Using Optical Methods to Monitor and Administer Photodynamic Therapy to Oral Bacteria

Yongji Fu

M.S., Tsinghua University (2002)

B.S., Tsinghua University (1999)

A dissertation submitted to the faculty of the

OGI School of Science & Engineering

at Oregon Health & Science University

in partial fulfillment of the

requirements for the degree

Doctor of Philosophy

in

Biomedical Engineering

March 2008

The thesis “Using Optical Methods to Monitor and Administer Photodynamic Therapy to Oral Bacteria” by Yongji Fu has been examined and approved by the following Examination Committee:

Steven L. Jacques, Ph.D., Thesis Advisor
Professor

Ruikang Wang, Ph.D.
Professor

Jorge Crosa, Ph.D.
Professor

Jack Ferracane, Ph.D.
Professor

Teresa Goodell, Ph.D.
Assistant Professor

ACKNOWLEDGEMENT

I would like to express my gratitude to so many people who have encouraged during my Ph.D study and supported me to achieve this thesis. Firstly I should thank my advisor Dr. Steve Jacques who has introduced the world of biomedical optics to me. He taught me how to conduct good research, how to communicate with colleagues efficiently with presentation and scientific paper and how to perform my best to be a good researcher. My career success will rest in these gifts. I will also thank Dr. Ruikang (Ricky) Wang who has continuously been encouraging and willing to help me. Ricky has been my model to pursue success in my career. My gratitude goes to Dr. Jorge Crosa. Jorge's brightness and humor always impressed me and let me feel research was such a wonderful work. I would like to thank Dr. Jack Ferracane for his kindly help and discussion about tooth relative topics. And I would also like to thank Dr. Teresa Goodell to share her great knowledge about Photodynamic Therapy and statistical analysis. I would also acknowledge Dr. Scott Prahl, Dr. Sean Kirkpatrick and Dr. Don Duncan in the biomedical optics group for their kindly help on my research. My thankfulness goes to Dr. Theresa Madden from School of Dentistry for her advice on periodontology.

I would like to acknowledge researchers in microbiology department. Dr. Hiroaki Naka helped me to culture bacteria and answered many microbiology questions. Dr. Moqing Liu also helped me on microbiology topics. Dr. Lidia Crosa gave me a lot of advice on research, career and life. My thankfulness goes to acknowledge researchers in Oregon Medical Laser Center. Dr. Michael Rutten allowed me to use the confocal system in OMLC and Kirstin and Amanda spent a lot of time to work with me on the confocal system.

I would like to thank my fellow students. Former student now Dr. Kirstin Engelking taught me a lot when I just came to this lab. David was always a good

people to chat with and he let me know a lot of interesting stuff from different culture. Ravi worked with me for the confocal microscope research and had great discussion on scientific topics as well as food, movie and everything. It was always nice to get a greeting email from Laurel in a sunny afternoon and thanks to introduce the Powell's bookstore to me. I also want to thank other students Lian, Anusha, Niloy, Yinchu, Ted, Amanda, Dan, Crane, Yi, Chuanmao, Yali, Lin, and Elaine.

There are a lot of researchers who communicated with me for all discussions including the topics of tissue optics, microbiology, optical scattering theory, scientific calculations, dentistry and all the other respects of my thesis work. The names list is too long to be listed. Although I have never seen them, their help will be always remembered.

Finally my greatest thankfulness goes to my family, my parents Liren Fu and Zhiping Liu who gave me all their supports and blessing from the other side of the ocean and my wife, Lifeng Liu, accompanying with me, sharing our achievement and frustration and letting me know I was not alone trudging the road.

TABLE OF CONTENTS

ACKNOWLEDGEMENTS…….. Iii

TABLE OF CONTENTS…….. V

LIST OF TABLES……..... Ix

LIST OF FIGURES…….. X

ABSTRACT……. Xii

CHAPTER 1 INTRODUCTION…….…… 1

1.1 PHOTODYNAMIC THERAPY AND ITS ANTIBIOTIC APPLICATIONS…… 1

1.2 ORAL BIOFILM PDT……... 5

1.2.1 Structure and components of tooth……... 5

1.2.2 Dental diseases and biofilm…….. 7

1.2.3 Streptococcus mutans and oral disease……. 11

1.2.4 Oral biofilm treatment…….. 12

1.2.5 Antibiotic PDT Selectivity Issue…….. 13

1.3 PS UPTAKE ANALYSIS WITH OPTICAL MEASUREMENT…….. 14

1.4 WORKING GOALS…….. 15

CHAPTER 2 PHOTOSENSITIZER: UPTAKE AND DISTRIBUTION PROFILE IN THE BIOFILM……. 19

CHAPTER 2A: AVERAGE PHOTOSENSITIZER UPTAKE MEASUREMENT OF ORAL BACTERIA IN PLANKTONIC AND BIOFILM STATES……... 20

2A.1 INTRODUCTION……. 20

2A.2 METHODS…… 22

2A.2.1 Planktonic Bacteria Culture Protocol…….. 22

2A.2.2 PS Preparison…….. 22

2A.2.3 TBO uptake process…… 22

2A.2.4 Separate the Bacteria from Solution…… 23

2A.2.5 Phantom Making…….. 23

2A.2.6 Optical Setup…… 24

2A.3 THEORY…… 26

2A.3.1 Total reflectance in a homogenous media……. 26

2A.3.2 Data Fitting…… 27

2A.3.3 Total reflectance for bacteria-polystyrene sphere phantom…….. 28

2A.3.4 Photosensitizer uptake measurement for biofilm…….. 29

2A.4 RESULT…….. 29

2A.5 DISCUSSION……. 32

CHAPTER 2B: USING A REFLECTANCE-MODE CONFOCAL MICROSCOPE TO DETERMINE PHOTOSENSITIZER DISTRIBUTION PROFILE A BIOFILM OF ORAL BACTERIA…….. 35

2B.1 INTRODUCTION……..... 36

2B.2 THEORY…….. 37

2B.2.1 Reflectivity and Attenuation in a Confocal Signal……. 37

2B.2.2 Heterogeneous Media……. 39

2B.3 MATERIALS AND METHODS……. 40

2B.3.1 Confocal System…… 40

2B.3.2 Phantom measurements…….. 41

2B.3.3 Biofilm culture protocol…… 43

2B.3.4 Imaging the biofilm…… 43

2B.4 RESULTS……. 45

2B.4.1 Phantom Results……. 45

2B.4.2 Biofilm results…….. 50

2B.5 DISCUSSION…….. 54

CHAPTER 3 LIGHT SOURCE CALIBRATION FOR EFFECTIVE PDT DOSAGE 57

3. 1. SPECTROMETER CALIBRATION…… 58

3. 2 EXTINCTION COEFFICIENT OF TOLUIDINE BLUE O…….. 61

3. 3 EFFECTIVE PDT DOSAGE CALCULATION……. 62

3.4 SUMMARY…… 63

CHAPTER 4 PHOTODYNAMIC THERAPY EXPERIMENT AND THE RESULTS: 64

SURVIVAL CURVES……

4.1 INTRODUCTION…… 65

4.2 MATERIALS AND METHODS…….. 65

4.2.1 Bacteria and Biofilm Culture Protocol…… 65

4.2.2 Photosensitizer Preparation ……. 66

4.2.3 Light Source …….. 66

4.2.4 Planktonic State PDT Process……. 67

4.2.5 Biofilm State PDT Process…….. 67

4.2.6 Uptake of Photosensitizer by Bacteria……. 67

4.3 RESULTS…….. 68

4.3.1 Uptake of Photosensitizer…….. 68

4.3.2 PDT Killing Effects…… 69

4.4 DISCUSSION…….. 70

CHAPTER 5 PHOTODYNAMIC THERAPY DOSAGE ANALYSIS…… 71

5.1 INTRODUCTION…… 70

5.2 THRESHOLD PDT DOSE, PDTTH…….. 72

5.3 DISCUSSION……. 73

CHAPTER 6 MONTE CARLO SIMULATION FOR LIGHT PROPAGATION IN 3D TOOTH MODEL…… 77

6.1 INTRODUCTION…… 77

6.2 THEORY…….. 78

6.2.1 Introduction…… 78

6.2.2 Light propagation…… 79

6.2.3 Photon termination……. 84

6.2.4 MCML geometry…… 85

6.3 3D MONTE CARLO TOOTH MODEL --- MCMB…… 85

6.3.1 Geometry Model and Optical Properties of Tooth……. 86

6.3.2 Data structure of MCMB…… 88

6.3.3 Light source implementation…….. 88

6.3.4 Function for photons crossing boundary……. 90

6.3.5 Monte Carlo Output…… 91

6.4 USE CASES……. 92

6.4.1 Light source comparison: broad beam vs. narrow (pencil) beam…….. 93

6.4.2 Compare incident light position…….. 95

6.5 CONCLUSION AND DISCUSSION…….. 98

CHAPTER 7 GENERAL DISCUSSION AND CONCLUSION…….. 99

7.1 CONFOCAL MICROSCOPY MODEL FOR PS DISTRIBUTION IN BIOFILM 99

7.2 PLANKTONIC STATE PS UPTAKE…… 101

7.3 LIGHT CALIBRATION AND PDT DOSAGE ANALYSIS……. 101

7.4 MONTE CARLO SIMULATION……. 102

7.5 ANTIBIOTICS PDT PERSPECTIVE…….. 103

BIBLIOGRAPHY …… 105

BIBLIOGRAPHICAL NOTES …… 115

LIST OF TABLES

TABLE 2.1 Fitting results for PS concentration parameters…… 33

TABLE 4.1 Survival results of bacteria after PDT …… .....…. 70

TABLE 6.1 Tooth optical properties …… 88

TABLE 6.2: Result for Case #2 …… 97

LIST OF FIGURES

FIG. 1.1. Photodynamic Therapy process ……. 2

FIG. 1.2. E.coli cells shape change during PDT process …….. 3

FIG. 1.3. Cell wall structure of Gram positive and Gram negative bacteria …….. 4

FIG. 1.4. Tooth Structure …… 5

FIG. 1.5. Tooth under periodontitis attacks …… 8

FIG. 1.6. Tooth under dental caries attacks ……. 9

FIG. 1.7. Polymicrobic biofilm …….. 10

FIG. 1.8. Gram stain of S. mutans, Source: CDC Public Health Image Library …… 11

FIG. 2.1 reflectance phantoms …… 24

FIG. 2.2. Reflectance-mode spectroscopy measurement ……. …….. 25

FIG. 2.3 Reflectance measurement data processing; solid squares are known factors and dash squares are unknown factors ……. 27

FIG. 2.4. Fitting program …….. 28

FIG. 2.5. Absorption coefficients derived from fitting program …… 30

FIG. 2.6. Uptake concentrations for S. mutans cells …….. 31

FIG. 2.7. TBO uptake vs. time …….. 32

FIG. 2.8. Confocal reflectance signal R(z) vs. depth z. The [dimensionless] and [cm-1] are the local reflectivity and attenuation coefficient, respectively …… 39

FIG. 2.9. Reflectance-mode confocal scanning laser microscope …….. 3?

FIG. 2.10. Holder for phantoms made with polystyrene microspheres as scatterer and TBO photosensitizer as absorber …… 42

FIG. 2.11. Biofilm holder for confocal microscope imaging ……. 44

FIG. 2.12. Protocol for exposure of biofilm to TBO ……. 45

FIG. 2.13 Phantom experiments ……. 46

FIG. 2.14 Phantom results …….. 48

FIG. 2.15 Analysis grid …….. 49

FIG. 2.16 Biofilm images before and after exposure to TBO …… 50

FIG. 2.17, Effect of TBO absorber in biofilm on the confocal reflectance signal. … … 52

FIG. 2.18 TBO concentration profile versus depth …….. 53

FIG. 2.19 Image of TBO concentration distribution ……. 54

FIG. 3.1 HeNe laser spectrum from an OceanOptics spectrometer ……. 58

FIG. 3.2 total power (in counts) from the spectrum measurement …….. 59

FIG. 3.3 LS-1 Spectrum from spectrometer measurement (red) and from vendor ……. 60

FIG. 3.4 Conversion number spectrum. …… 60

FIG. 3.5 Extinction coefficient of Toluidine Blue ……. 61

FIG. 3.6 Tungsten filament spectrums from OceanOptics spectrometer …… 62

FIG. 4.1. PDT survival curves for planktonic and biofilm states S.mutans …… 69

FIG. 5.1. TBO uptake in the S.mutans cells (planktonic) after 60 minutes waiting in dark. a: TBO concentration in cell vs. TBO concentration in the surrounding medium; b: TBO concentration ratio (cell/medium) vs. TBO concentration in the surrounding medium. 74

FIG. 5.2. Survival curve fitting for $H_{th.planktonic}$, $H_{th.upper}$ and $H_{th.lower}$. …….. 75

FIG. 6.1. Three phase functions …… 82

FIG. 6.2. Result comparison for 3 different phase functions …… 83

FIG. 6.3. Geometry of MCML ……. 85

FIG. 6.4 a.Tooth structure for Monte Carlo simulation, b. Tooth dimension in Monte Carlo model …….. 86

FIG. 6.5. Light sources in tooth model. ……. 89

FIG. 6.6. An example of MCMB output …… 92

FIG. 6.7. Use case #1: Board Beam vs. Narrow Beam …….. 94

FIG. 6.8. Use case #2: Comparison between 2 incident point of doctor's choice …….. 96

ABSTRACT

Using Optical Methods to Monitor and Administer Photodynamic Therapy to Oral Bacteria

Yongji Fu

OGI School of Science & Engineering

at Oregon Health & Science University

March 2008

Thesis Advisor: Steven L. Jacques Ph.D.

Oral bacteria related disease such as periodontital disease and dental caries affects over 75% of adults over 35 years in the US. Resolving this issue becomes more difficult as antibiotic-resistance strains of bacteria in a biofilm pose an increasing challenge for dental care. Photodynamic therapy (PDT) is an antibiotic treatment that employs oxidation by a light-activated photosensitizer (PS) to kill targeted bacteria cells. PDT is a good alternative to regular antibiotics approaches because (1) the dual selectivity of PDT (PS can target to the bacteria cells and the illumination can be directed to the infected area), and (2) the difficulty for bacteria to develop resistance to PDT. The objective of this study is to understand the dosimetry of PDT for oral biofilm in order to design PDT protocols, using optical technologies.

Research on this antibiotic effect of PDT is still in its early stage needs contributions from many different areas such as microbiology, biomedical optics, dentistry and

biochemistry. This study presents the research using optical methods such as reflectance spectroscopy and confocal microscopy to monitor the uptake of photosensitizers (PS) into bacterial suspensions (planktonic state, using reflectance spectroscopy) and bacterial biofilms (biofilm state, using confocal reflectance) dosimetry. The threshold PDT dose (photons absorbed by PS per g of cells) was determined as $3.6x10^{21}$ by cell survival studies following increasing light exposures, for both planktonic and biofilm states of bacteria. However the threshold radiant exposure H_{th} for biofilm (18 J/cm^2) was about 10-fold higher than H_{th} in the planktonic state (1.3 J/cm^2). This is because the photosensitizer concentration in the lower layer of biofilm is much less than the planktonic state photosensitizer concentration. The ability of treatment light to penetrate a tooth to achieve PDT both at surfaces and within the tooth, e.g., in cracks or fissures, was studied using a Monte Carlo program that simulates the structure of a tooth.

In summary, three topics were addressed: (1) uptake of PS by planktonic and biofilm bacteria, (2) the threshold PDT dose required to kill planktonic and biofilm bacteria, and (3) a Monte Carlo simulation of the tooth to asses the ability of PDT treatment light to reach different parts of a tooth. The significance of this work is that the tools (optical assessment of PS uptake, Monte Carlo model for light delivery) and dosage information (PDT threshold lethal dose) are pertinent to design of PDT protocols for antibacterial effect on oral bacteria.

Chapter 1
Introduction

1.1 Photodynamic therapy and its antibiotic applications

Disease-causing microbes that have become resistant to drug therapy, which is called antibiotics resistance [1], are an increasing public health problem. The mutation of bacteria helps a microbe to survive in the presence of an antibiotic drug and the new strain will quickly become predominant throughout the microbial population. Another major contributor to antibiotic-resistance is the inappropriate prescription of antibiotics [2, 3]. The emergence of antibiotic-resistance among pathogenic bacteria has led to a major research effort to find alternative antibacterial therapeutics, e.g. photodynamic therapy (PDT) [4, 5] which is going to be studied in this dissertation.

PDT employs a combination of photosensitizing drug, or photosensitizer (PS), and activating light, in the presence of oxygen, to kill targeted bacteria cells [5]. PS is converted to an excited-state by absorbing a photon. This excited-state PS then undergoes an intersystem crossing to a slightly lower energy, but a longer lived triplet-state, which may then react further via one of two pathways known as Type I and Type II photoprocesses [12], as shown in Figure 1.1 [5]. Type I pathway involves electron-transfer reactions from the triplet state of PS with the participation of a substrate to produce radical ions that then react with oxygen to produce cytotoxic species, such as superoxide, hydroxyl and lipid-derived radicals [13]. The Type II pathway involves energy transfer from the triplet-state PS to ground-state oxygen to produce an excited-state singlet oxygen, which can oxidize biological molecules, such

as proteins, nucleic acids and lipids, and can lead to cytotoxicity [14].

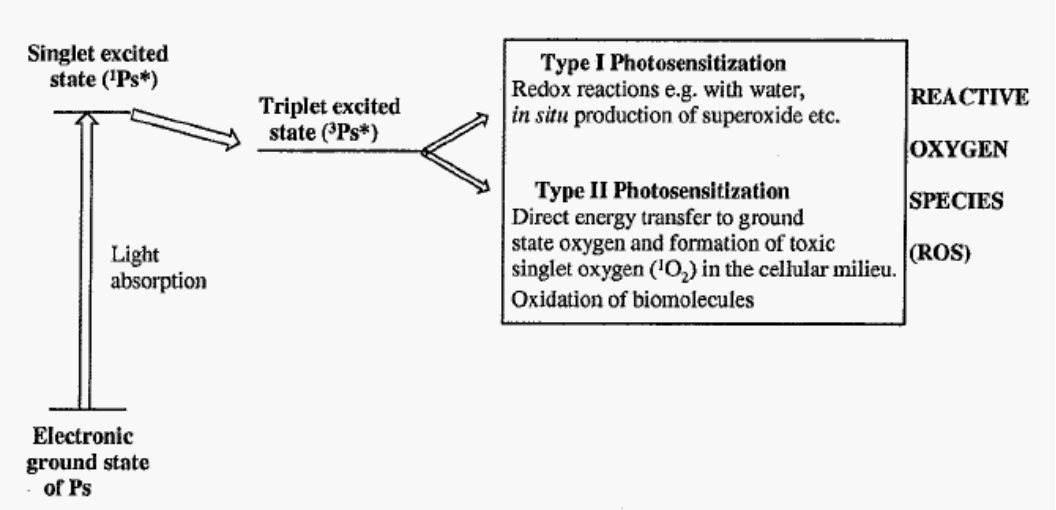

Figure 1.1 Photodynamic Therapy process

Researchers have successfully achieved PDT inactivation of bacteria in the laboratory. There are two basic mechanisms that have been proposed to account for the lethal damage of bacteria by PDT: (i) DNA damage [15, 16] and (ii) damage to the cytoplasmic membrane, causing leakage of cellular contents or inactivation of membrane transport systems and enzymes, as shown in Figure 1.2 [17]

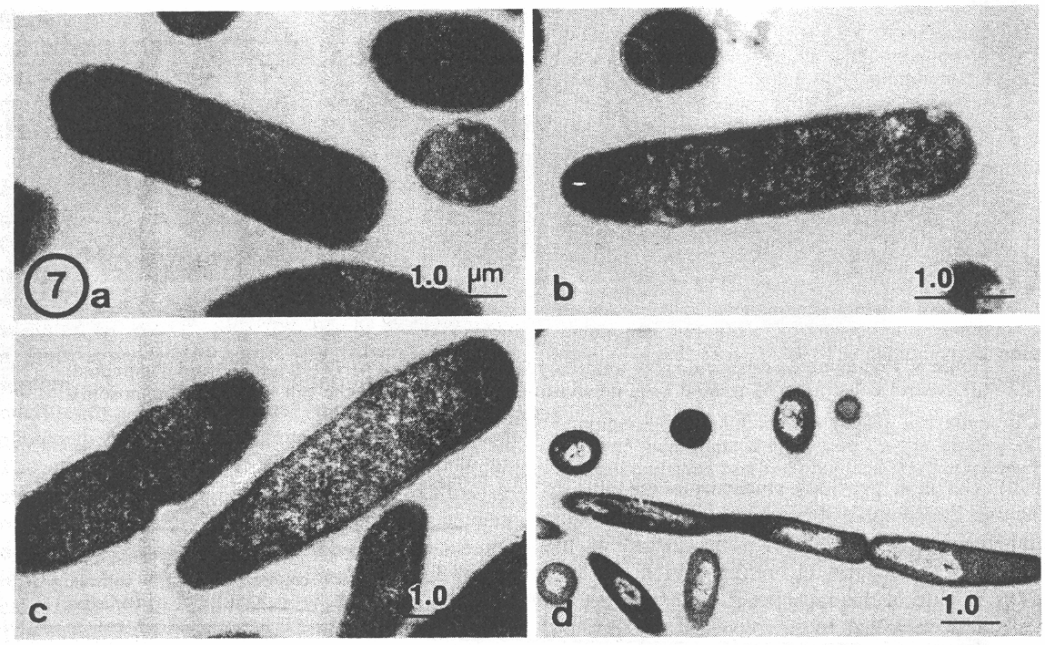

Figure 1.2 E.coli cells shape change during PDT process, Source: Reference [37]. a: untreated E.coli cells, b: treated with deuteroporphyrin (DP) and light illumination, c: treated with polymyxin nonapeptide (PMNP) and light illumination, d: treated with DP and PMNP and light illumination

PDT has significant future antibiotic applications [6]. Multi-antibiotic resistance of pathogens, especially bacteria, is a rapidly growing and alarming phenomenon and alternative antibiotics treatments are urgently being sought. In many localized infections, oral or systemically delivered antibiotics are not particularly effective. In recent years, clinical application of PDT has remained focused on the dosimetry of light and administered PS [7]. The concept of implicit dosimetry was introduced by Wilson et al. [8] and involves measuring various changing properties of a PS, such as the rate constant of photobleaching, or triplet decay time, to determine the singlet oxygen production during PDT.

The efficacy of PDT depends on a variety of parameters: the concentration of the PS [18, 19] at the time of treatment; the wavelength [20], fluence and irradiance of the treatment light [21]; and the availability of oxygen [23] within the illuminated space. The complicated conditions of PDT have resulted in variable treatment outcomes.

Therefore, methods which can instantly measure the PS uptake and simulate the light propagation will be very valuable for design of PDT protocols for clinical applications [10, 11].

Microbial cells have large differences in the cellular structure and organization between gram positive bacteria and gram negative bacteria as shown in Figure 1.3. These differences have dramatic effects in modulating the interaction of added photosensitize with cell constituents, hence in affecting the efficiency and the mechanism of the PDT killing processes. The outer wall of gram negative bacteria has an additional 10~15 nm thick structural element, which has a very heterogeneous composition, including proteins, lipopolysaccharide trimers and lipoproteins giving the outer surface a quasi-continuum of densely packed negative charges. Such a highly organized system inhibits the penetration of host cellular and humoral defense factors and triggers mechanisms of resistance against several antibiotic drugs including some commonly used photosensitizer. And that is the reason gram negative bacteria are more difficult to kill compared to gram positive bacteria. [19]

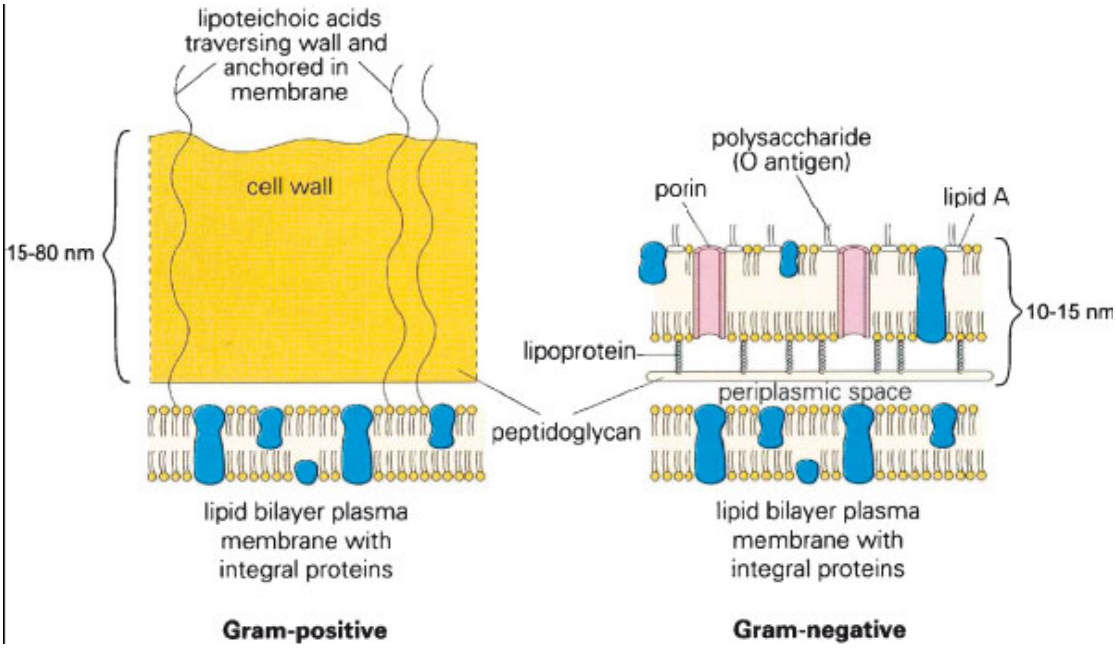

Figure 1.3 Cell wall structure of Gram positive and Gram negative bacteria

1.2 Oral biofilm PDT

1.2.1 Structure and components of tooth

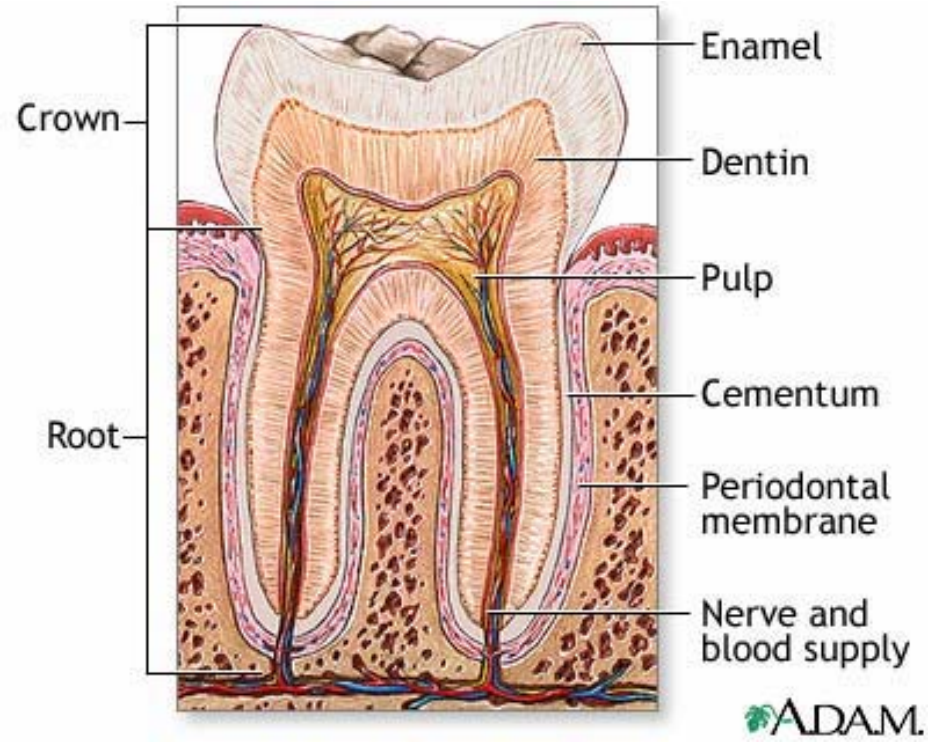

Figure 1.4 Tooth Structure

Figure 1.5 shows the tooth structure. Enamel and dentin, cementum, and dental pulp are the four major tissues which make up the tooth. Tooth enamel is the hardest and most highly mineralized substance of the body. It is the normally visible portion of a tooth and is supported by underlying dentin. Ninety-six percent of enamel consists of mineral, with water and organic material composing the rest [88]. The normal color of enamel varies from light yellow to grayish white. Enamel's primary mineral is hydroxyapatite, which is a crystalline calcium phosphate. This is the same material that is used in this work to grow biofilm: hydroxyapatite (HA) discs. The large amount of minerals in enamel accounts not only for its strength but also for its brittleness.

Dentin is covered by enamel or cementum and lays over the pulp. By weight, seventy percent of dentin consists of the mineral, hydroxylapatite, twenty percent is organic

material, and ten percent is water. However this content proportion varies and this is one of the reasons that the reported optical properties of dentin reported by different investigators significantly differ. Yellow in appearance, dentin greatly affects the color of a tooth due to the translucency of enamel. Dentin, which is less mineralized and less brittle than enamel, is necessary for the support of enamel. Dentin consists of microscopic channels, called dentinal tubules, which radiate outward through the dentin from the pulp to the exterior cementum or enamel border. These tubules contain fluid and cellular structures. As a result, tooth bacteria and biofilm can reside in dentin and tooth decay may be induced. According to this fact, we have to find some way to estimate the light deposition in the target region which may be inside the tooth in our PDT study [112].

The dental pulp is the central part of the tooth filled with soft connective tissue. This tissue contains blood vessels and nerves that enter the tooth from a hole at the apex of the root. The pulp is important when designing a treatment protocol because one must ensure that the light dose will not damage the pulp, which has a relatively high optical absorption coefficient [112].

Cementum is a specialized bony substance covering the root of a tooth. Because of its location and its size, cementum does not affect light propagation in the tooth. This structure is ignored in the tooth model presented in this thesis in order to simplify our model.

Besides the 4 components above, Gum (Gingiva) is part of the soft tissue lining of the mouth. It consists of the mucosal tissue that overlays the bone. It surrounds the teeth and provides a seal around them. Healthy gum is usually coral pink, but may contain pigmentation. Oral bacteria can lead to many gingival and periodontal disorders, including gingivitis or pyorrhea, which is the major cause for tooth loosening or being lost [112].

1.2.2 Dental diseases and biofilm

Dental diseases such as periodontital disease and dental caries are one of the most common diseases in the US. In fact, more than 75% of adults over 35 years in the US have dental diseases. Recent medical research has shown a direct correlation to periodontal disease and systemic health [9]. One of the periodontal diseases, periodontitis (Figure 1.6) is a dental disorder that results from the progression of gingivitis (inflammation of the gums) involving inflammation and infection of the ligaments and bones that support the teeth. The key factor of periodontal disease is dental plaque. Bacteria in the dental plaque around the teeth release enzymes (collagenases) that can damage and erode the gum tissues. The infected gums swell, bleed easily, recede, and loosen from the teeth. The dental caries (Figure 1.7) is a collection of infected material resulting from bacterial infection of the center (pulp) of a tooth. In the dental plaque there are bacteria which form acids. The acids decalcify the surface of the tooth so that the enamel becomes softer and chalk-white in color. This is the first sign of caries in a tooth. The bacteria and acids then move into the decalcified part and continue damaging the tooth. If the caries process is allowed to run its course without interruption, the tooth will decalcify until the dentin is reached and finally become sensitive to cold and sugars.

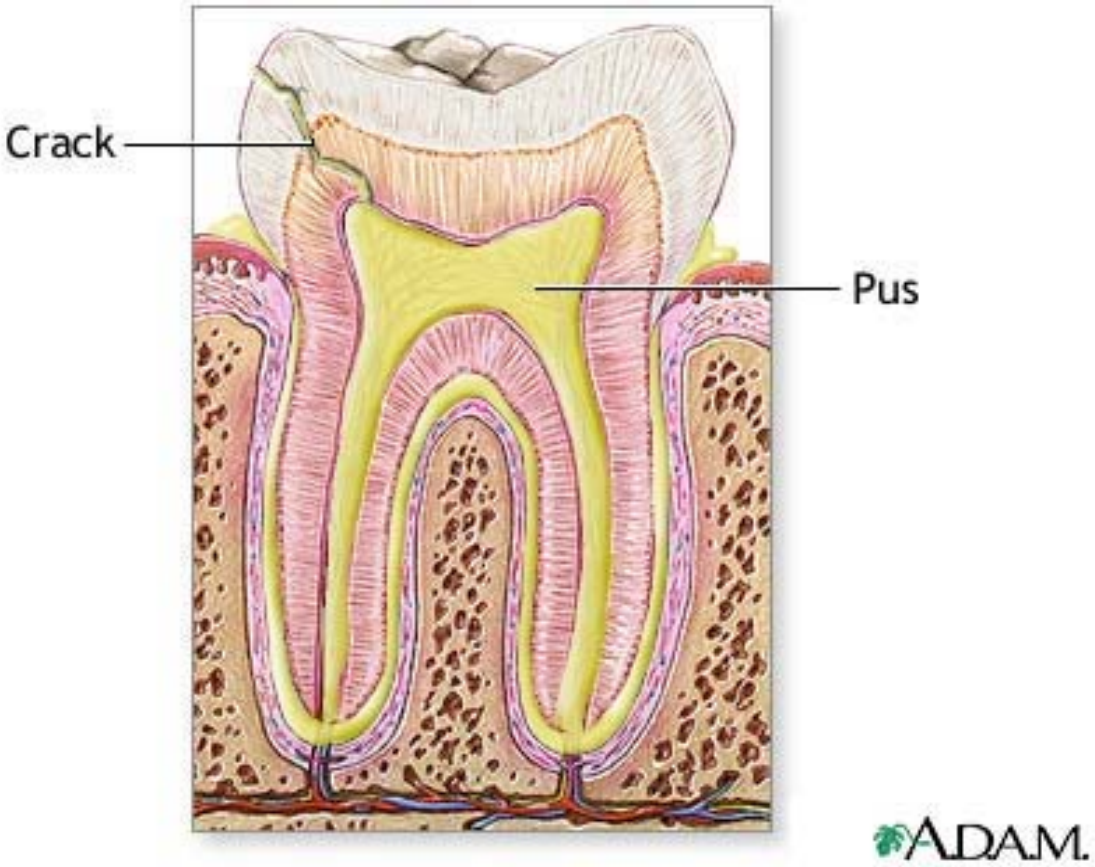

Figure 1.5 Tooth under periodontitis attacks

Source: the American Accreditation HealthCare Commission

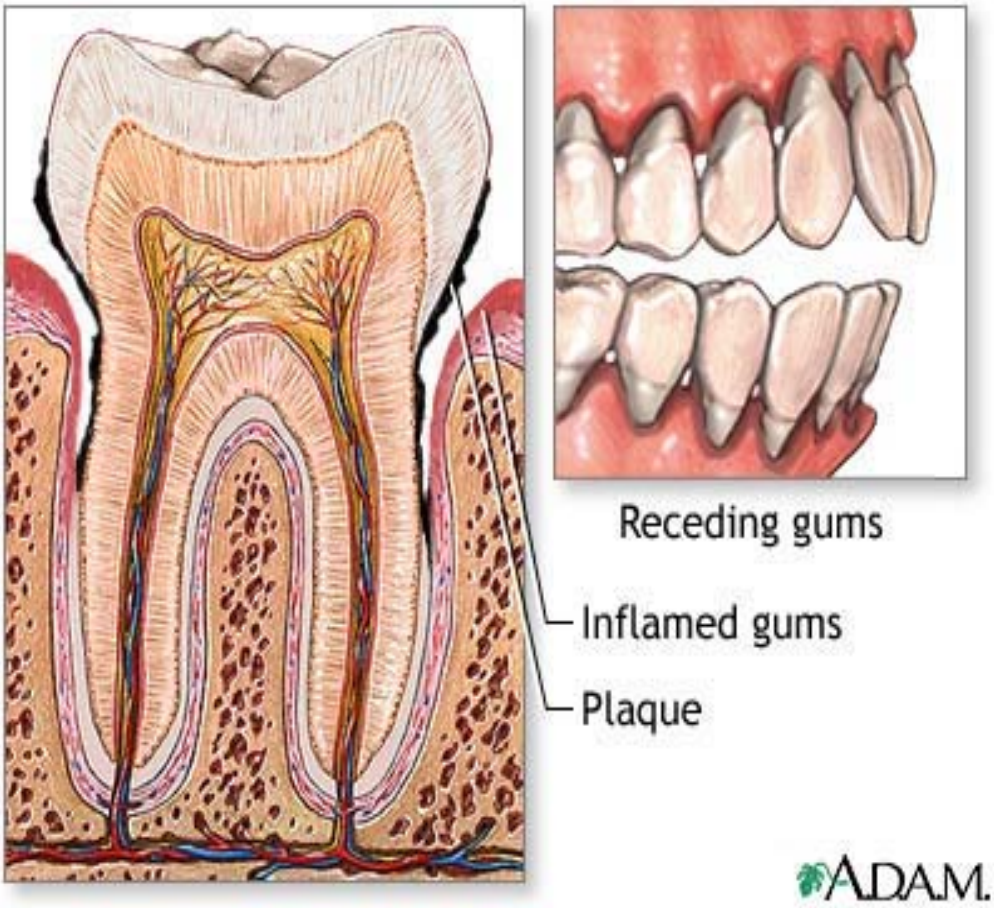

Figure 1.6 Tooth under dental caries attacks

Source: the American Accreditation HealthCare Commission

Since the end of the 20th century, dental researchers began to look at dental plaque as a microbial biofilm. Biofilm state microbes are broadly defined as adherent microorganisms within a polymeric matrix, typically comprising exopolysaccharide that develops into a complex community as shown in Figure 1.8 [24]. In contrast, bacteria suspended in a liquid medium are in the planktonic state. Growth of bacteria as a biofilm almost always leads to a large increase in resistance to antimicrobial agents, in comparison to planktonic state bacteria grown in conventional liquid media, with up to 1000-fold increases in resistance reported [26, 27]. Currently, there is no generally accepted mechanism to account for the broad resistance of microbial biofilms [28-31].

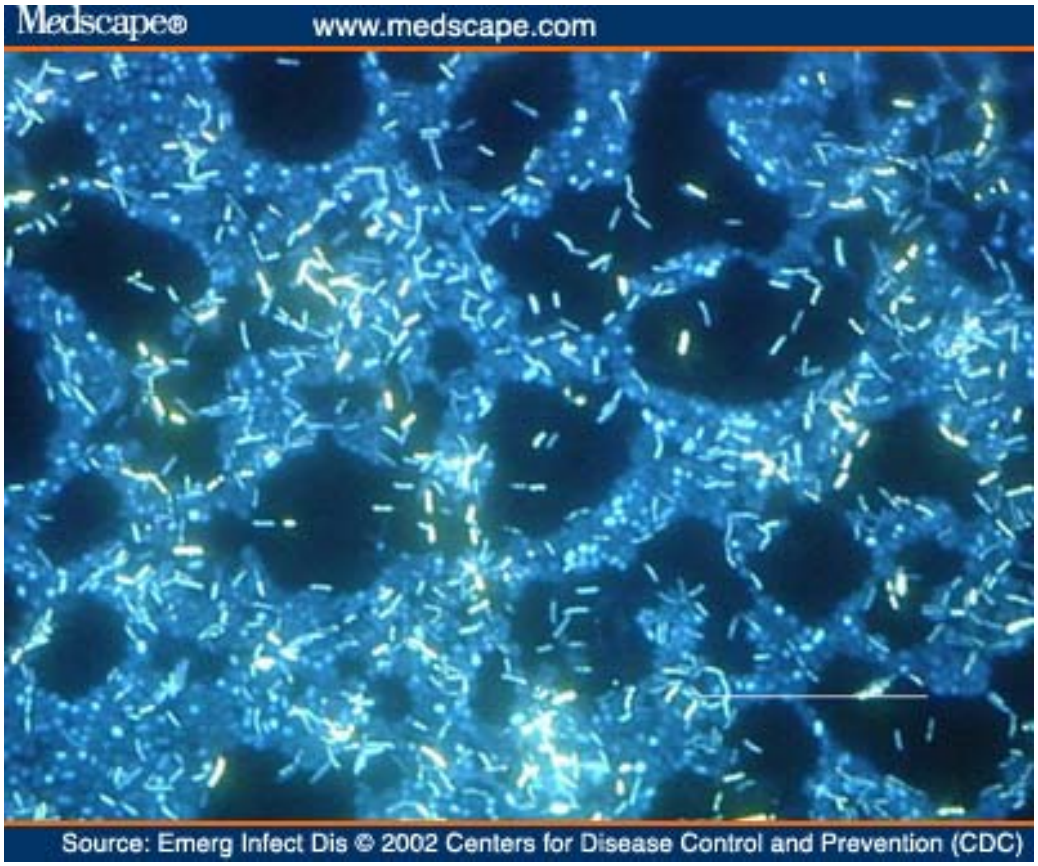

Figure 1.7 Polymicrobic biofilm grown on a stainless steel surface in a laboratory potable water biofilm reactor for 14 days, then stained with 4,6-diamidino-2-phenylindole (DAPI) and examined by epifluorescence microscopy. Bar, 20 µm. Photograph by Ricardo Murga and Rodney Donlan, CDC.

Periodontitis is an inflammatory disease of gingival tissue induced by the bacteria residing in the dental plaque on the subgingival tooth surface. The oral cavity is heavily colonized by a complex relatively specific and highly interrelated range of micro-organisms [38]. The inflammation leads to pocket formation in the gum tissue, attachment loss, bone destruction and possible tooth loss [33].

The contribution of biofilm to human infections [25] is also found in other sites of the human body, for example, the well-known device-related infections such as those associated with artificial joints, prosthetic heart valves and catheters [32]. Recent surveys indicate that catheter-associated bacteremia following catheter-related infection is by far the leading cause of nosocomial bloodstream infection in the

intensive care units [39]. A major part of the biofilm problem in nosocomial infections is transmission within the institute itself, i.e. hospital acquired infection (HAI). Hygiene practices that are quite adequate in everyday life are not acceptable in the health care system, owing to the greater propensity for disease development in already ill or immuno-compromised patients. There is a significant need for hospital treatments of patients with infections that does not require antibiotics, and PDT may be such a treatment [35].

1.2.3 Streptcoccucs mutans and oral disease

Streptococcus mutans is a gram-positive, facultatively anaerobic bacteria commonly found in the human oral cavity and is a significant contributor to tooth decay.[100] Figure 1.9 shows the strains of S.mutans bacteria.

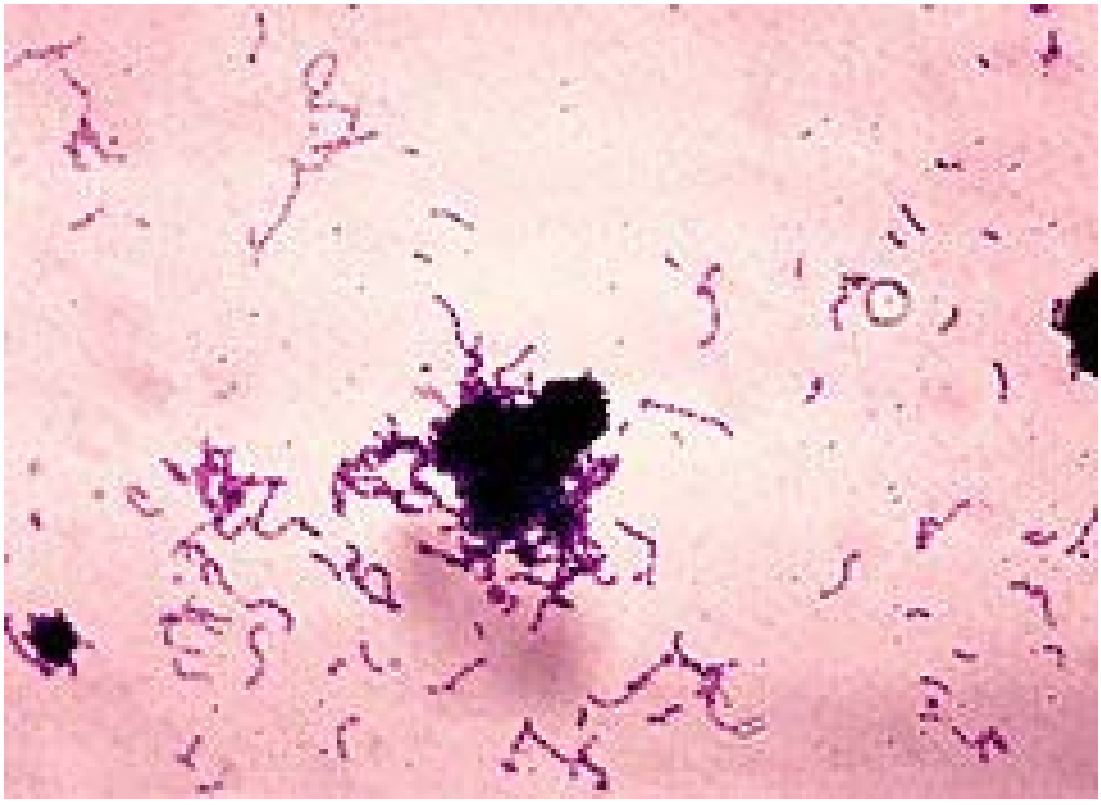

Figure 1.8 Gram stain of S. mutans, Source: CDC Public Health Image Library

S.mutans plays the key role in tooth decay, metabolizing sucrose to lactic acid [105]. The acidic environment created by S.mutans in the mouth causes the highly

mineralized tooth enamel to be vulnerable to dental decay. S.mutans is one of a few specialized organisms with receptors for adhesion to the surface of tooth. Sucrose is utilized by S.mutans to produce a sticky, extracellular, dextran-based polysaccharide that allows them to cohere to each other forming a biofilm. S.mutans produces dextran via the enzyme dextransucrase (a hexosyltransferase) using sucrose as a substrate in the following reaction:

$$n \text{ sucrose} \rightarrow (\text{glucose})_n + n \text{ fructose}$$

Sucrose is the only sugar that S.mutans can use to form this sticky polysaccharide [100]. It is also used to culture biofilm in experiments in this study.

Many other sugars such as glucose, fructose and lactose can be digested by S.mutans, but they produce lactic acid as an end product. It is the combination of biofilm (plaques) and acid that leads to tooth decay [106]. Due to the role that S.mutans plays in tooth decay, there have been many attempts to make a vaccine for the organism. So far, such vaccines have not been successful in humans [107]. Recently, proteins involved in the colonization of teeth by S.mutans have been shown to produce antibodies that inhibit the cariogenic process [108].

1.2.4 Oral biofilm treatment

The oral biofilm (plaques) are usually treated by mechanical methods such as tooth brushing and scraping. These kinds of methods will not totally remove the oral biofilm and the surviving biofilm will regrow. Some patients such as epidermolysis bullosa patients are not compatible with these mechanical methods. An alternative treatment is antibacterial drugs. There is no drug with significant antibiotic effect on oral bacteria and biofilm. The problems of antibacterial drug treatment include [54]: 1) increased resistance to most antibiotics used in periodontology, 2) an increased number of immune suppressed patients, 3) periodontal infections caused by many diverse pathogens requiring different antibiotics with different risks of adverse reactions.

PDT could be a good alternative approach to treat the oral biofilm causing periodontal diseases and dental caries diseases. PDT for oral biofilm has the advantage of dual selectivity: (1) PS can target the bacteria cells and the treatment light can be selectively delivered to the infected area. (2) reactive oxygen species produced by PDT are difficult for the microorganism to defend against [35]. Researchers have reported using PDT to treat oral biofilm with light from a helium/neon laser and greater than 95% of biofilm bacteria were killed [36]. Electron microscopic evidence for the destruction of biofilm structure has been reported for dental-type biofilms treated with a cationic PS, zinc phthalocyanine [37].

1.2.5 Antibiotic PDT Selectivity Issue

For the antibiotic use of PDT, it is very important that the PS binds selectively to bacteria and/or biofilm with negligible staining of the gum or other tissue. Binding is a prerequisite for the inactivation effect of PDT. Binding selectivity is crucial for PDT to avoid unwanted tissue damage.

Hamblin's group used P. gingivalis (gram positive bacteria), A. viscosus (gram negative bacteria) and HCPC-1 (epithelial cell) to test binding selectivity [50]. They found that the binding ratio of bacteria over epithelial cells is over 100:1 for cationic conjugate and 10:1to 50:1 for pL-C_{e6}. That is the reason why Toluidine Blue O (TBO) and Methylene Blue (MB), cationic dyes, can be the optimized photosensitizer for antibiotic PDT.

They also reported on the inactivation of *E. coli* in mouse wounds to prove that that bacteria-targeted PDT could be used as a treatment for localized infections, without unacceptable tissue damage [51]. They used a nonpathogenic bacterial strain that was eliminated in untreated control wounds over a period of 1-2 days. They also showed that PDT has an equal effect in treating infections caused by an invasive pathogen that, if left untreated, will inevitably cause death.

Another evidence for PDT binding is histological examination of the periodontal tissues of the rats following PDT [52]. The histological results showed no adverse effects, in that no ulcer formation on the epithelium or inflammation in the connective tissue was detected even with the highest light doses and Toluidine Blue O (TBO) concentrations used.

TBO, among other dyes, was reported to preferentially photosensitize carcinoma, or other tumor, cells and have lesser effects on normal cells [53]. A 90% reduction of the colonogenicity of human epidermoid carcinoma was achieved with 0.67 M TBO and 1 J/cm^2 of white light, whereas normal hamster ovary cells were highly resistant to the photosensitizing effects.

1.3 PS uptake analysis with optical measurement

PS uptake is a very important issue in PDT treatment. PS should be selectively taken up by bacteria cells to ensure that PDT will only kill the bacteria but not damage the surrounding tissue [34]. Another issue in PDT for biofilms is that PS should be taken up by bacteria throughtout the biofilm including the bottom layer of biofilm, so that oxidative treatment can occur throughout in the biofilm and all the bacteria in the biofilm will be killed.

Fluorescence measurement is a good approach to assess the PS uptake because most PS are fluorescent dyes or may be labeled with suitable fluorophores [55]. Fluorescence is increasingly used as a diagnostic tool to detect cancer, to monitor the intrinsic PDT dose, and to monitor fluorescent drug pharmacokinetics. However, quantitative models for the fluorescence signal have not been well developed.

To obtain quantitative information, such as fluorophore concentration, from the fluorescence measurement is complicated because of the complex photon propagation process [56]. Excitation light must penetrate the tissue to reach the fluorophores, and

fluorescence emission must escape the tissue to be observed. Light propagation in tissue is often expressed using diffusion theory, which depends on the two optical properties, the reduced-scattering coefficient μ_s' and the absorption coefficient μ_a, for both the excitation and fluorescence emission wavelengths Knowledge of local optical properties is essential for fluorophore quantification. A number of approaches to fluorophore quantification have been reported to minimize the effect of the optical properties of the medium on the detected signal [57-60]. In each of these techniques the detected signal is compared with a reference measurement (e.g. the signal from a known concentration in a tissue-simulating phantom), however the difficulty is that the fluorophore may have different properties in different environments, i.e. the absorption of excitation light and the efficiency of fluorescence emission.

1.4 Working Goals

In this study, two key factors in PDT, the PS distribution and the light dose, are investigated. These two factors are crucial for design of an oral antibiotic PDT protocol. The current research in this field has mostly focused on finding the proper PS for different bacteria and helping the PS penetrate into the biofilm. Quantitative analysis is still limited.

The threshold PDT dose for killing oral bacteria in planktonic and biofilm states will be determined. This determination relies on quantifying (1) the PS taken up by the bacteria, (2) the treatment light delivered to the bacteria, (3) the survival of bacteria after PDT treatment.

(1) PS uptake:

The PS concentration in planktonic bacteria is difficult to assess because of the small size of bacteria and the tiny amount of PS absorption. A method is presented based on a diffuse light reflectance measurement from a standard scattering solution to which bacteria with PS have been added. This method has been tested to be accurate and

robust. The method is used to study the dynamics of PS uptake by planktonic bacteria. This work is discussed in Chapter 3.

The PS concentration in biofilm is more difficult to measure because the distribution of PS in the biofilm is not homogenous. Researchers may use the fluorescence method to measure PS uptake, however fluorescence can only tell the amount but not the distribution of PS. Also, quantification is difficult because the PS fluorescence quantum yield is unknown and varies in different environments.

Some researchers break the biofilm and collect the cells to measure the PS concentration, but then the PS distribution information is missing. In the other words, the average PS concentration does not address the issue of PS distribution. The penetration of PS into the biofilm is a key issue that needs to be considered.

Instead of fluorescence measurement, this report relies on the absorption properties of the PS to assess uptake and distribution. A reflectance-mode confocal microscope is used to measure the biofilm with and without added PS. The difference in the confocal signal specifies the PS concentration. Hence, a 3D image of the PS concentration is acquired. Using this method, the dynamics of PS uptake are specified, and the uniformity of PS uptake is assessed. Additionally, the biofilm was broken up by vortex and resuspended and washed, then assayed by the reflectance spectroscopy method that was used for assay of uptake by planktonic bacteria.

(2) Treatment light:

The broad-band treatment light was characterized by spectroscopically specifying the power delivered per incremental wavelength, and specifying the absorption of this treatment light by the PS at each incremental wavelength. The product of (delivered light)(absorption) was integrated over the full wavelength range. The result is the light dose. For convenience, this dose could be described as equivalent to a specific power at one single wavelength, eg., 633 nm red light, times the absorption by PS at this

wavelength. Combined with the data on uptake of PS, and considering the volume of each bacterium, the light dose could be specified as the number of photons absorbed by PS per g of bacteria. This is the definition of a PDT dose.

(3) Survival studies:

Survival studies document the killing effect of PDT on planktonic state and biofilm state bacteria. Survival curves are recorded as colonies formation units (CFU) versus radiant exposure of treatment light (J/cm^2). For biofilms, after PDT treatment, the biofilm is broken up and resuspended in solution for plating to allow colony formation units.

The results of the studies of (1) PS uptake, (2) treatment light and (3) survival after PDT, the threshold PDT dosage is specified. The results show that PS uptake is a limiting factor for PDT treatment of biofilm. The results are consistent with both planktonic and biofilm having a similar sensitivity to PDT, expressed as a threshold PDT dose of $3.6x10^{21}$ photons/g, i.e., photons absorbed by PS per g of bacteria. However, the limited ability of PS to penetrate to the bottom layer of a biofilm allows a residual ~0.1% of the biofilm bacteria at the deepest layers of the biofilm to take up only about $1/71^{th}$ the amount of PS that is taken up by the bacteria in the superficial layers of the biofilm. Hence, the dose of light required for killing the bottom-most bacteria is increased about 71-fold, from a 1/e (63% killing) radiant exposure of 0.77 J/cm^2 to an exposure of 55 J/cm^2. Hence, the threshold PDT dosage for killing biofilm state bacteria appears to be much higher than the threshold for killing planktonic state bacteria. This conclusion is consistent with other group's work, and the PDT dosage is also compared with other target cell-PS couples. However, the difference is attributed in this report to the difficulty of PS to penetrate uniformly throughout the biofilm.

Finally, a study of light propagation in the tooth provides a design guide for planning light delivery to both the surface and interior of a tooth, eg., in cracks and fissures, for clinical practice. Sometimes the target bacterial cells are not located on the surface of

tooth, but in cracks or fissures. The light propagation model can guide the amount and location of irradiation that ensures sufficient PDT dose for killing bacteria. A 3D Monte Carlo simulation of light transport in a tooth is presented in Chapter 6. Example uses of tooth Monte Carlo program are also presented.

In summary, oral antibiotic photodynamic therapy will be studied with regard to photosensitizer uptake and distribution, light source calibration, threshold PDT dose analysis, and light propagation in a tooth model.

Chapter 2
Photosensitizer: Uptake and Distribution Profile in the Biofilm

This chapter includes two sections. In section A, reflectance method was yielded to access the photosensitizer uptake in the bacteria, for both planktonic and biofilm state. In section B, a confocal light propagation model was developed and validated to determine the photosensitizer distribution profile.

Chapter 2A:

Average Photosensitizer Uptake Measurement of Oral Bacteria in Planktonic and Biofilm States

Abstract

The average photosensitizer uptake by oral bacteria (S. Mutans) in both planktonic and biofilm states is determined using method based on optical reflectance. Bacteria that have taken up the photosensitizer Toluidine Blue O (TBO), either in planktonic or in biofilm that has been resuspended by vortex, were washed by centrifugation then added to a standard scattering medium consisting of polystyrene microspheres. The diffuse reflectance from the standard before and after adding the bacteria was measured. The bacterial TBO caused a drop in reflectance. Calibration was achieved by adding a known amount of TBO to the test standard scattering medium. This method allows measurements of low levels of TBO based on absorption because the scattering processed causes light to repeatedly expose each TBO molecule. Hence the absorption process is enhanced. Also, the difficulty of directly measuring a suspension of bacteria with its associated light scattering is avoided. The results show the time dynamics of TBO uptake by planktonic bacteria, in which bacteria achieve maximal concentrations after 15-20 min of exposure to a bathing solution with TBO. A typical number for planktonic state photosensitizer concentration was $3.1x10^3$ mg/L (40 mg/L solution concentration with 20 minutes waiting) and the biofilm state photosensitizer concentration was $1.1x10^3$ mg/L (80 mg/L solution concentration with 60 minutes waiting).

2A.1 Introduction:

Photosensitizer uptake is an important factor in Photodynamic Therapy because only

the photosensitizer in the bacteria cells have a killing effect. Photosensitizer concentration is much higher in the bacterial cell because the photosensitizer is selectively absorbed by bacteria in comparison to surround soft oral tissues [68-70]. To design a PDT treatment, the threshold PDT dose, PDT_{th} [photons absorbed by photosensitizer per g bacteria], should be carefully investigated. Equation 2.1 shows the factors that affect the dosage threshold [71, 72].

$$PDT_{th} = ET\ln(10)\varepsilon C_{ps}\frac{\lambda}{hc\rho} \qquad [photons/g] \quad [2.1]$$

In a photodynamic process, either singlet oxygen or another super oxidized molecule is generated. These molecules will kill the target cells [73, 78]. The singlet oxygen and super oxidized molecule have a very short lifetime [74]. Only the singlet oxygen and super oxidized molecules that are located within the target cells have a killing effect. Therefore only the photosensitizer in the target cells will contribute to the photodynamic therapy.

The photosensitizer (PS) has significant selectivity for the target bacterial cells. The concentration in the bacteria cells is much higher than the PS concentration in the surrounding media. The C_{ps} in the equation 2.1 is the photosensitizer concentration within the target cells. This chapter, will find an approach to measure this concentration.

PS selectivity is a very important feature for PDT process [76, 77]. Because of the PS selectivity, only the target cells will be killed by PDT and other cells will not be damaged. Therefore, finding the PS concentration for exposure to the target cells which yields good selectivity is one of the key tasks for researchers. For the subject bacteria cell S. mutans in this study, Toluidine Blue O (TBO) has been reported, along with other photosensitizers such as Methylene Blue and members of the porphyrin family [77].

In this chapter the photosensitizer concentration in cells will be studied and in chapter 2B the photosensitizer distribution in biofilm will be studied.

2A.2 Methods

2A.2.1 Planktonic Bacteria Culture Protocol

Streptococcus mutans (ATCC 25175) was used as subject bacteria. The bacteria were in planktonic state in the media.

1. Plating on brain heart infusion (BHI) agar of S mutants form -80°C glycerol stock and incubation at 37°C in a CO_2 incubator for 1 day.
2. Inoculation of S. mutans into 5ml BHI broth and Incubation at 37°C in a CO_2 incubator for 2 days.
3. Take 1ml culture and inoculate into 5ml BHI broth and incubate at 37°C in a CO_2 incubator with TBO solution for different incubation time (5 min, 10 min, 15 min, 20 min and 40 min).
4. Bacteria was diluted and grown on the BHI plate for 1 day in a CO_2 incubator for CFU counting.

2A.2.2 PS Preparison

Toluidine Blue O (TBO, Fisher Scientific, NY) was used as photosensitizer. TBO powder was put into distilled water to make the stock solution. The TBO stock solution was 160 mg/L.

2A.2.3 TBO uptake process

Different Concentration of TBO was put into the S. mutants to the test the uptake effect. Each well was put into 1 ml bacteria solution. In first five wells, 1 ml TBO stock solution was put into each well. In the second five wells, 0.5 ml TBO stock solution and 0.5 ml water was put into each well. In the third five wells, 0.25 ml TBO stock solution and 0.75 ml water was put into each well. The final TBO concentration was 80 mg/L, 40 mg/L, and 20 mg/L. And the final bacteria concentration was $5x10^8$

CFU/ml according to CFU counting. The bacteria TBO solution was put into dark environment and different waiting (incubation) time was tested.

The waiting time includes: 5 minutes, 10 minutes, 15 minutes, 20 minutes and 40 minutes. After the waiting process, the bacteria TBO solution was collected for next step: bacteria separation.

2A.2.4 Separate the Bacteria from Solution

The bacteria TBO solution was put into tube and centrifuge as speed 2000 RPM The residue after centrifuge was collected and washed twice. Then it was put into the tube and resolved for spectrometry measurement.

2A.2.5 Phantom Making

Polystyrene sphere (0.5 μm diameter, Duke Scientific, CA), S. mutans with TBO (in different initial concentration and different waiting time) and water were used to make a phantom for reflectance measurement. The stock polystyrene sphere concentration was 10% v/v.

1 ml polystyrene sphere solution; 0.5 ml bacteria solution (for each initial concentration and waiting time) and 0.5 mL water were put into each well. Three standard solutions were also made: 0.5 ml TBO solution (16 mg/L); 0.5 ml TBO solution (4 mg/L) and 0.5 ml water; in each phantom, 1 ml polystyrene sphere solution and 0.5 ml water was also added to each phantom. The final concentration of TBO in these phantoms is 4 mg/L and 1 mg/L.

Figure 2.1 shows the reflectance phantoms. First three rows are phantoms including polystyrene sphere and S. mutans cells with TBO uptake. There are 15 S. mutans and polystyrene sphere phantoms totally (3 different initial concentrations and 5 different waiting time) only 9 is shown in this figure. The phantoms in 4^{th} row are reflectance standards. The left one is polystyrene sphere (5% v/v) only phantom; the middle and

right phantoms are polystyrene sphere (5% v/v) with TBO solution (4 mg/L and 1 mg/L).

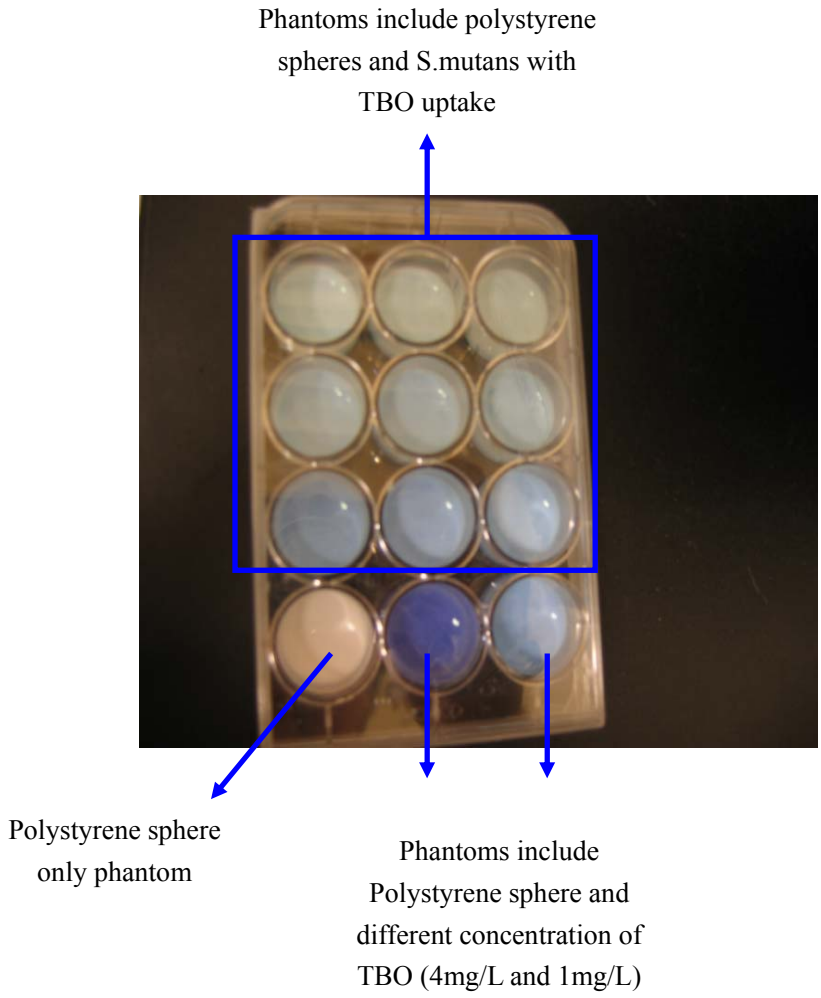

Figure 2.1 reflectance phantoms

2A.2.6 Optical Setup

Figure 2.2a shows the optical step for reflectance measurement of phantoms. Collimated light was irradiated to the phantom. A fiber collected lights reflected from the phantom. The fiber was connected with a spectrometer (OceanOptics, HR2000) and reflectance spectrum was recorded. This process is repeated for 18 phantoms. Figure 2.2b shows the optical setup for reflectance standard measurement. The collimated light was irradiated to a stack of white cards as reflectance standard. A fiber collected lights reflected from the phantom. The fiber was connected with the

OceanOptics spectrometer and reflectance spectrum of standard was recorded. Figure 2.2c shows the real optical setup for phantoms.

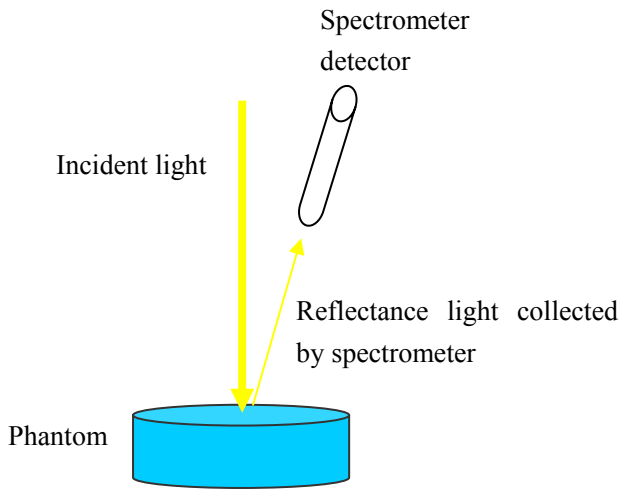

Figure 2.2a reflectance measurement of phantoms

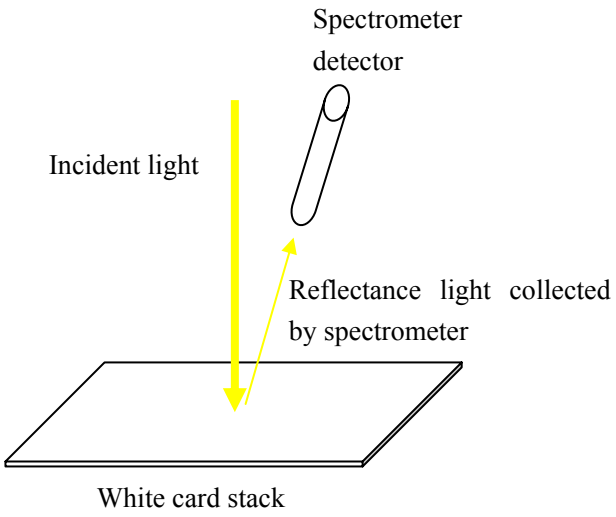

Figure 2.2b reflectance standard measurement

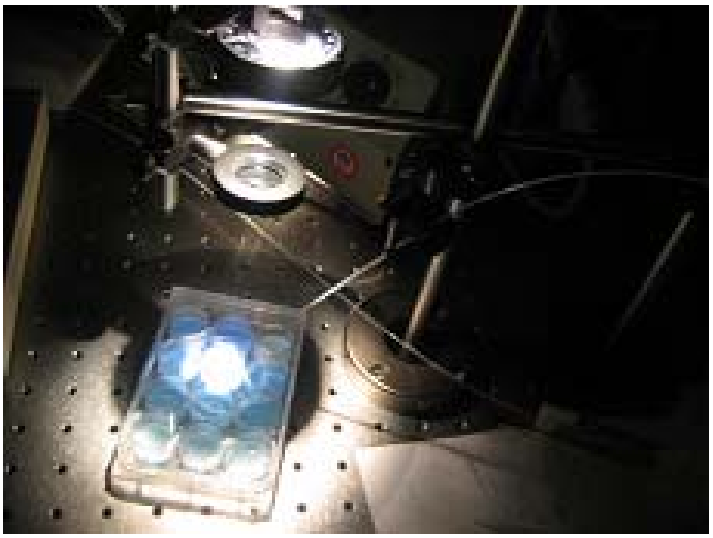

Figure 2.2c real optic setup for phantom measurement

2A.3 Theory

2A.3.1 Total reflectance in a homogenous media

Reflectance in a homogenous media depends on absorption coefficient and reduced scattering coefficient in the media [86], as equation 2.2

$$R_d \approx e^{(-A\delta\mu_a)} = e^{(-\frac{A}{\sqrt{3(1+N')}})}$$
$$\delta = 1 \Big/ \sqrt{3\mu_a(\mu_a + \mu_s')} \quad [2.2]$$
$$N' = \mu_s' \Big/ \mu_a$$

Reflectance R_d can be calculated with known absorption coefficient μ_a and reduced scattering coefficient μ_s'. If Reflectance R_d is known by measurement, and one of the absorption coefficient μ_a and reduced scattering coefficient μ_s' is also known, the other one will be also known using a fitting algorithm which will be explained later.

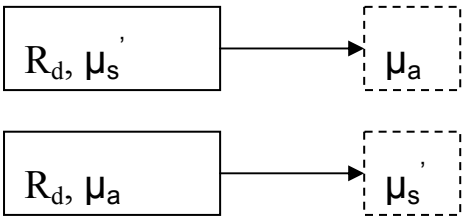

Figure 2.3 From measurements to unknowns; solid squares are known factors and dash squares are unknown factors

For reflectance spectrum each measurement, it includes the effects of light source S, effect of detector (spectrometer) D, geometry factor G and the reflectance R_d which we really want to know, as equation 2.3

$$M = SR_d GD \quad [2.3]$$

When we use this optical setup to measure a reflectance standard (a stack of name cards), effects of light source S, effect of detector (spectrometer) D, geometry factor G are not changed, reflectance of standard R_{std} is known to be around 0.9.

$$M_{std} = SR_{std} GD \quad [2.4]$$

If we take the ratio of equation 2.3 and 2.4 and reorganize this equation, the only unknown term is R_d and we can use this equation to get R_d.

$$R_d = \frac{M}{M_{std}} R_{std} \quad [2.5]$$

2A.3.2 Data Fitting

When we have R_d by the measurement described above, and we have known one of absorption coefficient μ_a and reduced scattering coefficient μ_s', we can use a fitting algorithm to get the other one.

To get the unknowns, there are no direct equations we can use. The approach we used was a fitting algorithm based on Matlab function fminsearch. The goal is to find the

best guess of unknown factor and the criteria is the Real reflectance measurement and the reflectance derived by guess value has least different.

Figure 2.4 is an example. In this example, the known factor is R_d and μ_a and we want to find the best fitting μ_s'. The main program will send R_d and μ_a to a subroutine called FitMusp through a Matlab function called "fminsearch", in FitMusp a serial of μ_s' will be selected as a "guess μ_s'" by a certain search strategy. The guess μ_s' and known μ_a will be sent to GetRd subroutine using equation 2.2 to get a "guess R_d". The guess R_d and measured R_d is compared and best matched guess R_d will be found which has least different with measured R_d. Finally the guess μ_s corresponding to the best matched guess R_d will be known as the fitting result.

The program is written in Matlab and it also works for known R_d and μ_s' to get μ_a.

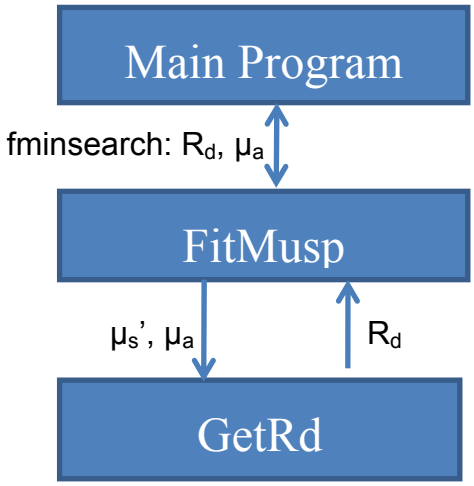

Figure 2.4 Fitting program

2A.3.3 Total reflectance for bacteria-polystyrene sphere phantom

In the bacteria with TBO uptake and polystyrene sphere solution, the reduced scattering coefficient mostly depends on the polystyrene sphere and the absorption coefficient mostly depends on the TBO in the solution. Polystyrene spheres' concentration, size, shape, reflectance index ratio are provided by the manufacture and Mie theory can be used to get the reduced scattering coefficient. However since the concentration in polystyrene sphere stock solution is not accurate (e.g. evaporation

effect), we will use known absorber (TBO solution) to calibrate the polystyrene sphere reduced scattering coefficient; the Mie theory calculation result will only be a reference value.

1 mg/L and 4 mg/L TBO with polystyrene sphere solution was used to as reflectance standard, polystyrene sphere without TBO will be another reflectance standard. The goal of reflectance standard is to calibrate the polystyrene sphere scattering coefficient. The TBO absorption coefficient has been measured using a transmission experiment with OceanOptics spectrometer. Reflectance R_d for the three phantoms has also been measured. In this case, the known factor is R_d and μ_a, using the fitting program μ_s' can be calculated and compared with the Mie theory result. As the scattering coefficient for polystyrene sphere is known, it will be used to get the TBO concentration in the bacteria.

2A.3.4 Photosensitizer uptake measurement for biofilm

To assess the photosensitizer uptake for a biofilm, the biofilm and 80 mg/L TBO was incubated in dark environment for 60 minutes. The biofilm was washed then vortexed vigorously for 60 seconds and washed again. Then suspended bacteria were collected by centrifugation and added to the polystyrene microsphere solution, as for the planktonic bacteria. The optical assessment of TBO uptake was the same as for the planktonic bacteria.

2A.4 Result

In the first step, three standard phantom R_d measurements (using equation 2.3 with white card measurement) were put into the fitting routine together with known absorption coefficient according to the added TBO concentration and measured TBO extinction coefficient. Since we have three groups of data (R_d and μ_a) and only one unknown μ_s', the three groups of data will be put into the fitting program together and the fitting criteria becomes the summation of three different R_d is least.

The scattering coefficient was 49.6 cm^{-1} using the fitting routine with measurement data and the result according to Mie theory with manufacture size information was 51.0 cm^{-1}. The measured reduced scattering coefficient of polystyrene sphere is lower than the value from Mie theory. That means the polystyrene sphere concentration is lower than the manufacture provided value. It might because the polystyrene sphere deposit in the bottom of the solution. Although it was well shaken before using it, we can still see the white polystyrene sphere on the bottom.

Using the measured scattering coefficient for polystyrene sphere and the measured R_d for all bacteria solution, the absorption coefficient of TBO in the bacteria can be calculated as shown figure 2.5

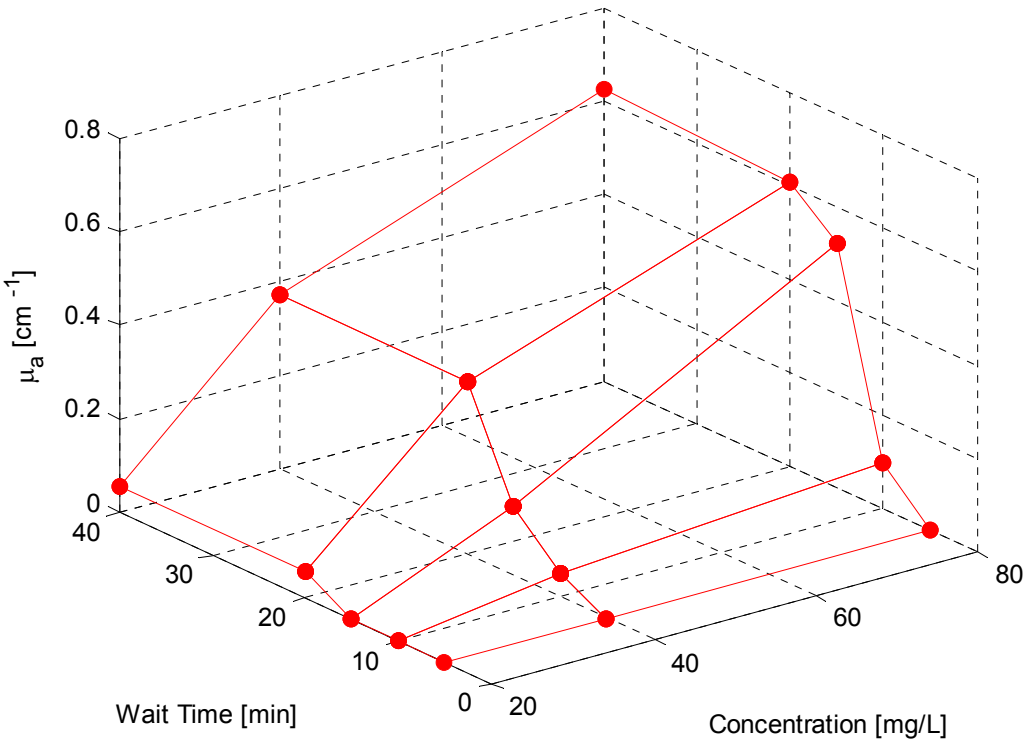

Figure 2.5 absorption coefficients derived from fitting program

From Figure 2.5, we can see the uptake trend with increase of initial TBO concentration and increase of waiting time. Using equation 2.6, μ_a and ε is known, C_{ps}

can be calculated. However, the C_{ps} is actually concentration in the bacteria cells and μ_a is the concentration in the bacteria solution. Bacteria volume is only a very small fraction of volume in the solution. The bacteria size is known and the CFU concentration of bacteria is also measured, the volume fraction can be calculated.

$$\mu_a = \log(10)\varepsilon C_{ps} \text{ [2.6]}$$

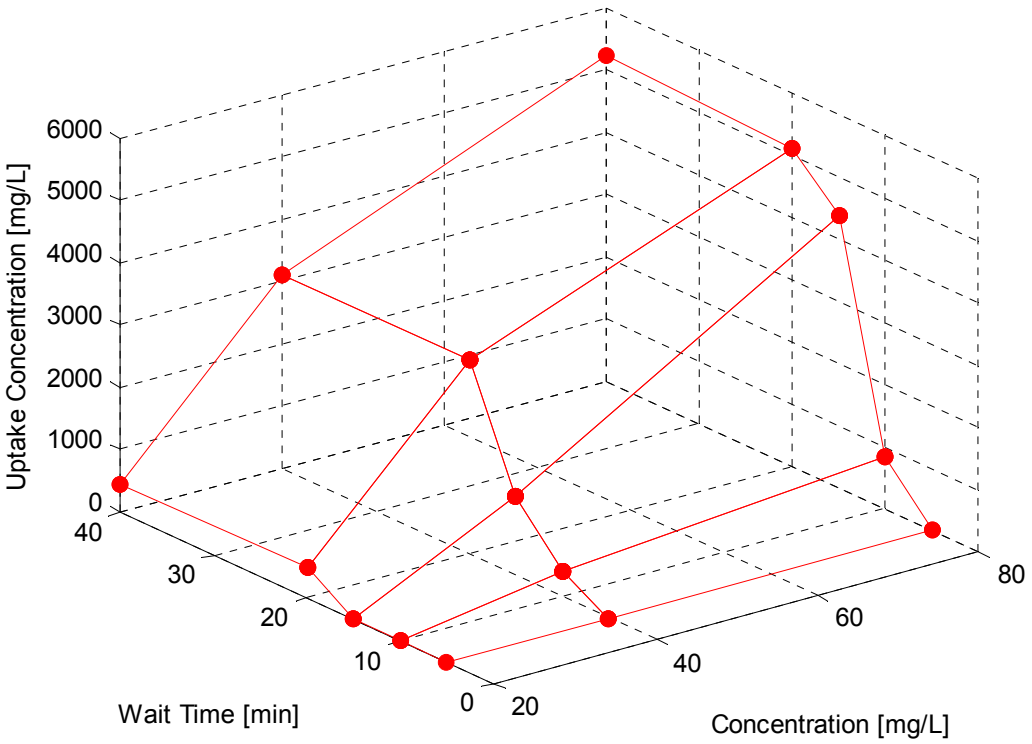

Figure 2.6 uptake concentrations for S. mutans cells

Figure 2.5 shows the final C_{ps} using equation 3.6 and the volume fraction conversion. (Only the bacteria with TBO has high absorption coefficient and the solvent is water which does not have significant absorption) We can see the photosensitizer concentration in the bacteria with different initial PS concentration and waiting time as shown in Figure 2.6.

The biofilm uptake was calculated as 1.1×10^3 mg/L for 80 mg/L initial bath solution using the same reflectance measurement and same fitting program as planktonic state S.mutans.

2A.5 Discussion

TBO uptake by S. mutans cells has relationship with the initial concentration. To show this relationship, Figure 2.7 uses another approach to organize the result of TBO concentration for different initial concentration and waiting time.

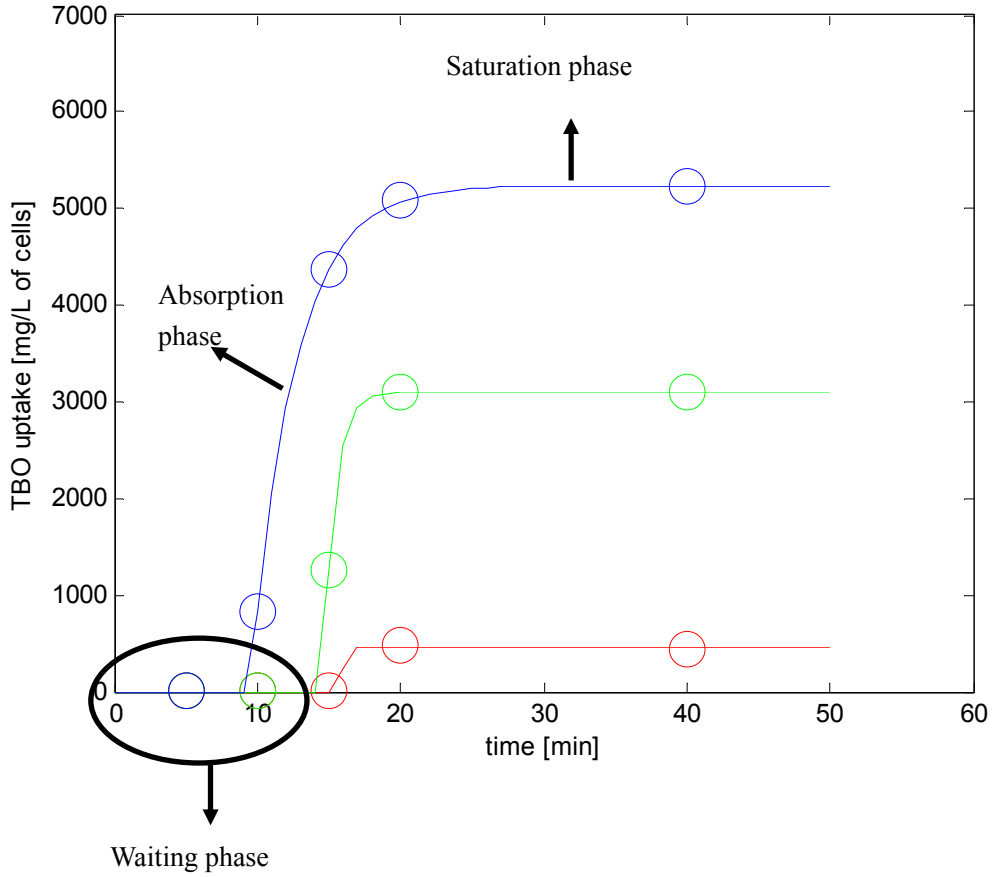

Figure 2.7 TBO uptake vs. time

Red: 20 mg/L, Green: 40 mg/L, Blue: 80 mg/L (TBO initial concentration)

Circles: concentration from reflectance measurement, lines: fitting results

In Figure 2.7, we can see that photosensitizer (TBO) diffusion in the bacteria has three phases: waiting phase, absorption phase and saturation phase. The photosensitizer has to overcome a barrier before it can diffuse into the bacteria cells. The waiting time is inverse proportional to the initial concentration of photosensitizer. After the waiting phase, photosensitizer begins to penetrate the cell wall and deposits into the bacteria

cell. We can this time period as “absorption phase”. The absorption (diffusion) rate of photosensitizer is proportional to the initial concentration of photosensitizer. And after the absorption phase, the concentration of photosensitizer in the bacteria cells won’t increase significantly. We call this time period as “saturation phase”. In the saturation phase, the final photosensitizer concentration is proportional to the initial concentration of photosensitizer.

We can summarize the three phases of photosensitizer concentration as the following equation 2.7

$$C = 0, t < t_w$$
$$C = C_s(1 - e^{-(t-t_w)/\tau}), t > t_w \quad [2.7]$$

In equation 3.7, C is the dynamic photosensitizer concentration in the bacteria cells; t is the current time from photosensitizer added into bacteria solution; t_w is the waiting time in waiting phase; C_s is the final concentration in the saturation phase; τ is relative to the slope of absorption curve.

A Matlab fitting routine based on “fminsearch” is developed to find the best fitting of t_w, C_s and τ for each group of measured photosensitizer time concentration. The solid curve in Figure 2.6 is the fitting results. The results are displayed for three different initial photosensitizer concentrations in Table 2.1

Initial Concentration	t_w (sec)	C_s (mg/L)	τ (sec)
20 mg/L	15.9	464	0.1088
40 mg/L	14.6	3.106	0.8427
80 mg/L	9.5	5.237	3.0570

Table 2.1 Fitting results for PS concentration parameters

For a practical photodynamic therapy protocol, it is a tradeoff to treat the patient in

the absorption phase or in the saturation phase. The absorption phase is earlier, which means patient does not need to wait very long time before the light irradiation. However, in the absorption phase, the photosensitizer concentration in the bacteria cells changes quickly, it is quite difficult to control the photosensitizer concentration.

If the light irradiation is the in the saturation phase, the photosensitizer concentration is well controlled. However, the first problem is patient has to wait longer time; secondly the photosensitizer concentration in the bacteria doesn't has significant change, which means the residue of the photosensitizer will be deposited into the surrounding tissue, when the light irradiate to those region, the surrounding tissue will be damaged as well.

Based on the discussion above, we still recommend clinician to use the absorption phase; a relative low dosage of initial concentration of photosensitizer will make the photosensitizer control easier. For the S. mutans with TBO, we found 40 mg/L is better than the other two cases, according to the photosensitizer diffusion control and the final PDT results.

Chapter 2B

Using a Reflectance-mode Confocal Microscope to Determine Photosensitizer Distribution Profile a Biofilm of Oral Bacteria

Abstract

Reflectance-mode confocal scanning laser microscopy was used to measure the spatial distribution of an absorbing dye that has penetrated an oral bacteria biofilm (S. mutans) grown on hydroxylapatite disc. The dye was Toluidine Blue O (TBO), which is a photosensitizer that is being studied as a means of conducting photodynamic therapy of oral bacterial biofilms. The method quantifies the non-uniform distribution of dye penetration in the biofilm, despite the background light scattering properties of the biofilm. The method yielded the scattering coefficient ($\mu_s \approx 25$ cm^{-1}) and the anisotropy of scattering ($g \approx 0.55$) of a biofilm at 633 nm wavelength. With exposure to an absorbing dye, TBO, the method could document the spatial distribution of the absorption coefficient (μ_a = 20-200 cm^{-1}) after the biofilm absorbed TBO. The experiments showed maximum errors of 10-15% in optical properties. The study showed that TBO penetration into biofilm after a 60 s exposure to solution containing TBO (40 mg/L) achieved a non-uniform distribution of biofilm, with the superficial layers nearly equilibrating with the bathing solutions TBO levels, but the deepest layers approaching a very low level that was below the detection limits (<5 mg/L) of the method.

2B.1 Introduction

The accumulation of photosensitizer (PS), a light-activatable dye, in a target tissue site for the purpose of photodynamic therapy (PDT), a light-activated chemotherapy, is a key factor is planning a PDT treatment [40-43]. Monitoring PS uptake during the PDT is a topic of clinical interest [44-46]. In this report, we report on the use of an optical method, reflectance-mode confocal scanning laser microscopy, to monitor the uptake of PS into a biofilm of an oral bacteria (*Streptococcus mutans*) grown on a hydroxylapatite disc.

Fluorescence measurement has been widely used to determine the kinetics of drug uptake, including photosensitizers [47-49]. However quantification of PS with a fluorescence measurement is difficult. The quantum yield is usually an unknown factor that is affected by the environment [61]. If the quantum yield is small, the fluorescence signal will be weak and the measurement accuracy will be poor. The fluorescence signal also depends on the optical properties (absorption and scattering at wavelengths for both excitation and fluorescent emission) of the tissue in the light path, which are usually unknown [62, 63].

Optical absorption measurements have been used to estimate photosensitizer concentration in tissues [64-66]. Most of the work assumes that the photosensitizer is homogeneously distributed in the measurement region. But the uptake of topically applied PS by a biofilm of oral bacteria cannot be assumed to be uniform. In this study, an optical method of measurement based on optical absorption by PS is presented, which accounts for background scattering by the tissue.

2B.2 Theory

2B.2.1 Reflectivity and Attenuation in a Confocal Signal

The confocal signal of reflected optical intensity decreases as the focus of the microscope is scanned down into the medium (biofilm), falling as an exponential decay,

$$R(z) = \rho e^{-\mu z} \quad [2.8]$$

where R(z) [dimensionless] is the collected confocal signal recorded at the depth of z. Figure 1 illustrates a generic measurement, where ρ [dimensionless] is the local reflectivity and μ [cm^{-1}] is the attenuation coefficient of the biofilm. The attenuation coefficient μ can be expressed as:

$$\mu(g, \mu_s, \mu_a, NA) = \left(\mu_s a(g) + \mu_a\right)\ 2G(g, NA) \quad [2.9]$$

In this equation, μ_s [cm^{-1}] is optical scattering coefficient, g [dimensionless] is the anisotropy of scattering, and μ_a is the optical absorption coefficient. The factor G is a geometry factor that describes the average pathlength of photons as they travel to the focal volume at depth z, which depends on the numerical aperture (NA) of the objective lens and only slightly depends on g. The value of G was calculated to be ~1.37 for a 0.90 NA lens, with only a slight dependence on g. The factor 2 accounts for the photon path into and out of the biofilm. The factor $a(g)$ accounts for how forward-directed light will still reach the focus despite scattering. As the anisotropy of scattering, g, becomes close to 1, which is the case for very forward-directed scattering, the value of $a(g)$ goes to zero because scattering does not prevent the photon from reaching the focus. When scattering is isotropic, $g \approx 0$, then $a = 1$ and scattering is optically effective in preventing photons from reaching the focus. The behavior of $a(g)$ has been explored by Monte Carlo simulations [79-81]:

$$a(g) = 1 - e^{-(1-g)^b / K} \quad [2.10]$$

where b = 0.6651 and K = 0.1555.

The reflectivity ρ can be expressed as:

$$\rho(\mu_s, NA, g) = \mu_s L_f b(NA, g) \quad [2.11]$$

where L_f is the axial distance extending over the confocal volume within which detectable scattering occurs. The product $\mu_s L_f$ is the fraction of light reaching the focal volume that is scattered by the focal volume. The factor b(NA,g) specifies the fraction of scattered photons that would successfully return to the objective lens if there were no attenuation induced by scattering or absorption events. Hence, b(NA,g) depends on the numerical aperture (NA) of the collection lens and the scattering function of the biofilm in the confocal volume, p(θ) [sr^{-1}]:

$$b(NA, g) = \frac{\int_{\pi - \arcsin(NA)}^{\pi} p(\theta)\ 2\pi \sin(\theta) d\theta}{\int_{0}^{\pi} p(\theta)\ 2\pi \sin(\theta) d\theta} \quad [2.12]$$

where p(θ) is the scattering function, and θ is the angle of photon deflection by the scattering event. The p(θ) used here is the Henyey-Greenstein function [67], which has been shown to be a good approximation of the scattering by tissue [82]. The Henyey-Greenstein p(θ)is uniquely specified by the anisotropy g, hence b(NA,g) is specified by the anisotropy of scattering.

Before adding PS to the biofilm, the background μ_a of the biofilm was negligibly small relative to the μ_s. Hence, Eq. 2.10 could use experimental measurements of ρ and μ to specify the background μ_s and g of the biofilm. After uptake of PS by the biofilm, the μ_a was appreciably increased but the μ_s and g remained the same. Since μ_s and g were known, Eq. 2.10 could specify the μ_a due to added PS.

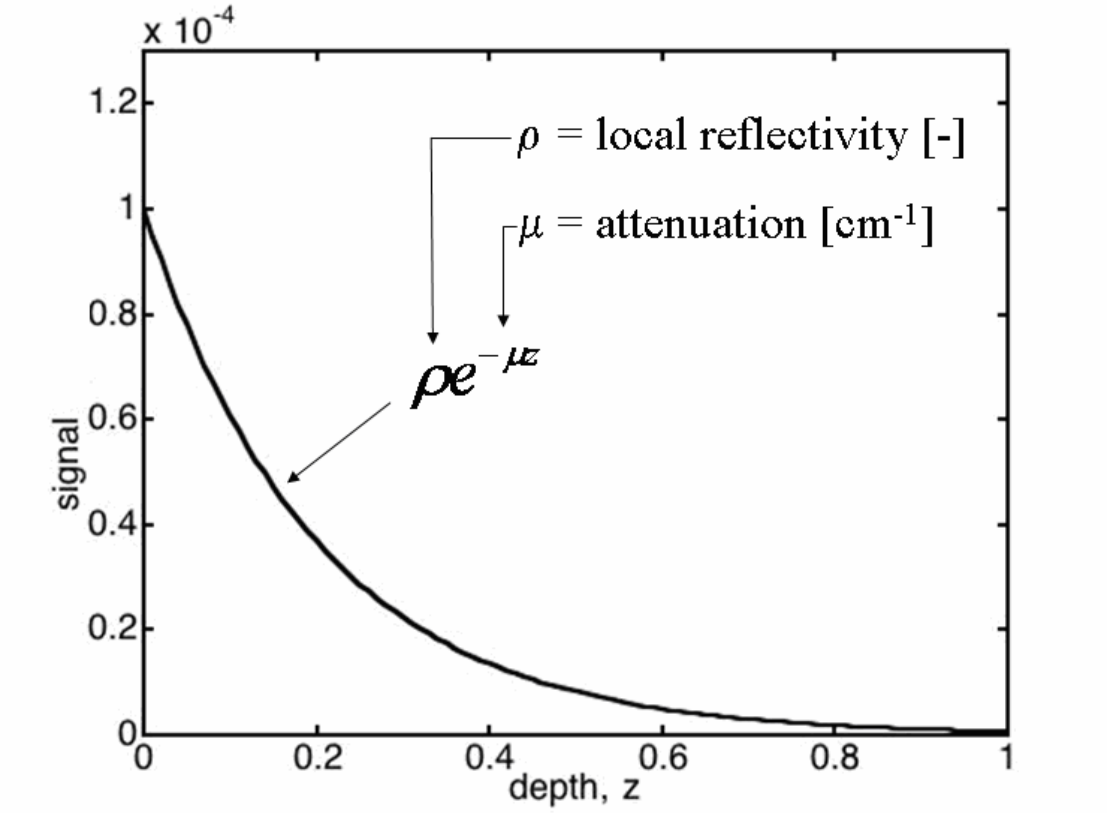

Figure 2.8 Confocal reflectance signal R(z) vs. depth z. The ρ [dimensionless] and μ [cm^{-1}] are the local reflectivity and attenuation coefficient, respectively.

2B.2.2 Heterogeneous Media

A biofilm is not homogenous, and the PS uptake can not be assumed to be uniform. Equation 1 can be restated to account for a heterogeneous biofilm:

$$R(z) = \rho(z) e^{-\int_0^z [\mu_s(z)a + \mu_a(z)]2G dz} \qquad [2.13]$$

In this expression, the optical depth over which photons travel in/out of the biofilm is proportional to the integral of $(\mu_s a + \mu_a)2G$ from the surface to the depth of the focal volume, z. If one takes the ratio of the measurement S before and after exposing the biofilm to dye, the addition attenuation is due to dye uptake:

$$\frac{R_{afterDye}(z)}{R_{beforeDye}(z)} = e^{-2G\int_0^z \mu_a(z)dz} \qquad [2.14]$$

The depth profile of absorption due to dye, $\mu_a(z)$ can be deduced by stepwise evaluating the ratio first at the surface layer and sequentially at incremental depths. The final $\mu_a(z)$ can be converted into concentration by:

$$C(z) = \frac{\mu_a(z)\ MW}{\varepsilon\ \ln(10)} \quad [2.15]$$

where MW is the molecular weight [g/mole] of the dye and ε is the extinction coefficient [$cm^{-1}\ M^{-1}$] of the dye.

2B.3 Materials and Methods

2B.3.1 Confocal System

The reflectance mode confocal system is shown in Fig. 2.9. A HeNe laser (Melles Griot, 25 LHP, 632.8nm, 5mW) was the light source. The laser passed through a beam expander to yield a broader collimated beam (~1 cm dia.), then reflected off a pair of scanning galvanometric mirrors (Nutfield Technologies) and a pair of relay lenses for the lateral x-y scanning. The collimated beam at this point was entering the objective lens at varying angles, which caused the focus to scan laterally in x and y. The objective lens (Newport Inc., water-dripping lens, NA 0.90, 60x magnification) was coupled to the test sample (biofilm or phantom) by water. The reflected light from the focal volume within the test sample was returned through the scanning system, through the beam splitter and through a pinhole (50-μm dia., corresponding to the Airy diameter of the Gaussian beam radial profile) to reach a photomultiplier tube (PMT) detector (Hamamatsu H5773-01). The phantom was placed on a piezo-controlled stage that moved the sample along the z axis to focus the laser at different depths.

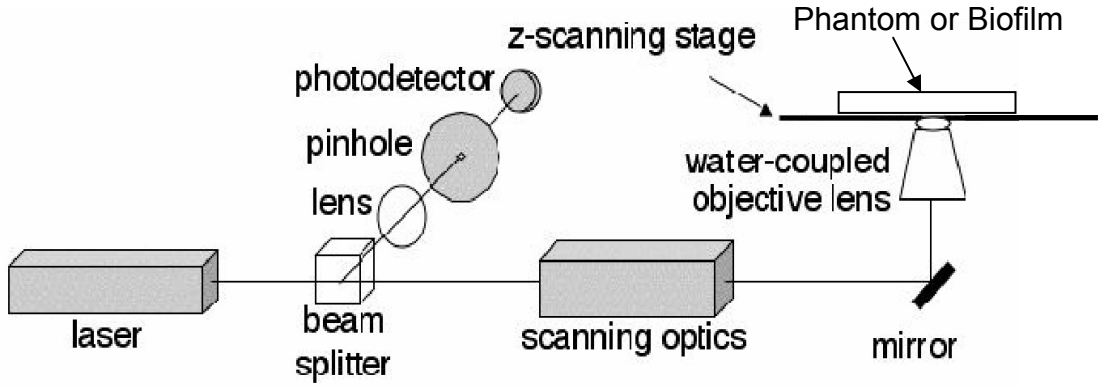

Figure 2.9 Reflectance-mode confocal scanning laser microscope.

A test sample was placed on the microscope stage and the confocal microscope was scanned through the phantom, acquiring a 512x512 x-y image at each z step along the z axis. The choice of step number depended on where the air-solution interface was located and where the signal dropped into the noise floor. Typically, 35-70 3-5-μm steps were taken along the z axis. The reflected signal was recorded in Volts by a data acquisition card (National Instruments). A measurement, V_{og} [Volts], of an oil/glass interface was used to calibration the system. The reflectance signal recorded,V(z) [Volts], was converted to reflectance R [dimensionless] by the expression:

$$R(z) = \frac{V(z)}{V_{og}} R_{og} \quad [2.16]$$

where the reflectance of an oil/glass interface is $R_{og} = ((1.46\text{-}1.52)/(1.46+1.52))^2 = 4.05\text{x}10^{-4}$.

2B.3.2 Phantom measurements

Polystyrene spheres in solution (diameter = 0.1μm, stock concentration 10% w/w, Duke Scientific Inc., refractive index n = 1.59) were used as scatterers. The photosensitizing dye Toluidine Blue O (TBO made from powder with distilled water, stock solution 1683 mg/L, Sigma Inc.) was used as absorber. The polystyrene sphere

solution was sonicated before mixing to avoid aggregation. The volume fraction of spheres in the solution was varied over 2, 4, 6 and 8%.

The extinction coefficient ε of TBO was measured to be 3.20×10^4 [$cm^{-1}M^{-1}$] using a transmission experiment with an optical fiber spectrometer (OceanOptics Inc.). The wavelength was 632.8 nm. The scattering coefficient of polystyrene sphere stock solution was estimated to be 107.5 cm^{-1} using Mie theory [83].

Polystyrene spheres in water were mixed at different concentrations with no added absorber to create *scattering-only* phantoms. Spheres at each of two scatterer concentrations (μ_s = 59 and 236 cm^{-1}) were prepared with different amounts of added absorber (TBO). When sufficient TBO was added, the solution became an *absorption-dominated* phantom. Groups 1-4 were the *absorption-dominated* cases ($\mu_a \geq \mu_s$) and groups 5-8 were the *scattering-dominated* cases ($\mu_s \geq \mu_a$). All the mixed solutions were shaken and sonicated to achieve good mixing, then a 1 ml volume was placed into the phantom holder (Fig. 2.10) for measurement by the confocal system. Phantoms were 1 ml in volume. For imaging phantoms, the axial step size was 5 μm and the step number was 35-50.

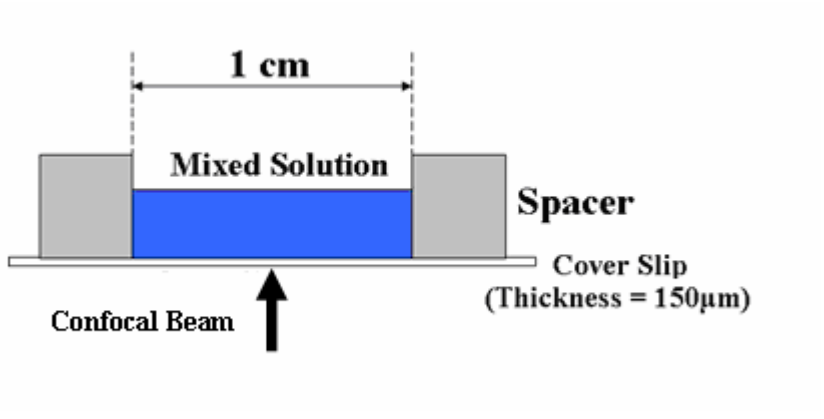

Figure 2.10 Holder for phantoms made with polystyrene microspheres as scatterer and TBO photosensitizer as absorber.

2B.3.3 Biofilm culture protocol

Streptococcus mutans was cultured using the following protocol.

1. *Streptococcus mutans* ATCC 25175 was streaked on a BHI plate and incubated at 37°C in 5% CO_2 for 2 days without agitation.
2. 1ml of overnight culture of Streptococcus mutans ATCC 25175 was added to 2 ml BHI with a hydroxylapatite disc (0.5 cm in diameter and 0.05 cm to 0.06 cm thickness, from HiMed Inc.; alternatively, from Old Bethpage Inc., NY) in a 24-well titer plate.
3. After supplementation with sucrose (final concentration was 0.2 M), the plate was incubated at 37°C in 5% CO_2 for 3 days without agitation.

2B.3.4 Imaging the biofilm

The biofilm was imaged with the confocal microscope twice, once before and once after exposure to dye (or water as a control). The two images needed to be co-registered for comparison, therefore the registration method was carefully considered. Figure 2.11 shows the biofilm holder for the confocal microscope. Two stacks of cover slips (3 pieces in each stack) were placed on top of a glass slide to serve as spacers. Glue was put at the edge of the cover slip stack to affix the cover slips to the glass slide. The hydroxyapatite (HA) disc was placed on top of the two spacers creating a chamber approximately 450 μm thick x 3 mm x 10 mm in dimension. The biofilm surface was on the bottom of the HA disc oriented toward the chamber. During the experiment, either TBO solution or water filled the chamber for exposure to the biofilm.

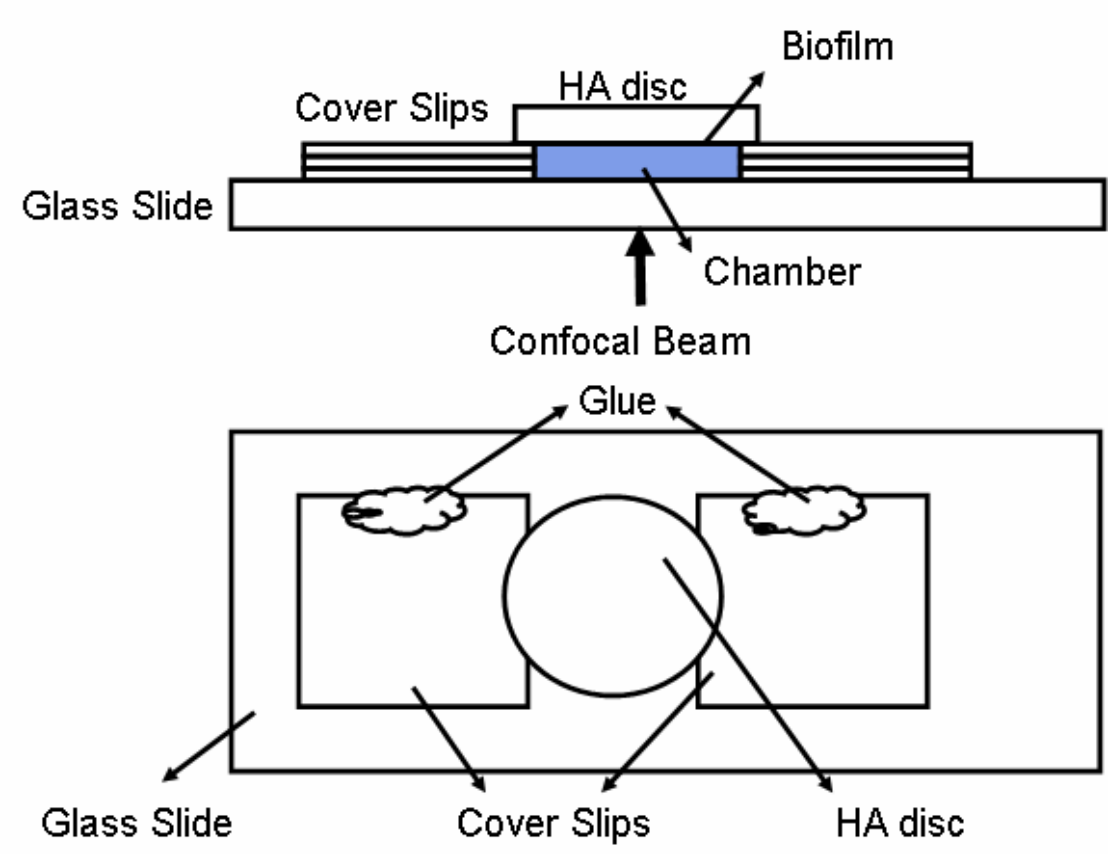

Figure 2.11 Biofilm holder for confocal microscope imaging. The TBO solution is introduced region labeled "chamber" which allows absorption of TBO by biofilm. After exposure for 20 min, the residual TBO is washed out. Images are acquired before exposure and after exposure and washout.

Figure 2.12 shows the protocol for exposing biofilm to TBO and taking co-registered images. First, water was placed in the chamber to pre-equilibrate the biofilm, and a set of images was acquired. Second, a solution of TBO (40 mg/L) was placed in the chamber for 30 min in a dark environment to allow TBO to penetrate the biofilm. Third, the chamber was washed with water to remove the TBO in the chamber. The biofilm retained the TBO that had penetrated into the biofilm. A second set of images was acquired. For the images of biofilm, the axial step size was 3 μm and the step number was 70.

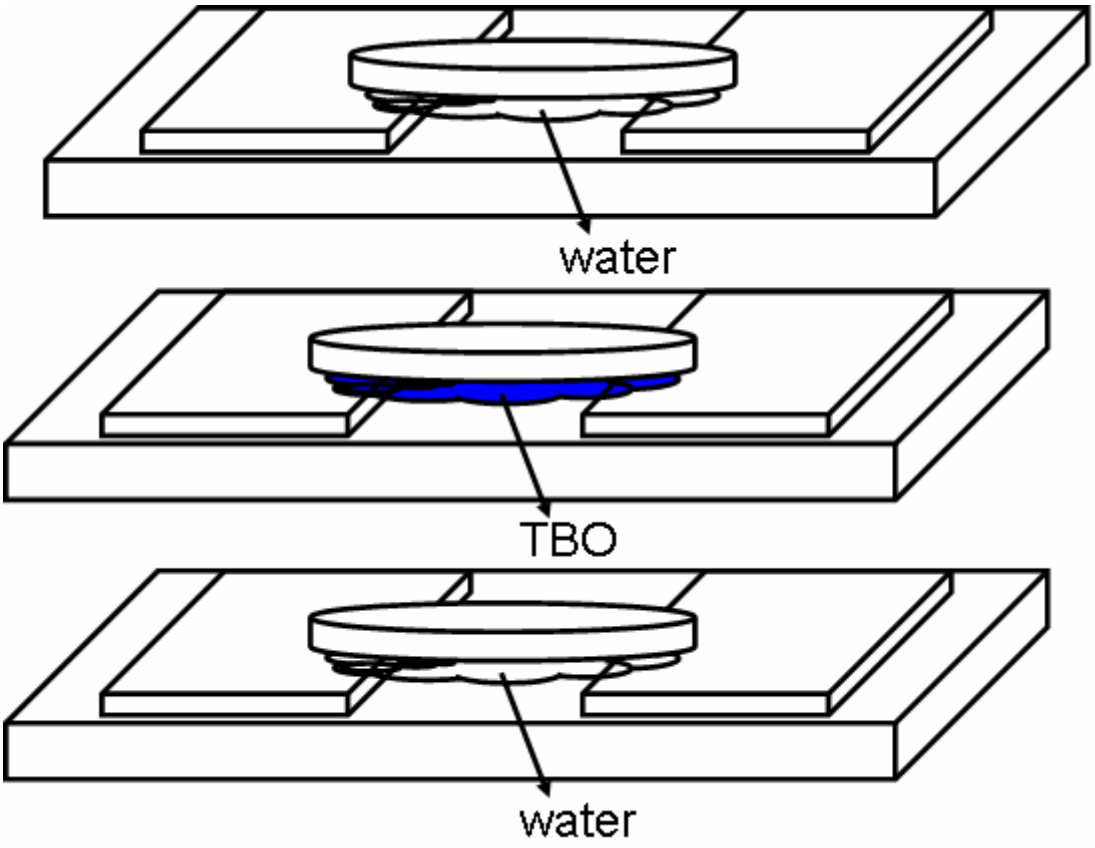

Figure 2.12 Protocol for exposure of biofilm to TBO. (a) Water in chamber contacts biofilm. (b) TBO solution introduced into chamber for absorption by biofilm. (c) Water flushes residual TBO from chamber after TBO uptake by biofilm.

2B.4 Results

2B.4.1 Phantom Results

Figure 2.13a is a typical confocal side view image, showing an R(x,z) image at one position y. The phantom had 2% volume fraction of polystyrene spheres. At each x position, the R(z) along a vertical line shows the axial decay of reflectance. Figure 2.13b shows the R(z) axial profile corresponding to the vertical line in Figure 2.13a.

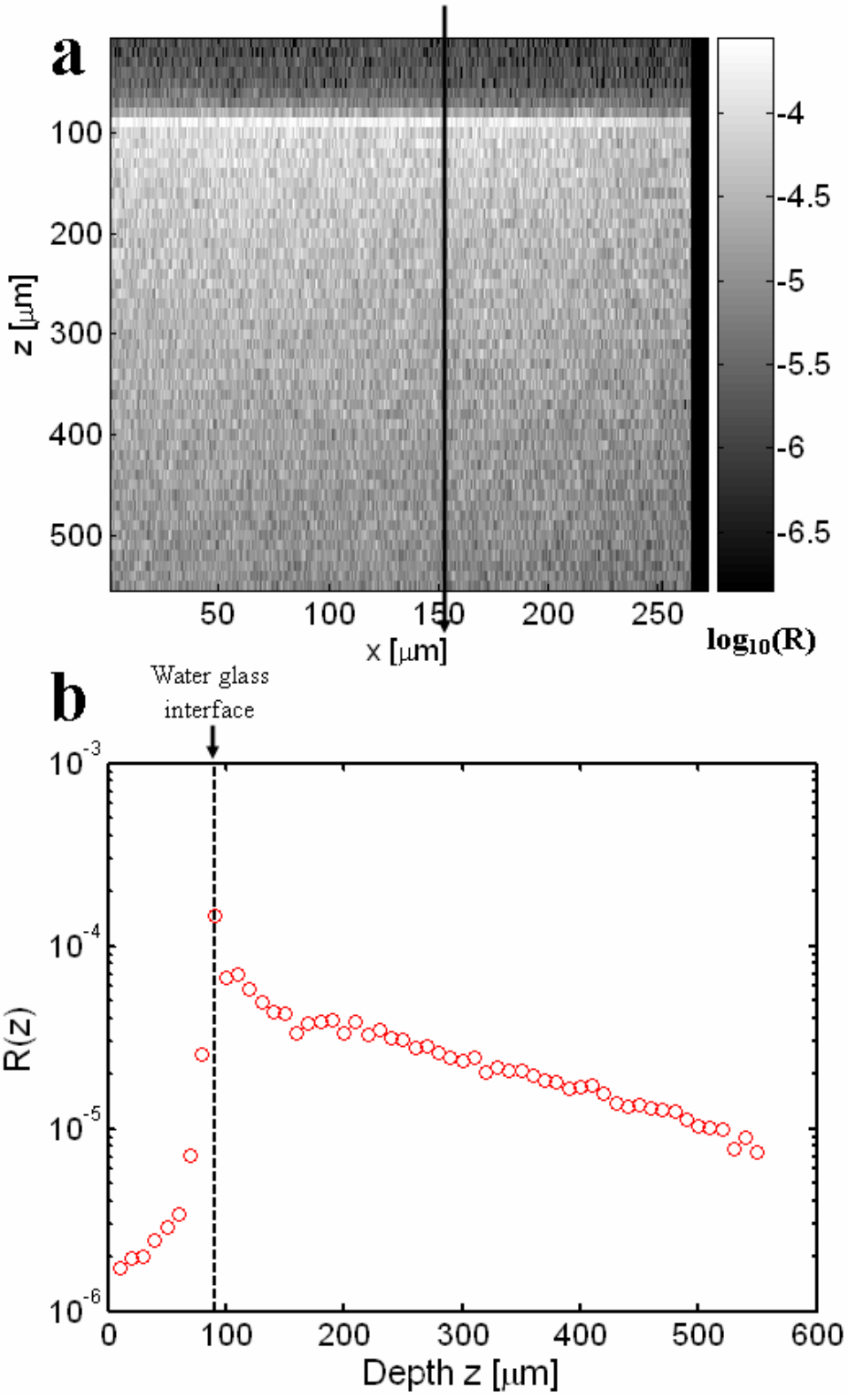

Figure 2.13 Phantom experiments. (a) Side view (x-z) of reflectance confocal image for a homogeneous phantom. (b) Confocal signal R(z) as a function of depth z along the vertical black arrow in Fig. 6a. A dashed line indicates the water/biofilm surface.

For each phantom image, the R(z) signal was randomly selected for different positions in the confocal image stack. The average of 100 R(z) profiles was calculated from a 10 by 10 pixel neighborhood of x-y positions. This average R(z) was fitted with the equation 1 to yield the values of ρ and μ. This procedure was repeated on 10 sites within the phantom and the mean and standard deviation of the 10 μ values are plotted in Figs. 2.14a and 2.14b. Figure 2.14a shows *scattering–only* case, both the data for μ versus added scatterer and the predicted behavior (dashed line) based on the stock solutions and using Mie theory to predict the scattering of the microspheres, according to their size, refraction index and concentration at the 632.8 nm wavelength. The error of the prediction was less than 10%. Figure 2.14b shows the data and predicted behavior (dashed lines) μ versus added absorber, for both the *absorber-dominated* case (μ_s = 21.5 cm^{-1}) and *scatter-dominated* case (μ_s = 86.8 cm^{-1}). The error of the prediction was less than 15%.

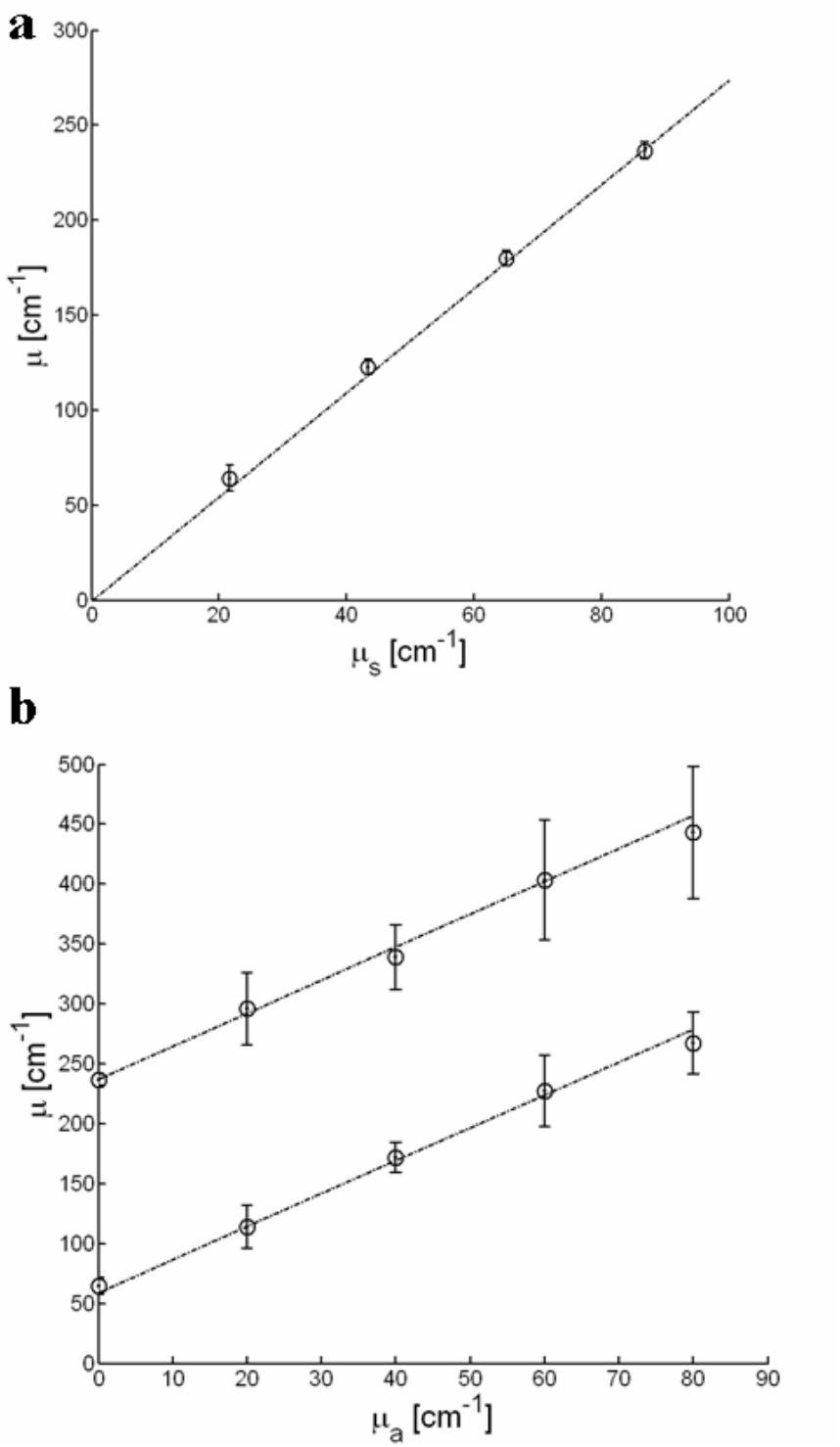

Figure 2.14 Phantom results, showing predicted μ versus added scatterer only (μ_s, in Fig. 2.14a) and scatterer with added TBO absorber (μ_a, with μ_s = 21.5 cm^{-1} (lower curve) and 86.8 cm^{-1} (upper curve), in Fig. 2.14b). Measurements (circles) and analysis model (dashed line), which is $\mu = (\mu_s a(g) + \mu_a)2G$.

Figure 2.15 shows the analysis grid of experimental μ and ρ values for particular μ_s and g values, and the experimental data for the *scattering-only* phantom (μ_a = 0) (circles) and the phantoms with added TBO absorber (squares). The experiment was repeated 3 times for each phantom. The g value for 0.1-μm dia. spheres ($n_{particle}$ = 1.59, n_{medium} = 1.33) at 632.8 nm wavelength is 0.0755, which corresponds to an $a(g)$ of 0.9978, which is nearly unity. The, μ_s was specified:

$$\mu_s = \frac{\mu}{2aG} \quad [2.17]$$

where the factor 2aG equals (2)(0.9978)(1.37) = 2.734. This figure illustrates the relationship between experimental observations and the underlying optical properties of the test sample.

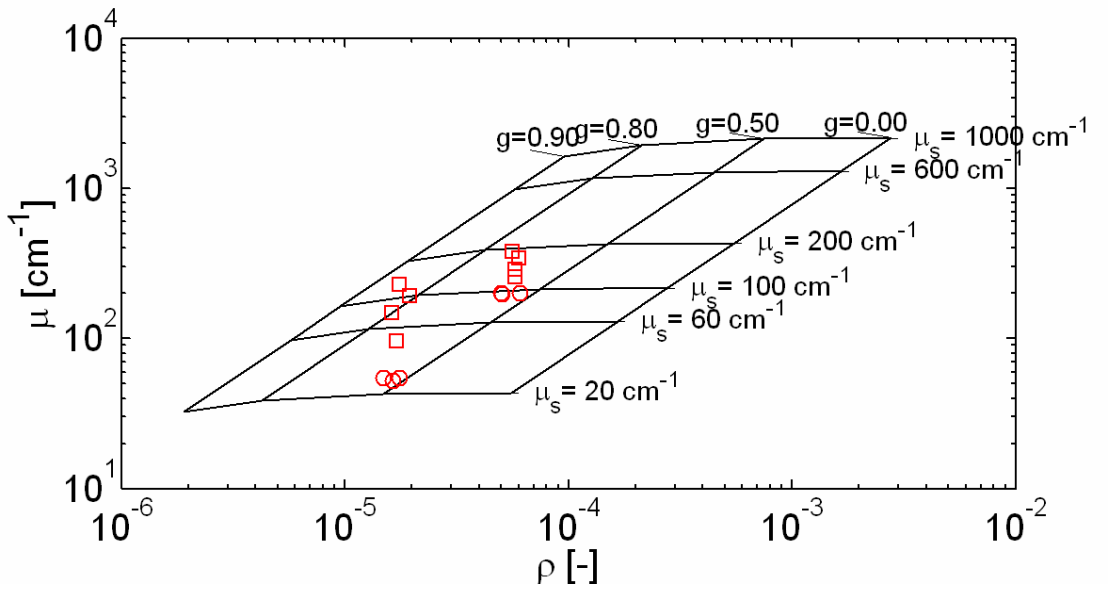

Figure 2.15 Analysis grid, converting experimental measurements (ρ, μ) to optical properties (μ_s, g). Scattering only phantoms (circles) and phantoms with added TBO absorber (squares) are shown. Diamonds show measurements on biofilm.

2B.4.2 Biofilm results

Figure 2.16 shows side-view confocal microscope images of the $\log_{10}(R)$ for a biofilm before exposure to TBO (Fig. 2.16a) and after exposure to TBO with subsequent washout of excess TBO in the chamber (Fig. 2.16b). There is little difference between these two figures. Figure 2.16c shows the difference image, $\Delta(\log_{10}(R)) = \log_{10}(R_{berore.TBO}) - \log_{10}(R_{after.TBO})$, which indicates there are differences which are strongest at the deepest depths where the incremental effects of TBO absorption at each incremental depth have integrated to yield the strongest total effect.

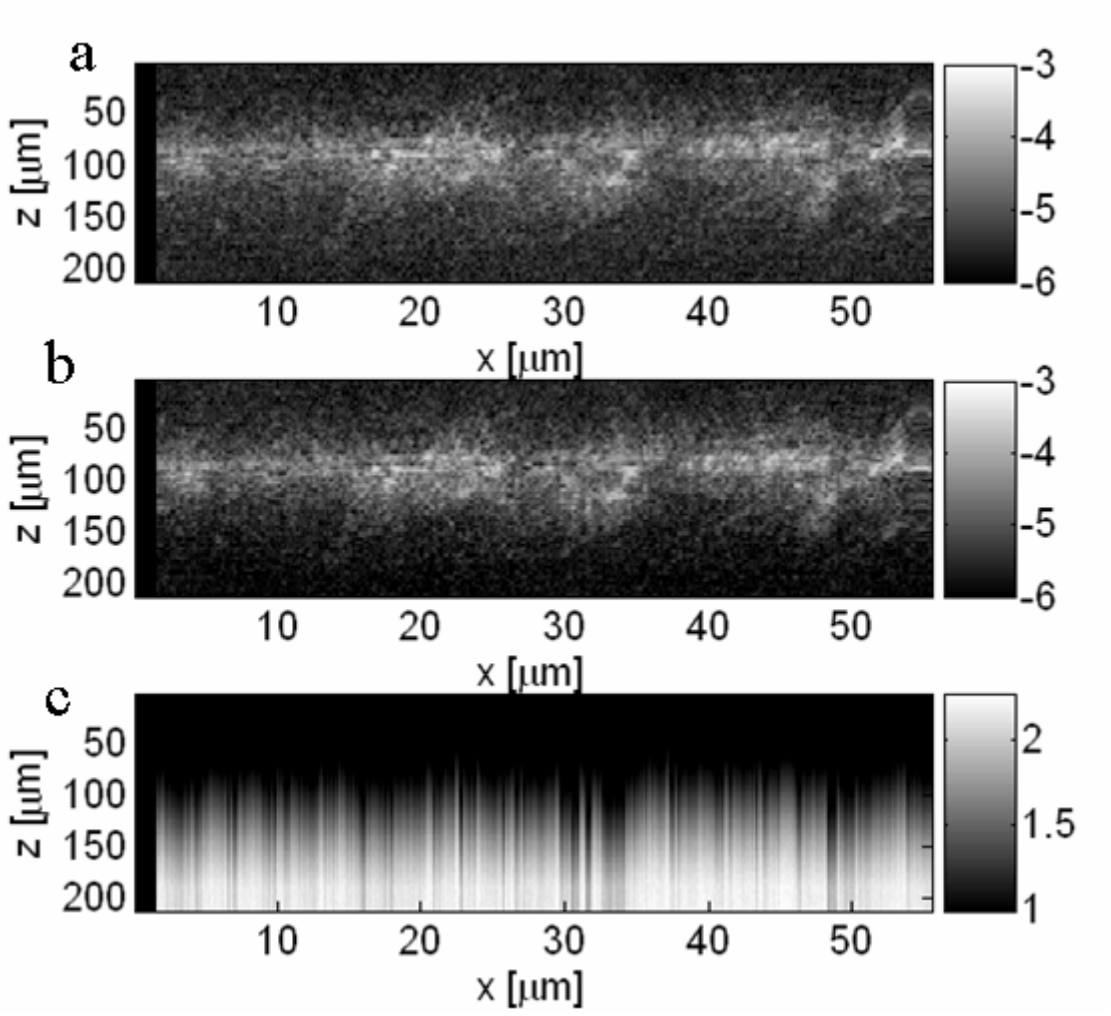

Figure 2.16 Biofilm images before and after exposure to TBO, plotting $\log_{10}(R)$. (a) Before TBO. (b) After TBO. There is little discernible difference in these images. (c) Difference image, $\log_{10}(R_{before}) - \log10(R_{after})$, shows the effect of absorbed TBO.

Figure 2.17a shows the average confocal signal R(z) in one 10 by 10 x-y neighborhood of pixels, for the biofilm before and after TBO exposure that was shown in Fig. 2.6. Circles correspond to the biofilm before adding TBO and the triangles correspond to biofilm after adding TBO. In the range z = 0-80 μm, the two signals have little significant difference, because this is the chamber outside the biofilm. For z = 80-210 μm, the reflectance signal is from the biofilm, and the reflectance before adding TBO was larger than the signal after adding TBO. After taking up TBO, the biofilm was more absorbing and the reflectance dropped.

Figure 2.17b shows the ratio of $R_{after.TBO}/R_{before.TBO}$. The ratio is unity in the chamber outside the biofilm, and then drops with increasing depth z within the biofilm. Also shown are a series of lines that indicate the expected exponential decay of the ratio if the TBO was uniformly distributed in the biofilm. The curves for TBO concentrations of 8, 16, 24, 32, 40 mg/L are shown. Note that the ratio for the biofilm initially falls exponentially as if the TBO concentration was 32 mg/L, which is close to the 40 mg/L solution that was used. But at deeper depths the data departs from this curve for uniform TBO, as if there were less TBO.

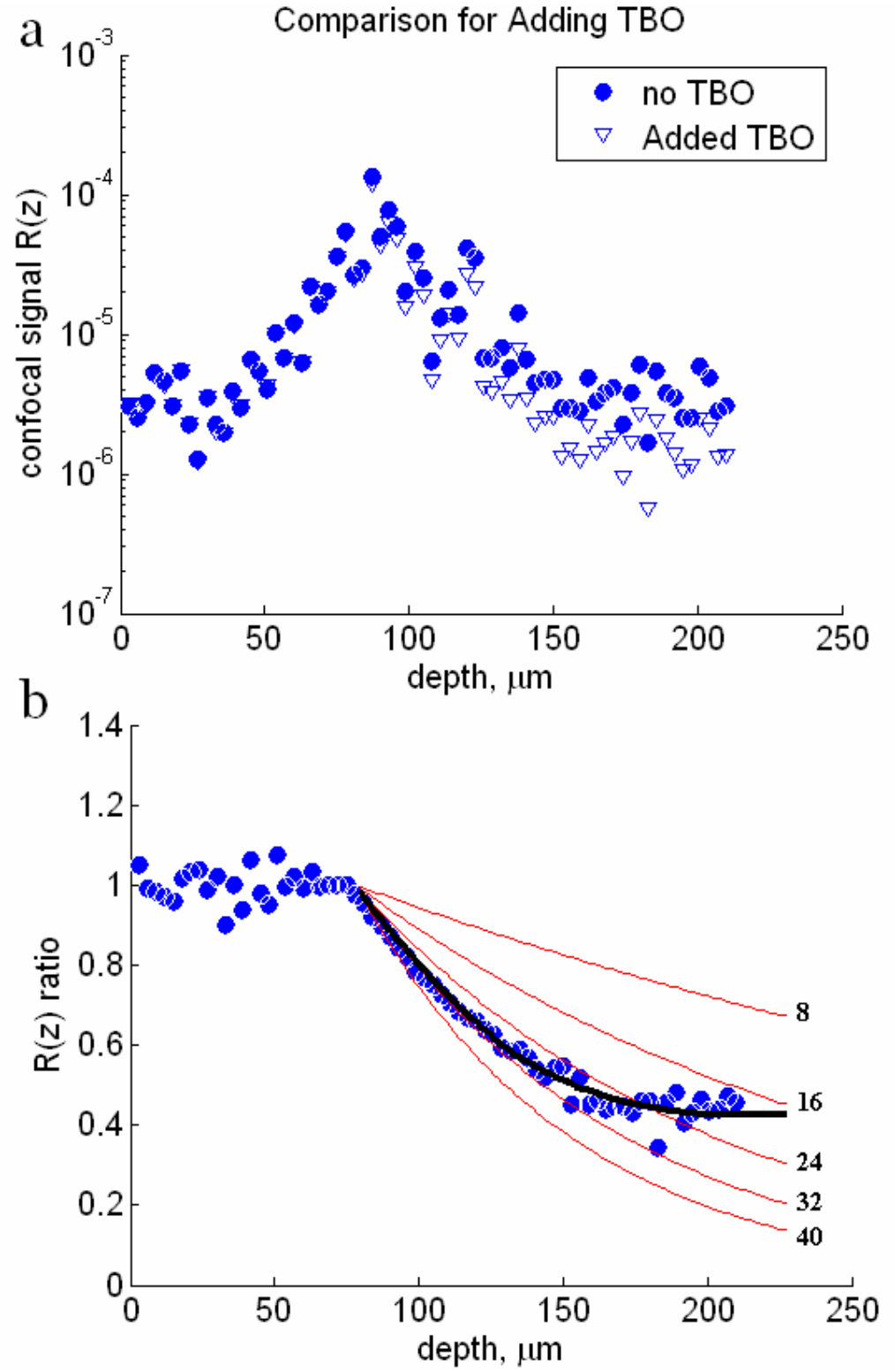

Figure 2.17, Effect of TBO absorber in biofilm on the confocal reflectance signal. (a) R(z) signal before and after TBO uptake. (b) The ratio $R(z)_{after}/R(z)_{before}$. The family of curves show the expected behavior for homogenous absorber in the biofilm. The experimental data initially falls as if the TBO concentration was 32 mg/L, but at deeper depths the curve departs from the ideal curve, indicating less TBO deeper in the biofilm. The black line through the experimental data is the prediction based on

the TBO concentration profile versus depth shown in Fig. 2.18.

Figure 2.18 shows the concentration of TBO as a function of depth based on the ratio in Fig. 2.16b using the method described in Eqs. 2.13 and 2.14. The residual TBO concentration in the chamber was only about <5 mg/L, likely due to slight leakage of TBO from the biofilm into the chamber. The TBO concentration within the biofilm was close to 40 mg/L near the surface of the biofilm and dropped to <5 mg/L (the approximate limit of detection, given the variability of the signal) at about 100 μm below the biofilm surface. Figure 2.19 shows an image depicting the TBO concentration in the biofilm, with brighter gray color indicating more TBO. There is more TBO in the superficial layers of the biofilm than in deeper depths. The surface is quite rough, consistent with the rough surface of the biofilm.

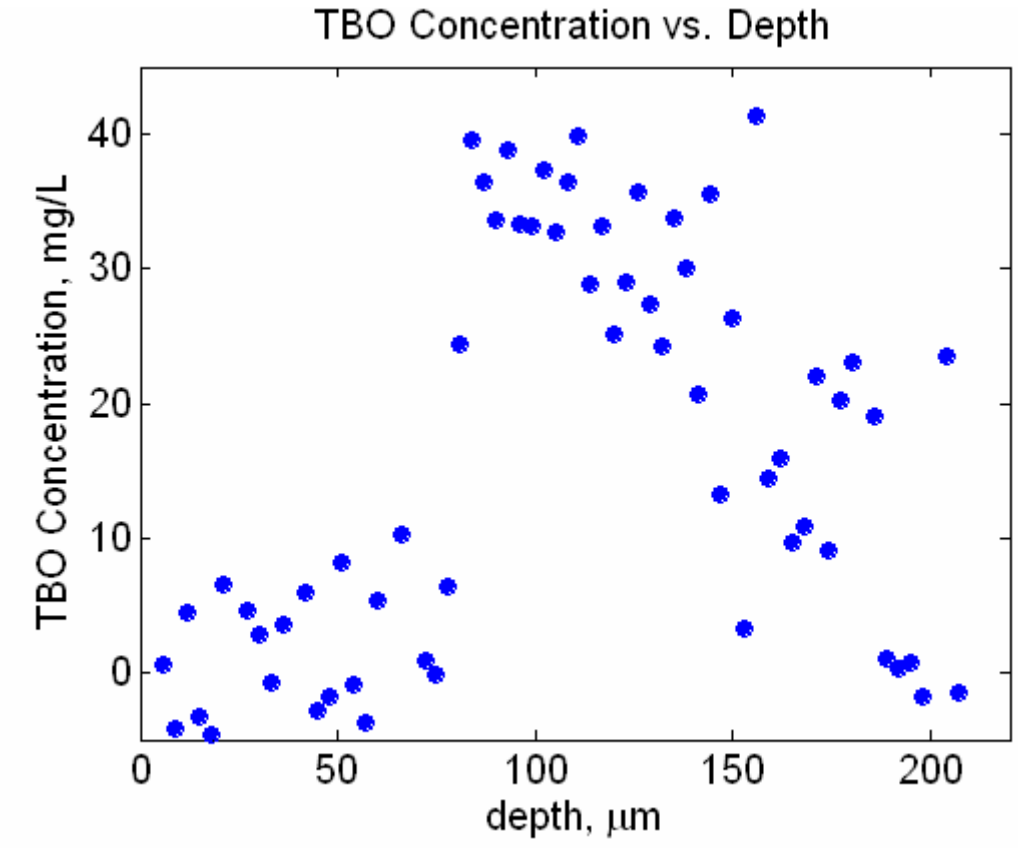

Figure 2.18 TBO concentration profile versus depth. The biofilm surface is at z ≈ 80 μm, showing about 35-40 mg/L concentration, which matches the 40 mg/L solution in the chamber that bathed the biofilm. The TBO concentration drops to <5 mg/L at about 120 μm below the surface.

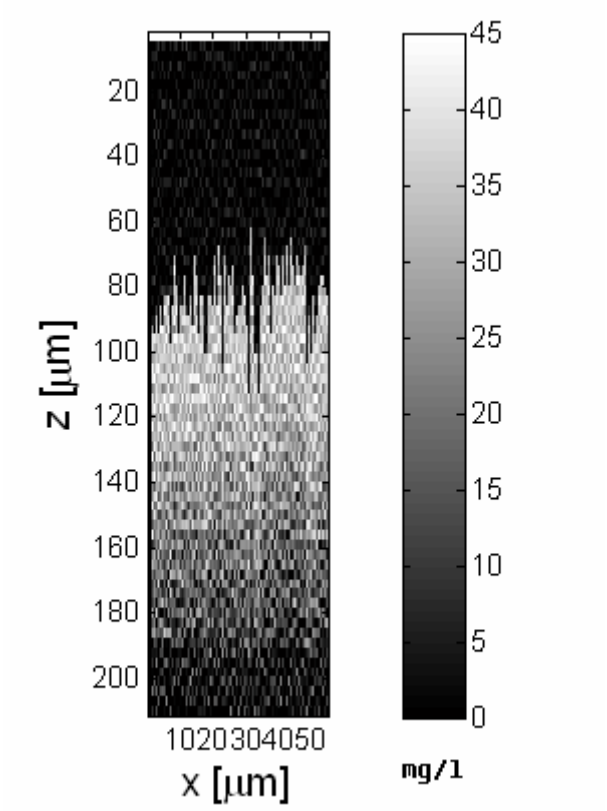

Figure 2.19 Image of TBO concentration distribution, C(x,z) [mg/L], in a bacterial biofilm.

2B.5 DISCUSSION

One of the main sources of inaccuracy during the calibration was the aggregation of TBO-polystyrene spheres in the solution. Several steps were taken to eliminate the aggregation such as sonicating the polystyrene spheres, and mixing the polystyrene sphere and TBO at a warm temperature. However, such aggregation could not be totally avoided. The aggregation was greater for higher concentrations of polystyrene

sphere and TBO. This is a possible reason that the larger standard deviation for the higher scattering coefficient.

Another issue which affects the results is the start point and end point of the exponential curve in confocal signal S(z) to be fitted by Eq. 2.8 to yield ρ and μ. In the region near the front surface of the phantom, the signal was affected by reflectance from the water/glass interface. Therefore, around 10~15 μm of S(z) (around 2~3 points) were ignored in the fitting.

Previously, researchers have usually used two methods to estimate photosensitizer uptake. The first method is fluorescence [84], [85] and [79]. Fluorescence methods can specify the spatial variation of the photosensitizer but the estimate of the photosensitizer concentration is not accurate. The reasons are (1) fluorescence measurement depends on quantum efficiency which is environmental dependent and difficult to measure, (2) incident light and fluorescence light are at different wavelengths, and the optical model for delivery of excitation light and collection of fluorescence is a bit complicated, especially for a heterogeneous medium such as biofilm. The second method is to break the biofilm and measure the optical density to determine the biofilm photosensitizer uptake.

This report shows that the concentration of photosensitizer (TBO) is not homogenously distributed in the biofilm. This method can not give any position information about photosensitizer uptake. Depth information is very important in planning a PDT therapy because although the average concentration is enough for the PDT effect, the deeper layers may not have enough photosensitizer, which results in incomplete treatment and regrowth of bacteria.

Another difficulty of the method using the reflectance confocal measurement is image registration for the two images, one before and one after TBO exposure. The confocal signal must be exactly in the same position before and after TBO exposure. In the method section, a method to accomplish image registration was presented. Sometimes this method still fails if there is slight movement during the experiment process (adding/removing TBO). An alternative method for image registration is to make a mark in the biofilm, perhaps using the sharp edge of a blade, to facilitate post registration the two images.

In summary, an optical method for measuring photosensitizing dye uptake by a bacterial biofilm was presented that is based on images acquired using a reflectance-model confocal laser scanning microscope. The method yielded the scattering coefficient ($\mu_s \approx 25$ cm^{-1}) and the anisotropy of scattering ($g \approx 0.55$) of a biofilm. With exposure to an absorbing dye, TBO, the method could document the spatial distribution of the absorption coefficient (μ_a = 20-200 cm^{-1}) after the biofilm absorbed TBO. The experiments showed maximum errors of 10-15% in optical properties.

Chapter 3
Light Source Calibration for Effective PDT Dosage

Abstract

A tungsten filament was used as PDT light source. To determine the light energy efficacy of PDT and to compare the dosage result with other groups (using other light source), the tungsten filament was calibrated for effective PDT dosage at a certain wavelength (633nm). The effective PDT dosage result was 285.4mW for the tungsten filament source as a HeNe laser (633nm) for TBO absorption in the PDT experiment with OceanOptics spectrometer.

3.1 Spectrometer Calibration

OceanOptics spectrometer was calibrated to get power (mW) from arbitrary unit (counts). A HeNe laser (633nm) was measured by the spectrometer from 11.7, 15.5 and 16.7 cm and the spectrum of 11.7cm is shown as an example in Figure 3.1. The total power in the spectrum was calculated and plotted as a function of distance as Figure 3.2. The power of the HeNe laser was also measured using MELLES GRIOT broadband power meter as 5.46mW.

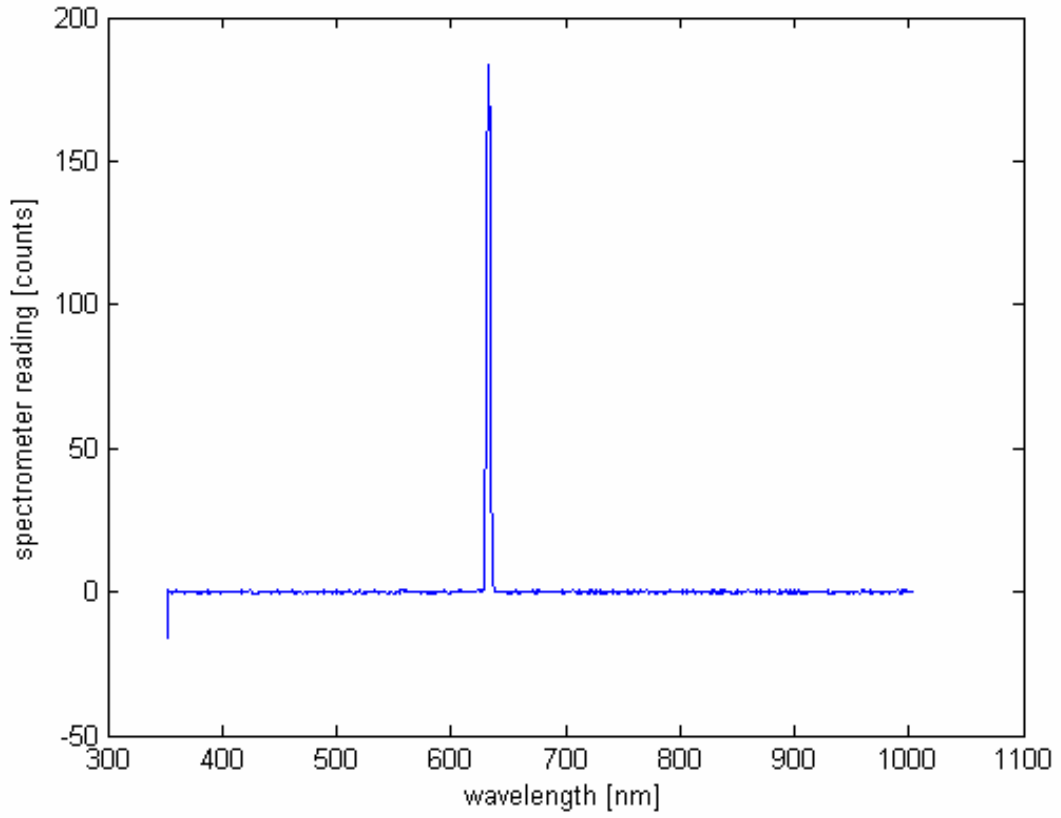

Figure 3.1: HeNe laser spectrum from an OceanOptics spectrometer

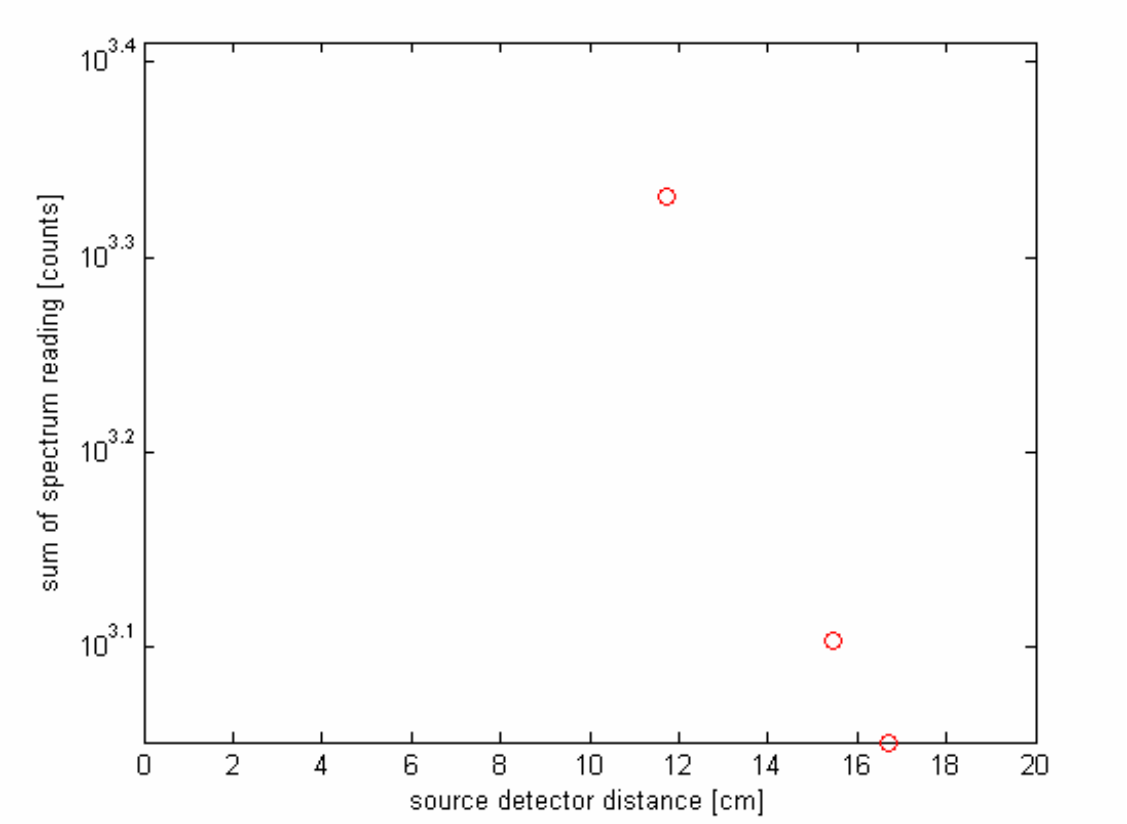

Figure 3.2: total power (in counts) from the spectrum measurement

From these measurements, we know that the conversion number around 633nm for the OceanOptics spectrometer to be 6.0±0.2x109 count/W/ms.

Tungsten light (OceanOptics LS-1) was measured using the spectrometer as shown in Figure 3.3 red curve. The emission spectrum of the light source was provided from the vendor as shown in Figure 3.3 black curve. From these 2 spectrums we can calculate the whole conversion curve. And we also know the conversion number at 633nm, so we can know all the conversion numbers in the conversion curve as shown in Figure 3.4.

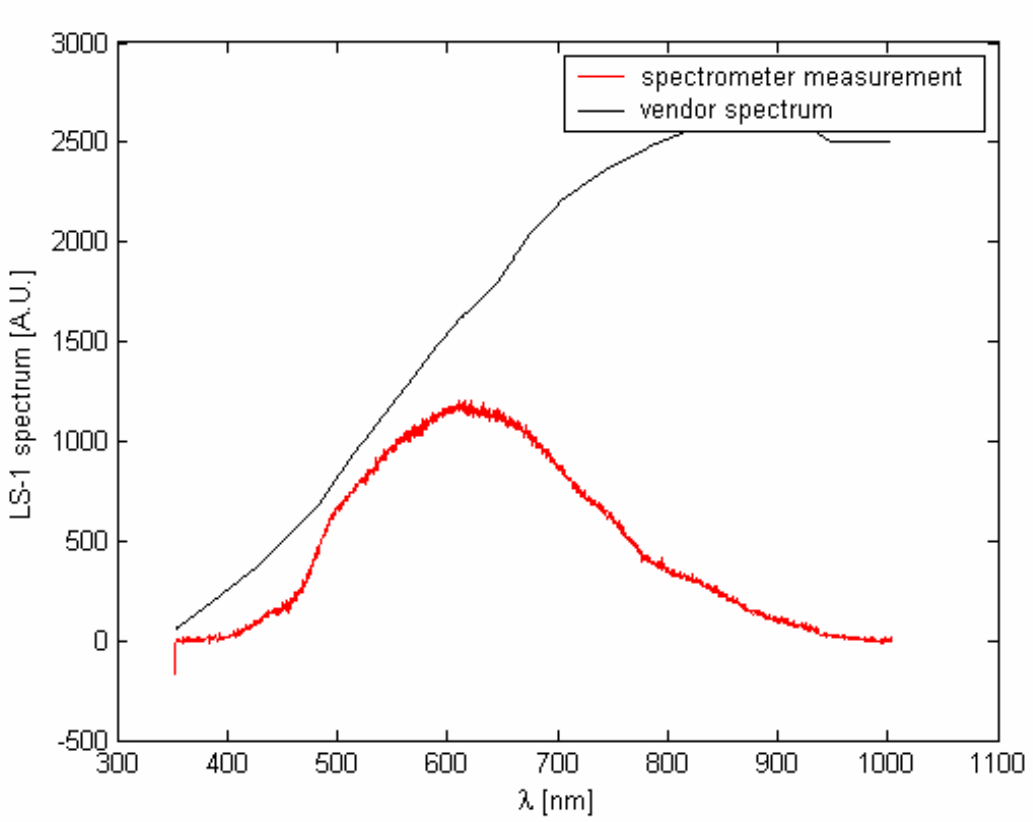

Figure 3.3: LS-1 Spectrum from spectrometer measurement (red) and from vendor (black)

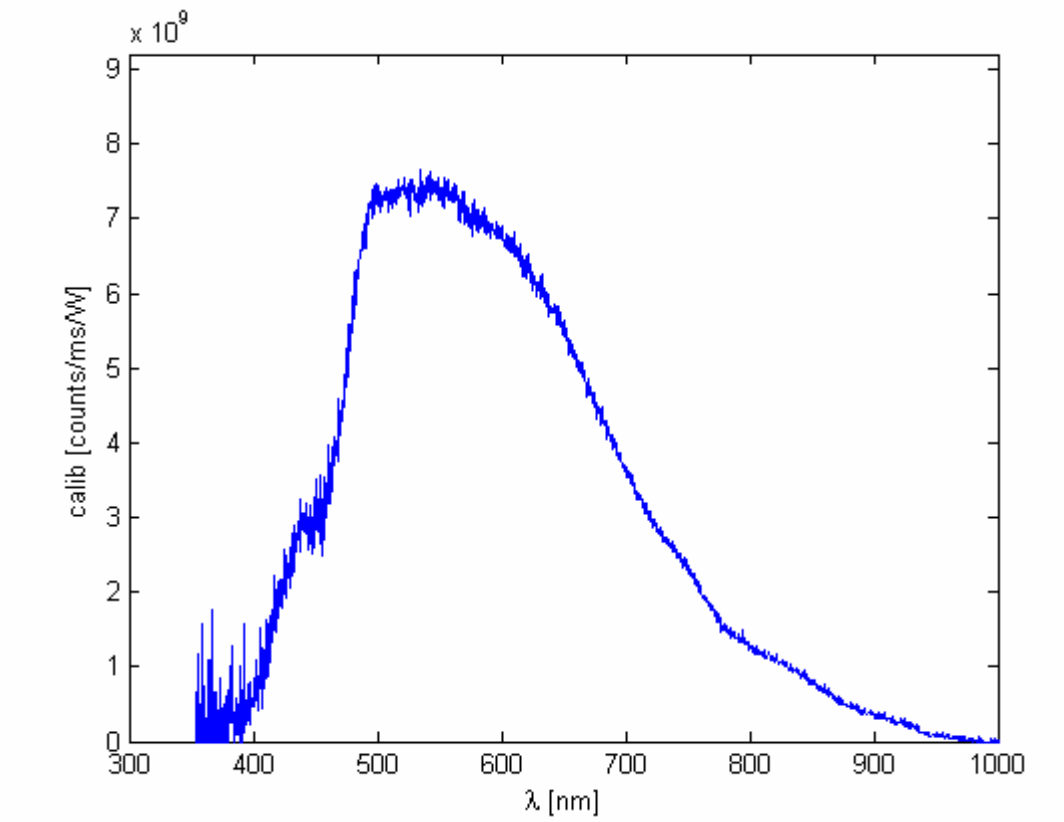

Figure 3.4: Conversion number spectrum

3.2 Extinction Coefficient of Toluidine Blue O

The extinction coefficient of TBO was measured using a transmission experiment with OceanOptics spectrometer. TBO was put into dilute water to get 1mg/L TBO solution. TBO solution was put into a cuvette (path length = 1 cm) to take a transmission measurement with OceanOptics spectrometer. Dilute water was also put into the cuvette to take a standard measurement. The extinction coefficient was calculated and plotted as the Figure 3.5 below.

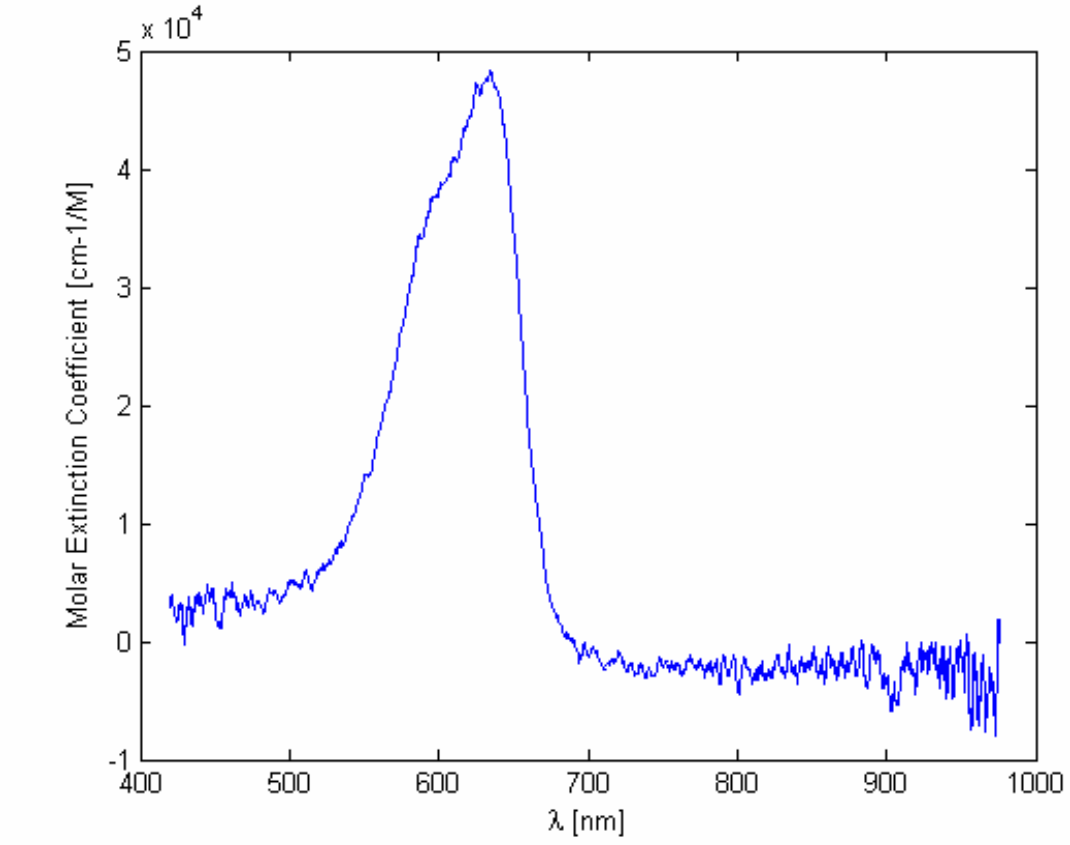

Figure 3.5: Extinction coefficient of Toluidine Blue

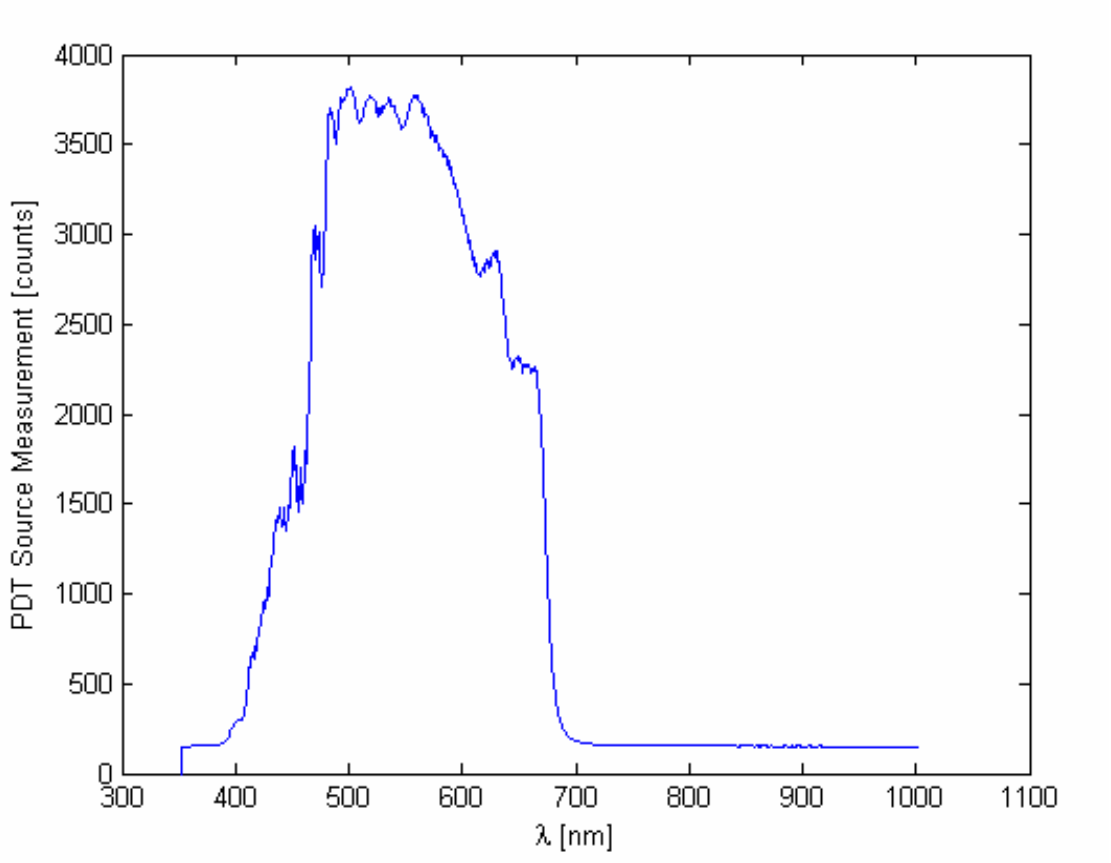

Figure 3.6: Tungsten filament spectrum from OceanOptics spectrometer (Right)

3.3 Effective PDT Dosage Calculation

The actual light source using in PDT is a 500W tungsten filament. This tungsten filament was also measured with OceanOptics spectrometer and shown as Figure 3.6. There was water place in the pathway to block infrared effect and prevent the biofilm to become warm.

The effective dosage for PDT is defined as how much of the laser power (@633nm) is equal to the tungsten filament we are using in the PDT experiment. It can be calculated as:

$$P_{Effect} = \int M_0(\lambda) \frac{S_{cuvette}}{a} \frac{r_s^2}{r_c^2} \frac{\varepsilon(\lambda)}{\varepsilon(633)} D(\lambda) absorb_{water}(\lambda) d\lambda \quad [3.1]$$

$M_0(\lambda)$ is the spectrum measurement of tungsten filament as Figure 3.6; $S_{cuvette}$ is the irradiation area of cuvette; a is the surface area of spectrometer fiber; r_s is the distance

between spectrometer detector and tungsten filament; r_c is the distance between cuvette and tungsten filament; $\varepsilon(\lambda)$ is the extinction coefficient spectrum and $\varepsilon(633)$ is the extinction coefficient at 633nm; $D(\lambda)$ is the conversion number curve as Figure 5.5; $absorb_{water}(\lambda)$ is the absorption effect of water; From this measurement, we know that the effective dosage of the tungsten filament light source is 285.4mW.

3.4 Summary

In this chapter, the tungsten filament light source was calibrated for effective PDA dosage which is the current PDT light source (tungsten filament) is equal to how much of the light power at 633 nm. Firstly the OceanOptics spectrometer was calibrated from arbitrary unit (counts) to real unit (W). Secondly the extinction coefficient spectrum was measured for TBO (photosensitizer in PDT). Thirdly the tungsten filament source was measured using the calibrated spectrometer and the effective dosage was calculated as 285.4 mW at 633nm.

Chapter 4
Photodynamic Therapy Experiment and the Results: Survival Curves

Abstract

Streptococcus mutans, a key factor for dental caries disease, was treated with photodynamic therapy (PDT) in both its planktonic state and biofilm state. The photosensitizer was Toluidine Blue O (TBO) and the light source was a tungsten filament. When exposed to TBO in solution, the bacteria concentrated the TBO 100-fold above the concentration of the solution. After PDT treatment, the biofilm was resuspended. Bacteria were then plated and survival assessed by colony formation. The PDT showed a 10^4 killing effect. The threshold radiant exposure H_{th} was determined for planktonic state (1.3 J/cm^2) and biofilm state (18 J/cm^2).

4.1 Introduction

Photodynamic therapy (PDT) uses a light-activated oxidative injury to achieve cell death. Its ability to kill even drug-resistant bacteria has spurred interest in PDT for bacteriocidal treatments. This paper considers the use of PDT to kill oral bacteria growing in either the planktonic state or as a biofilm.

In this paper, PDT of *S.mutans*, one of the oral bacteria growing in oral biofilms, was studied using TBO as the photosensitizer. The uptake of TBO by planktonic and biofilm was determined using optical methods. The light was quantified in terms of the delivered light that would be absorbed by TBO. The survival after PDT treatment was assayed by colony formation.

4.2 Materials and Methods

4.2.1. Bacteria and Biofilm Culture Protocol

Streptococcus mutans strain ATCC 25175 was used in this study. *S. mutans* was grown in brain heart infusion broth (BHI) or on BHI containing 1.5% agar (Difco, Detroit, MI, USA) at 37°C in a CO_2 incubator without agitation. For liquid culture, 1 ml of a 2-day-old culture of *S. mutans* was diluted into 5 ml of BHI broth and incubated until *S. mutans* growth reached exponential phase. For biofilm experiments, 1 ml of an overnight culture of *S. mutans* was added into 2 ml of BHI broth supplemented with 0.2 M sucrose to enhance biofilm formation on a hydroxylapatite disc placed in the solution (1-cm diameter, 0.05-0.06 thickness, HiMed, Inc., Old Bethpage, NY, USA) within a 24-well titer plate, incubated for 3 days.

Bacterium grown as a biofilm was resuspended for assay of TBO uptake and for assay for colony formation. The disc was transferred to a 50 ml sterile polypropylene conical tube (Becton Dickinson Labwere, NJ, USA) with 5 ml BHI broth and vortexed vigorously for 60 seconds. Control experiments showed that this procedure did not kill bacteria. Then 100 μl samples from serial dilutions of the bacterial

suspension using BHI broth were plated onto BHI plates for colony formation. After two days of incubation, the number of colony forming units (CFU) per plate was counted.

4.2.2 Photosensitizer Preparation

Toluidine Blue O (Acros, New Jersey, USA) was used as photosensitizer. Stock solution was 200 mg/L, in PBS (phosphate buffer saline). The TBO solution was prepared 15 minutes prior to the experiment and kept in a dark environment. The concentration of TBO in the PDT experiments was varied as mentioned in the PDT protocols.

4.2.3 Light Source

The details about light source calibration were presented in Chapter 3. The light source for PDT was a 500-W tungsten filament. The spectral power output, $P_{tungsten}(\lambda)$ [W/nm], was calibrated by a spectrometer (Ocean Optics, Inc.). The integral of the product of light source irradiance E [W/cm^2] and TBO extinction coefficient ε [$cm^{-1}M^{-1}$] was calculated, and equated to the product of a laser at 633 nm wavelength with a power P_{633nm}:

$$P_{633nm}\varepsilon(633nm) = \int_{400}^{800} P_{tungsten}(\lambda)\varepsilon(\lambda)\ d\lambda \qquad [4.1]$$

The tungsten light source behaved equivalent to a 633-nm-wavelength laser with power 57.4 W, with respect to its ability to activate TBO photosensitizer. Hence, the irradiance cited in this report for the irradiance E [W/cm^2] is the equivalent 633-nm power P_{633nm} normalized by the area of the beam of light exposure:

$$E = P_{633}\frac{S_{cuvette}}{4\pi r_s^{\,2}} \qquad [4.2]$$

The value of E is 285.4 mW. $S_{cuvette}$ is the surface area of the plate for irradiation and

r_s is the distance between light source and cuvette. Water was placed in the light pathway between the light source and the target cells or biofilm to block infrared radiation and prevent the cells or biofilm from warming.

4.2.4 Planktonic State PDT Process

The photosensitizer TBO was added to the cell suspension of *S. mutans* to yield a TBO concentration of 40 mg/L. The *S.mutans* density was ~5x10^6 CFU/ml. The *S. mutans* cells were incubated in the TBO solution in the dark environment for 20 min to allow TBO uptake. The cell solution was put into a serial of cuvette. Each cuvette had 100-µl S.mutans with TBO. The light path was around 0.1 cm. The transmission through plate with the TBO solution was 0.4; marginal effect on light exposure due to the background TBO was not very significant. The 100-µl samples from each the cell solution in the cuvette were irradiated for different times of exposure to light for use in the CFU assay, as described above. The irradiation times were 0, 30, 60 120 s. Three control groups were also tested: light only (L+ PS-), TBO only (L- PS+) and no light no TBO (L- PS-).

4.2.5 Biofilm State PDT Process

The biofilm state of *S.mutans* was also tested with PDT. The biofilm was washed twice in the BHI solution and then put into the 80 mg/L TBO solution for 60 minutes incubation in dark environment. Four samples were tested and irradiation time were 0, 5, 10 and 20 min, respectively. Three control groups were also tested including light only (L+ PS-), TBO only (L- PS+) and no light no TBO (L- PS-). Water was placed in the light pathway to block infrared effect and prevent the biofilm to be warm.

4.2.6 Uptake of Photosensitizer by Bacteria

The details about photosensitizer uptake by the bacteria were presented in Chapter 2A. An aliquot of 0.5 ml of planktonic state *S.mutans* cells were incubated with 40 mg/L TBO for 30 min in a dark environment. The cells were suspended in a 1 ml solution containing polystyrene microspheres (0.5 µm diameter, Duke Scientific, CA, stock solution 10% v/v) and 0.5 ml water was also added, to yield a final solution with cells

that had taken up TBO, and 6.6% v/v microspheres. The addition of microspheres provided a background optical scattering that dominated over the inherent scattering by the bacteria. The TBO within the cells provided the absorption. The scattering by microspheres provided multiple passes of light through each bacterium so the sensitivity of the diffuse optical reflectance of the solution was especially sensitive to the TBO concentration.

Reflectance measurements were made by delivering white light to the surface of the solution held in the well of a 24-well plate. The total diffuse reflectance $R_{bacteria}$ and $R_{added.TBO}$ were calculated using diffusion theory, based on the absorption coefficient, μ_a [cm^{-1}], and reduced scattering coefficient, μ_s' [cm^{-1}] of the solution. With the measured absorption coefficient μ_a, final concentration of TBO in the cells was calculated.

To assess the photosensitizer uptake for a biofilm, the biofilm and 80 mg/L TBO was incubated in dark environment for 60 minutes. The biofilm was washed then vortexed vigorously for 60 seconds and washed again. Then suspended bacteria were collected by centrifugation and added to the polystyrene microsphere solution, as for the planktonic bacteria. The optical assessment of TBO uptake was the same as for the planktonic bacteria.

4.3 Results

4.3.1 Uptake of Photosensitizer

The study indicated the TBO concentration in the planktonic state bacteria to be $3.1x10^3$ mg/L ($1.01x10^{-2}$ M) and in the biofilm to be $1.1x10^3$ mg/L ($3.6x10^{-3}$ M). Both of the concentrations were much higher than the initial TBO concentrations (40 and 80 mg/L, respectively). The planktonic bacteria concentrated TBO 78-fold and the biofilm cells on average concentrated the TBO 45-fold.

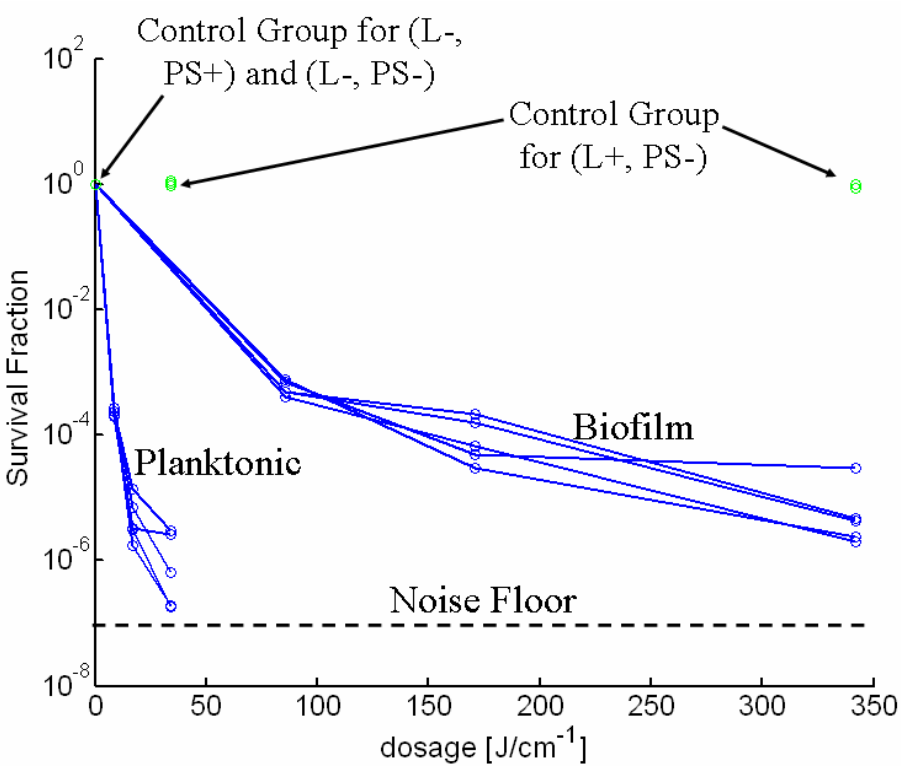

Figure 4.1 PDT survival curve for planktonic and biofilm states S.mutans

4.3.2 PDT Killing Effects

The survival after PDT was scored as colony forming units (CFU) after 2-day incubation. Figure 4.1 shows the survival of planktonic bacteria and biofilm bacteria as a function of radiant exposure, H [J/cm^2]. Survival dropped to at least 10^{-5} for both bacteria types, but the dosage required to achieve this killing was 10-fold greater for the biofilm than for the planktonic state. The results for 5 repetitions of the experiment are shown. The noise floor at 10^{-7} survival corresponds to one CFU on the plate with the highest dilution of cells.

The initial drop in survival was approximated by an exponential decay:

$$survival = e^{-H/H_{th}} \qquad [4.3]$$

evaluated using the data at 10-4-10-3 survival, (H, survival) = (7.7, 0.0030) for planktonic and (85.2, 0.0084) for biofilm.

4.4 Discussion

The value of H_{th} was 1.3 J/cm^2 for planktonic bacteria and 18 J/cm^2 for biofilm. The biofilm H_{th} values are comparable to the H_{th} for S.mutans biofilm with TBO results from other groups [103, 104], as listed in Table 4.1.

State	Radiant exposure, H [J/cm^2]	Survival	Threshold radiant exposure H_{th} [J/cm^2]	Citation
Planktonic	7.7	$3.0x10^{-3}$	1.3	This study
Biofilm	85	$8.4x10^{-3}$	18	This study
Biofilm	231	$1x10^{-5}$	20.1	Queen Mary University of London, UK [5]
Biofilm	13.9	0.05	8.6	State University of Campinas, Brazil [4]

Table 4.1: Survival of bacteria after PDT

From the survival curves result, both planktonic state and biofilm state PDT successfully killed the bacteria. The killing effect was at least 10-4 significant. The Threshold radiant exposure H_{th} was comparable to the peer studies. The biofilm state has 10-fold higher PDT resistant than the planktonic. The reason is clear but we will discuss this in the next chapter.

Chapter 5

Photodynamic Therapy Dosage Analysis

Abstract

With the information from the last 3 chapters, effective PDT dosage for light, photosensitizer uptake by bacteria cells and the PDT survival curves were determined and used to calculate PDT dosage. The threshold PDT dosage (photons absorbed by TBO per g bacteria, [photons/g]) for killing 63% of bacteria was $3.6x10^{21}$ photons/g for S.mutans bacteria. The biofilm was 10-fold more resistant to PDT treatment than bacteria in the planktonic state because of lower photosensitizer concentration.

5.1 Introduction

In 1990, a practical "photodynamic dose threshold", PDT_{th} [photons/g], was defined by Patterson, Wilson, and Graff [1] as the number of photons absorbed by photosensitizer per gram of target tissue. For tumors, the typical range for PDT_{th} is ~10^{18}–10^{20} photon/g, which varies for different photosensitizers [2]. The expression for PDT_{th} is

$$PDT_{th} = Et\ln(10)\varepsilon C_{ps}\frac{\lambda}{hc\rho} \qquad [photons/g] \quad [5.1]$$

where E is the irradiance of treatment light [W/cm^2], t is the time of exposure to light[s], ε is the extinction coefficient of photosensitizer [cm^{-1}/M], C_{ps} is the photosensitizer concentration [M], λ is the irradiance wavelength [nm], h is Planck's constant [Js], c is the speed of light [cm/s] and ρ is the density of the target tissue or

cells [g/cm^3]. The product Et is the radiant exposure, H [J/cm^2], of treatment light.

In a preliminary study on bacteria, the PDT_{th} for *Eschericha coli* using Methylene Blue (MB) as the photosensitizer was determined to be ~1.5x10^{21} photons/g. This value is much higher than the typical range of PDT_{th}, consistent with *E.coli* being a Gram (-) bacteria that is more difficult to kill with PDT [6].

In this chapter, PDT of *S.mutans*, one of the oral bacteria growing in oral biofilms, was studied using TBO as the photosensitizer. The uptake of TBO by planktonic and biofilm was determined using optical methods as Chapter 2. The light was quantified in terms of the delivered light that would be absorbed by TBO as Chapter 3. The survival after PDT treatment was assayed by colony formation as Chapter 4. The values of PDT_{th} for S.mutans are reported and discussed. These results are pertinent to efforts to design PDT protocols for antibiotic treatment of oral bacteria.

5.2 Threshold PDT Dose, PDTth

In both bacteria experiment and biofilm experiment, tungsten filament (from 8cm away) was used as light source. The effective dosage was measured as 285.4mW.

The photosensitizer uptake in biofilm is studied in Chapter 2A using reflectance spectroscopy measurement. PDT dosage threshold (photons absorbed by PS per gram cells) that achieved inactivation was calculated. Since the diffusion of singlet oxygen was very limited (diffusion distance is less than 20 nm), only the photosensitizer that had accumulated inside the cell or was adherent to the bacteria cells was effective for PDT. For planktonic state, the average concentration was measured as 3.1x10^3 mg/L. Biofilm was broken using vortex method and the bacteria was collected and put into the curette with polystyrene sphere (same method for planktonic bacteria) and the average concentration was measured as 1.1x10^3 mg/L and used for PDT dosage threshold calculation.

The dosage threshold for S.mutans-TBO PDT was expressed as the number of photons absorbed by TBO inside S.mutans per 1 cm^3 volume of S.mutans cells that prevented colony formation. With the equation 4,1, the photons absorbed by TBO was calculated based on the energy threshold denoted as ET = H_{th}, which can be known from the survival curve experiment in Chapter 4 as Table 4.1. H_{th} was 1.3J/cm^2 for planktonic state and 18 J/cm^2 for biofilm state.

The PDT threshold dose, PDT_{th}, for *S.mutans* –using TBO as the photosensitizer was calculated using the values of H_{th} for the product ET in Eq.4.1. The concentration of TBO in the cells was also used. The values of PDT_{th} were $3.64x10^{21}$ photons/g for planktonic bacteria. The PDT_{th} for biofilm should be close to the PDT_{th} for planktonic. However the TBO concentration in the biofilm is not homogenous which case the H_{th} in the biofilm was not uniform. The H_{th} in upper layer of the biofilm was much less than the lower layer.

5.3 Discussion

Consider the possibility that bacteria in both the planktonic and biofilm state have a similar PDT_{th}. It is possible that the bacteria in the upper layers of the biofilm were quickly killed by PDT due to the high TBO levels, while the bacteria in the deeper layers of the biofilm required more light exposure to achieve the PDT_{th} due to the low TBO levels. This possibility would be consistent with the biofilm bacteria survival curve, where an early population may have responded quickly but a residual population required far more light for killing due to a lower TBO level. The threshold dose PDT_{th} could be the same for both types of bacteria, and the differences attributed simply to non-uniform TBO concentration within the biofilm.

According to the results from a separated experiment, in the planktonic state, the TBO uptake in the cells and the TBO concentration in the surrounding medium after 60 minutes waiting time in dark environment are as Figure 5.1a. In Figure 5.1b the ratio

of bacteria TBO uptake over surrounding medium TBO concentration after 60 minutes waiting in dark is also plotted. Another separate experiment not reported here used confocal reflectance measurements to quantify the penetration of TBO into the biofilm. Those studies showed the surface of the intact biofilm having a concentration comparable to the bathing solution, and the concentration falling as a function of depth within the biofilm on the HA disc. Near the surface, the bacteria in the biofilm might be expected to concentrate the TBO 70-fold (Fv) above the surrounding solution, like the planktonic bacteria, although this assumption could not be tested.

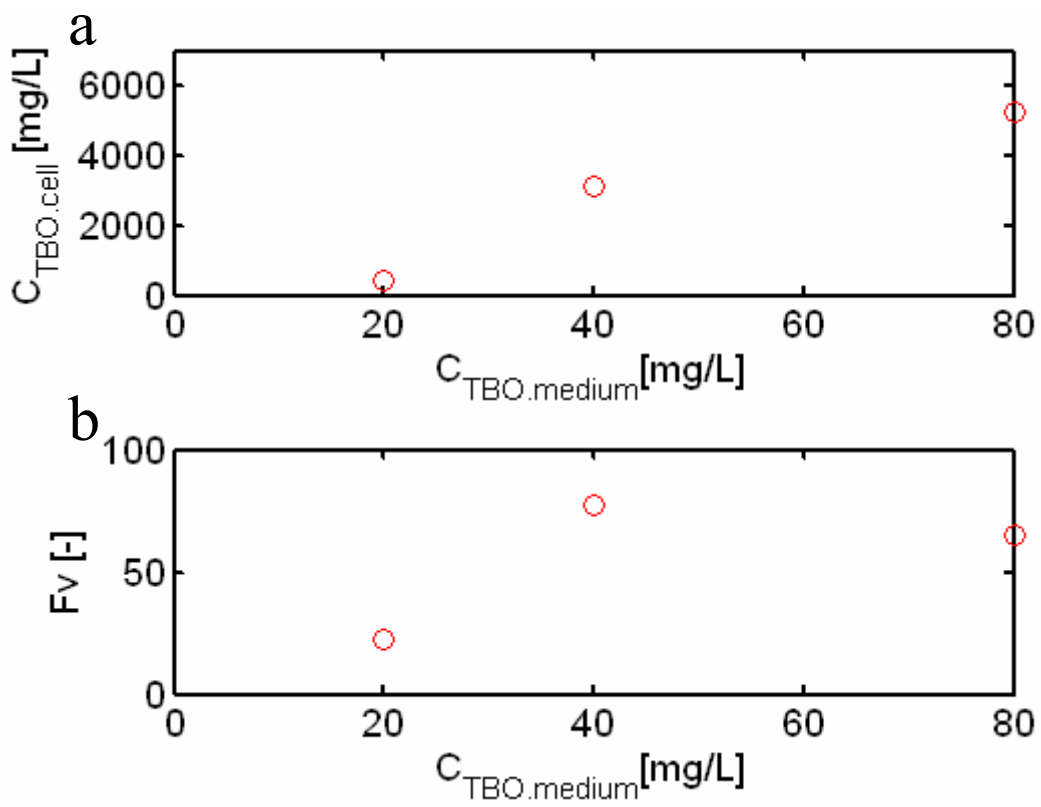

Figure 5.1 TBO uptake in the S.mutans cells (planktonic) after 60 minutes waiting in dark. a: TBO concentration in cell vs. TBO concentration in the surrounding medium; b: TBO concentration ratio (cell/medium) vs. TBO concentration in the surrounding medium.

According to Figure 5.1a, TBO higher concentration in the surrounding medium yields a higher cell uptake. Therefore, in the biofilm case, TBO concentration in the upper layer biofilm was around 80 mg/L which corresponded 5.2×10^3 mg/L TBO in

bacteria cells.

Because PDT_{th} for both planktonic and biofilm state are very similar,

$$C_{planktonic} H_{th.planktonic} = C_{upper} H_{th.upper} \quad [5.2]$$

The left side of the equation is for planktonic state and the right side is for the upper layer of the biofilm. $H_{th.upper}$ is resolved as 0.77 J/cm2 since all other terms are known in Eq 5.2. (Cplanktonic = 3.1×10^3 mg/L, $H_{th.planktonic}$=1.3 J/cm^2) Figure 5.2 shows the upper layer survival curve with $H_{th.upper}$.

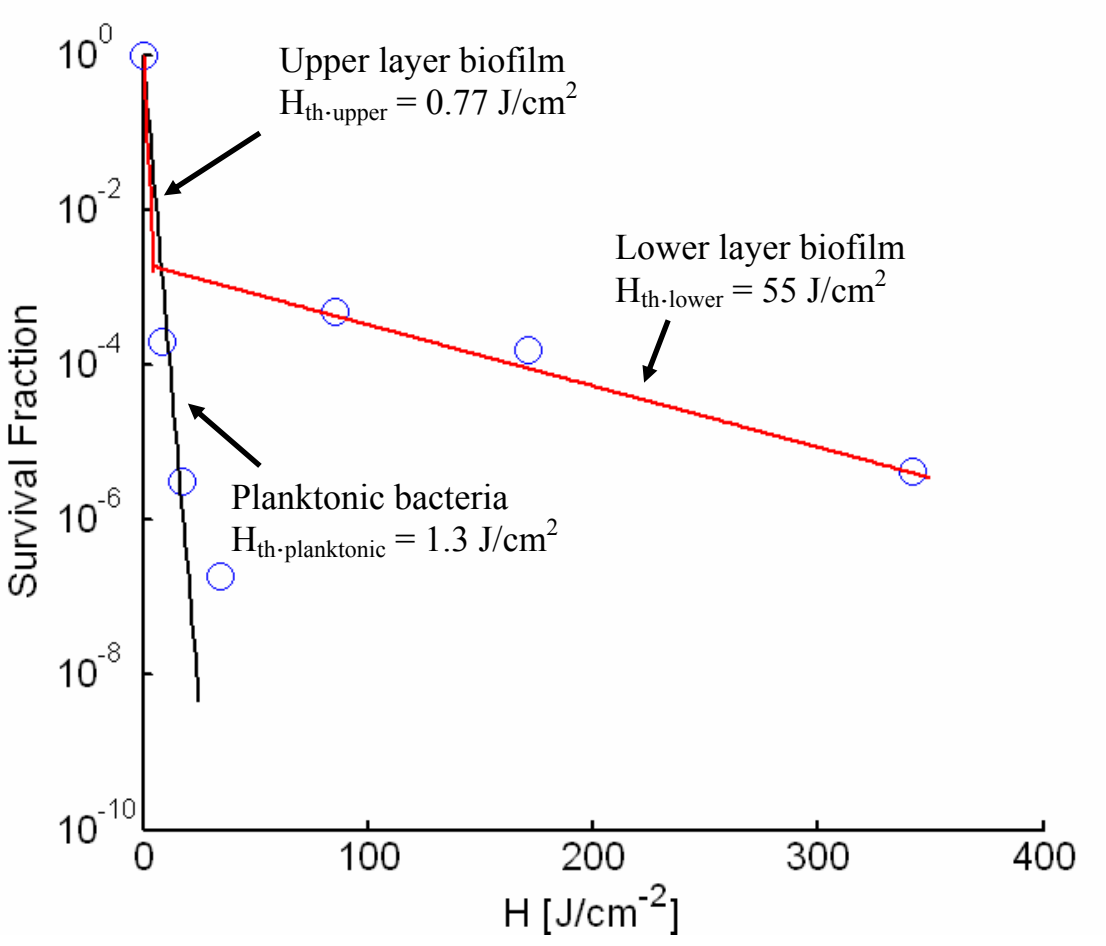

Figure 5.2 Survival curve fitting for $H_{th.planktonic}$, $H_{th.upper}$ and $H_{th.lower}$.

Because the TBO concentration in the lower layer is much less, the lower layer bacteria has a much higher H_{th} (55 J/cm^2 by fitting results, which is also shown in

Figure 4.3) corresponding to the bacteria in the lower layer biofilm. From Eq 5.3, C_{lower} is also calculated as 73 mg/L.

$$C_{planktonic}H_{th.planktonic} = C_{lower}H_{th.lower} \quad [5.3]$$

Assuming TBO concentration drop in linear and surface layer was 80 mg/L and bottom layer was 0 mg/L. The average TBO uptake in the cells was $1.1x10^3$ mg/L. The average Fv in the biofilm was around 27.5. This number is much lower than the Fv (~70) in planktonic state if the surrounding concentration in 40 mg/L. It is most likely the Fv in the biofilm lower layer is quite low.

Chapter 6
Monte Carlo Simulation for Light Propagation in 3D Tooth Model

Monte Carlo simulation is implemented in a three dimension model to simulate the light propagation in the tooth and presented in this chapter. The goal of this research is to estimate the light energy deposition in the target region in the tooth with given light source information, tooth optical properties and tooth structure. With this Monte Carlo model, we can find the proper light source/dosage and incident point to meet the photodynamic therapy dosage requirement.

6.1 Introduction

For photodynamic therapy or other optical therapy for the tooth, input light dosage needs to be estimated according to the required dosage in the target site [89]. According to the nature of the disease, the target site could be inside the tooth [90]. (Please refer the introduction of oral disease in Section 1.2 “oral biofilm PDT”.) A model is necessary to simulate light propagation in the tooth. When the geometry model is very complicated, analytical solution for the light propagation will become quite difficult. One of the alternative approaches is the Monte Carlo simulation, which is a statistic based method, to resolve this problem. [91]

MCML program is the most famous Monte Carlo program in biomedical optics field [92]. It has been validated and widely applied to many different applications. However, MCML is a multi layer model which won’t fit for our tooth structure [93].

A three dimensional multi block Monte Carlo model has been developed and implemented. The program is designate for tooth geometry model. It is a good tool for the photodynamic therapy dosage estimation. The implementation of Monte Carlo tooth model and 2 use cases are presented in this chapter.

6.2 Theory

6.2.1 Introduction

Monte Carlo simulation has been used to solve a variety of physical and mathematical problems, as well as finance analysis [94]. In all applications of the Monte Carlo method, a stochastic model is constructed in which the expected value of a certain random variable (or of a combination of several variables) is equivalent to the value of a physical quantity to be determined [95]. The essential of this method is statistical sampling for complicated system usually with at least two degree of freedom. The term Monte Carlo was coined in the 1940s by physicists in the Los Alamos National Laboratory.

For light propagation application, Monte Carlo simulation offers a flexible and rigorous approach toward photon transport in turbid tissues. Monte Carlo simulation describes local rules of photon propagation. The photon propagation rules include:
1) Probability distributions for the step size of photon movement between sites of photon-tissue interaction;
2) Angles of deflection in a photon's trajectory when a scattering event occurs.

Monte Carlo method is statistical based and relies on computing the propagation tracks of a large number of photons. Monte Carlo method also defines the termination of photon tracking, which is actually the mechanism to decide to kill a photon or add more weight if the photon weight is very low.

As a result of statistical sampling, this method requires a large amount of computation

time. It will be relatively difficult for real time calculation. Also the inversion problem of Monte Carlo method is difficult; usually a lookup table will be necessary and the computation load will be even huger.

Wang and Jacques published the MCML program and released the source code for biomedical optics research. The tooth model Monte Carlo program MCMB is developed based MCML. Therefore MCML will be used as an example to discuss the details of general Monte Carlo model for light propagation and its implementation.

6.2.2 Light propagation

Absorption coefficient μ_a is defined as the probability of photon absorption per unit pathlength, and the scattering coefficient μ_s is defined as the probability of photon scattering per unit pathlength. In the other words, the higher value of μ_a or μ_s means there will be more absorption/scattering possibility in certain pathlength. The total interaction coefficient μ_t, which is the summation of the absorption coefficient μ_a and the scattering coefficient μ_s, is also defined. The anisotropy g is the average of the cosine value of the deflection angle during the scattering. The anisotropy will affect the light propagation in the phase function, which is the possibility distribution function for the deflection angle for each scattering events.

If we know the absorption coefficient μ_a or scattering coefficient factor μ_s, we will be able to determine the distribution of the free path between two scattering/absorption events.

$$P\{s \geq s_1\} = e^{(-\mu_t s_1)} \quad [6.1]$$

The equation 5.1 represents the possibility distribution function for free path with given total interaction coefficient μ_t. If there is a uniform distributed random number ξ, the following equation will convert this random number to a free path distribution:

$$s_1 = \frac{-\ln(1-\xi)}{\mu_t} \quad [6.2]$$

With the random number in the free path distribution, a step size s_1 is determined. The photon will move from the original position to the new position and the distance between these two positions is s_1. In the MCML program, the position of the photon packet is updated by:

```
Photon_Ptr->x += s1*Photon_Ptr->ux;
Photon_Ptr->y += s1*Photon_Ptr->uy;
Photon_Ptr->z += s1*Photon_Ptr->uz;
```

As the above codes shown, the photon position is Photon_Ptr->x, Photon_Ptr->y, and Photon_Ptr->z; the movement direction is Photon_Ptr->ux, Photon_Ptr->uy, and Photon_Ptr->uz.

When the photon has moved to a new position, an absorption/scattering event happens. A fraction of the photon's current weight W, will be deposited into the new position. The amount of deposited photon weight ΔW is as below:

$$\Delta W = W \frac{\mu_a}{\mu_t} \quad [6.3]$$

The corresponding codes in Monte Carlo are as:

```
dwa = Photon_Ptr->w * Photon_Ptr->mua/(Photon_Ptr->mua+Photon_Ptr->mus);
Photon_Ptr->w -= dwa;
```

When the photon has a scattering event, there will be a deflection angle $\theta \in [0, \pi)$ and azimuthal angle, $\psi \in [0, 2\pi)$. The probability distribution for the cosine of the deflection angle, $\cos\theta$, is defined as phase function. Phase function depends on the anisotropy g. Henyey Greenstein function is experimentally found to be suitable for

the tissue phase function:

$$p(\cos\theta) = \frac{1-g^2}{2(1+g^2-2g\cos\theta)^{3/2}} \quad [6.4]$$

The conversion equation from a uniform random number to Henyey Greenstein distribution is:

$$\text{If g>0}, \cos\theta = \frac{1}{2g}\{1+g^2-[\frac{1-g^2}{1-g+2g\xi}]^2\}$$

$$\text{If g=0}, \quad \cos\theta = 2\xi - 1 \qquad [6.5]$$

Although Henyey Greenstein function [98] is mostly used as phase function in Monte Carlo simulation, there are a few phase function may be yielded and which one is the best is still not clear. For example, Henyey Greenstein function does not reproduce the backscattering well, the double Henyey Greenstein function as equation 7.6 is yielded for better reproduce of light scattering [96]. P_{DHG} is the double Henyey Greenstein function, P_{HG} is the Henyey Greenstein function, a is a constant number around 0.9.

$$P_{DHG}(\theta, a, g_1, g_2) = aP_{HG}(\theta, g_1) + (1-a)P_{HG}(\theta, g_2) \quad [6.6]$$

Figure 5.1 shows three different phase functions. The scatterers are 1 micron diameter spheres, refraction index ratio is 1.128 and the incident light wavelength is 0.65 micron. Anisotropy g is 0.932. Transform method was used [97] to generate random numbers following the scattering angle distribution for each corresponding phase function from a uniform distributed random number.

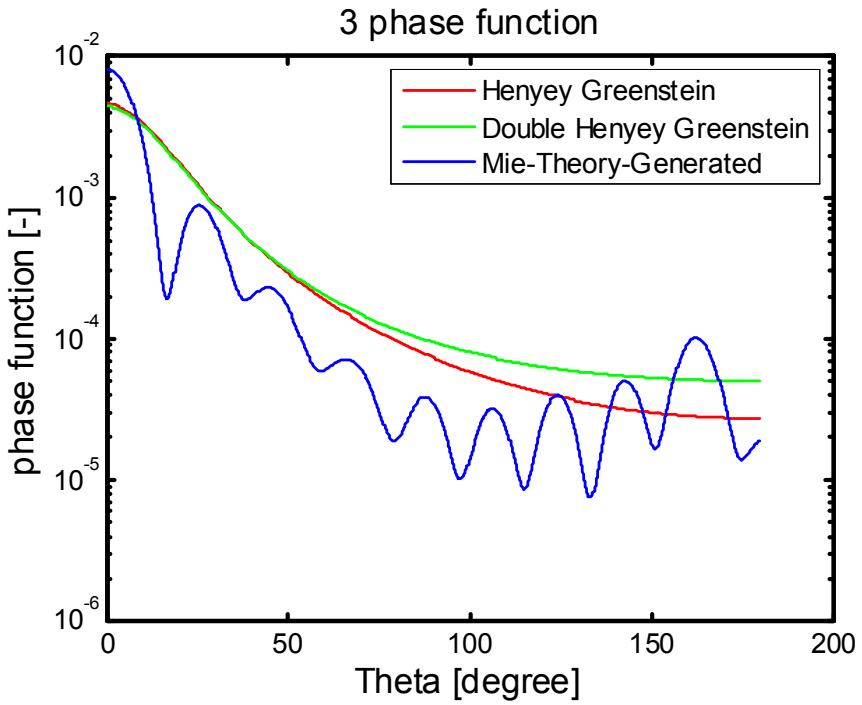

Figure 6.1 Three phase functions

Three phase functions, including Henyey Greenstein function, Double Henyey Greenstein function and Mie-theory-Generated phase function into the Monte Carlo simulation program. With the same anisotropy, we compared the difference of Monte Carlo results (in the form of the reflectance flux as function of radius R(r)) for the 3 phase function and found that there is significant difference when light source is collimated beam and focused beam. The light sources were collimated pencil beam (radius equal to 0); the incident light wavelength was 0.65 μm.

The phase function effect region includes the 3.4% of the total reflectance light. The phase function effect region is 0.105cm. It's about one mean free path (0.1cm).We found that the main effect of phase function is close to the incident point.

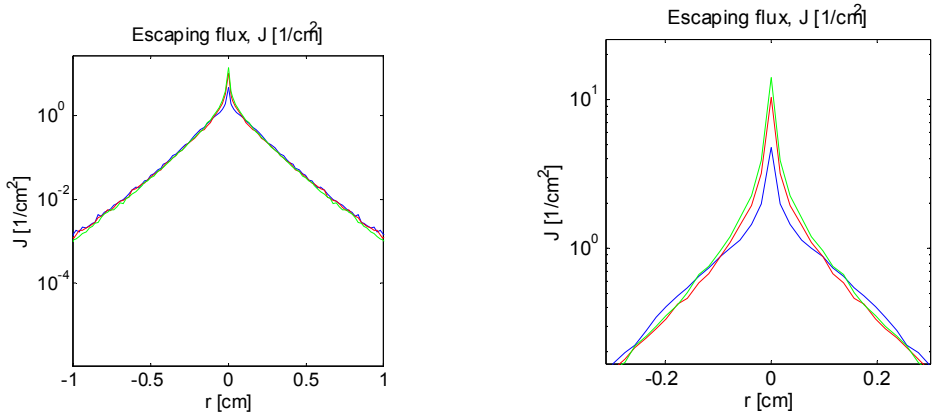

Figure 6.2 Result comparison for 3 different phase functions, Green: Henyey Greenstein, Red: Double Henyey Greenstein, Blue: Mie theory Phase function; Left: Macro image, Right: Micro image

However in the tooth model, our target is the region deep inside the incident point. Therefore, the phase function will not have significant effect on this case and we will use the Henyey Greenstein function as phase function for this program.

The azimuthally angle follows a uniformly distribution in the interval 0 to 2π, therefore, it can be calculated as the following equation. ξ is the uniformed random number.

$$\psi = 2\pi\xi \quad [6.7]$$

Here the corresponding codes for deflection angle change in function "spin"; The first line "SpinTheta" is the function to generate phase function distributed reflectance angle.

```
cost = SpinTheta(g);          /* get the deflection angle from phase function. */
sint = sqrt(1.0 - cost*cost);  /* sqrt() is faster than sin(). */


psi = 2.0*PI*RandomNum();  /* spin psi 0-2pi. */
cosp = cos(psi);
if(psi<PI)
```

```
    sinp = sqrt(1.0 - cosp*cosp);
        /* sqrt() is faster than sin(). */
  else
    sinp = - sqrt(1.0 - cosp*cosp);

  if(fabs(uz) > COSZERO)  {  /* normal incident. */
    Photon_Ptr->ux = sint*cosp;
    Photon_Ptr->uy = sint*sinp;
    Photon_Ptr->uz = cost*SIGN(uz);
        /* SIGN() is faster than division. */
  }
  else  {       /* regular incident. */
    double temp = sqrt(1.0 - uz*uz);
    Photon_Ptr->ux = sint*(ux*uz*cosp - uy*sinp)
                          /temp + ux*cost;
    Photon_Ptr->uy = sint*(uy*uz*cosp + ux*sinp)
                          /temp + uy*cost;
    Photon_Ptr->uz = -sint*cosp*temp + uz*cost;
  }
```

6.2.3 Photon termination

During the photon movement, a photon will be terminated automatically if it is out of the tissue. For a photon that is still propagating inside the tissue, if the photon weight W is below a threshold value W_{th} after many absorption events effect, it will be also terminated. This is because further propagation of the photon will give little information and calculation time will increase. Proper termination should be implemented such that the final energy deposition will be equal to the initial input energy. Russian roulette is used to handle the photon termination when $W<W_{th}$.

The roulette technique gives the photon packet one of m (e.g., m = 10) chance to

survive with new weight of mW. If the photon packet does not survive in the roulette, the photon weight is reduced to zero and the photon is terminated.

$$W = \begin{matrix} mW, if \xi \le 1/m \\ 0, otherwise \end{matrix} \quad [6.8]$$

6.2.4 MCML geometry

In MCML, Monte Carlo simulation program deals with the transport of an infinitely narrow photon beam perpendicularly incident on a multi-layered tissue as shown as Figure 6.3 Each layer is infinitely wide, the thickness, the refractive index, the absorption coefficient μ_a, the scattering coefficient μ_s, and the anisotropy factor g is defined by the user. The output result is stored as energy deposition and fluence rate.

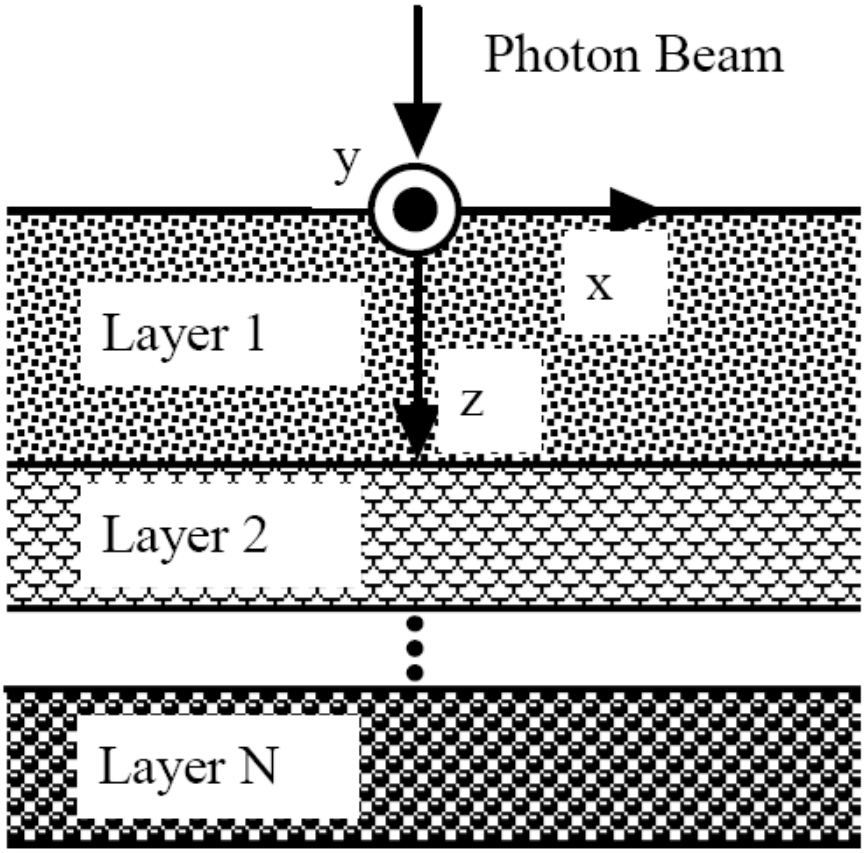

Figure 6.3 Geometry of MCML

6.3 3 D Monte Carlo Tooth Model --- MCMB

MCML has been well validated and widely applied and it is a very good reference for

this study. MCMB is developed based on MCML; the update for the 3D tooth model will be described in this section.

6.3.1 Geometry Model and Optical Properties of Tooth:

The Figure 6.4 shows the geometry of the MC tooth model. The tooth is divided into four parts which are corresponding to enamel, gum, dentin and pulp according the real tooth structure. Please refer the introduction chapter for details about the tooth structure.

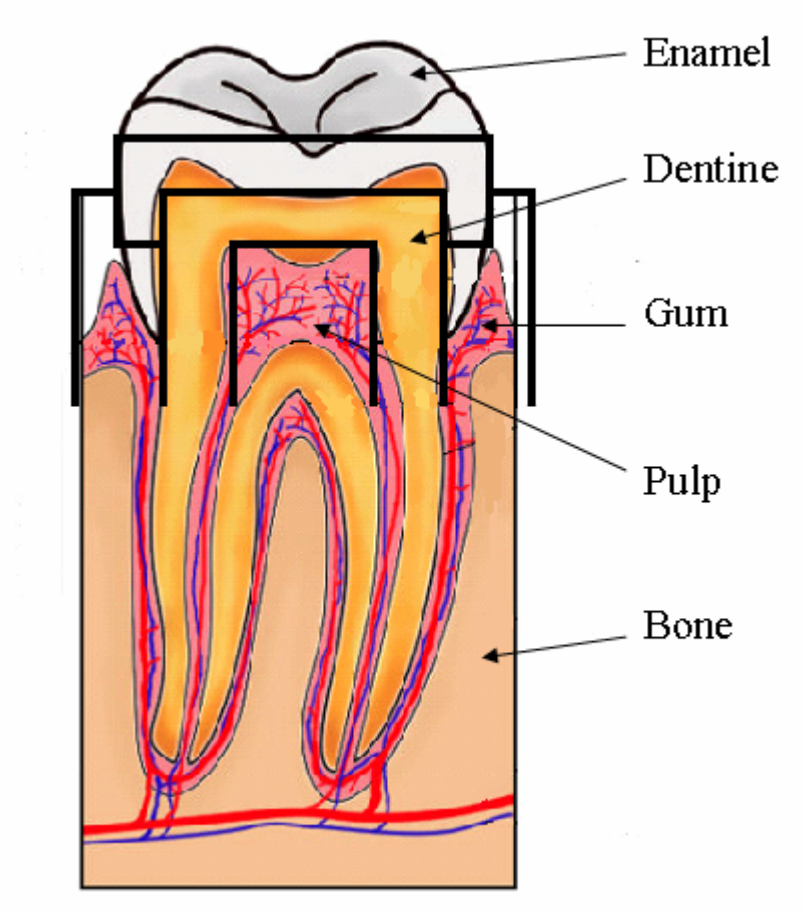

Figure 6.4a Tooth structure for Monte Carlo simulation

In Figure 6.4a, the tooth structure has been simplified to reduce the calculation load. This model is cylindrical symmetrical system as MCML model. However, we will not store the result in a cylindrical coordinate system as MCML. The reason will be

discussed lately in the result store section. Each pixel in this tooth model is a 0.01x0.01x0.01 cm cube. The size of tooth (crown part) is 100 pixel x 100 pixel x 50 pixel. Please refer Figure 6.4b for details of the geometry model for tooth.

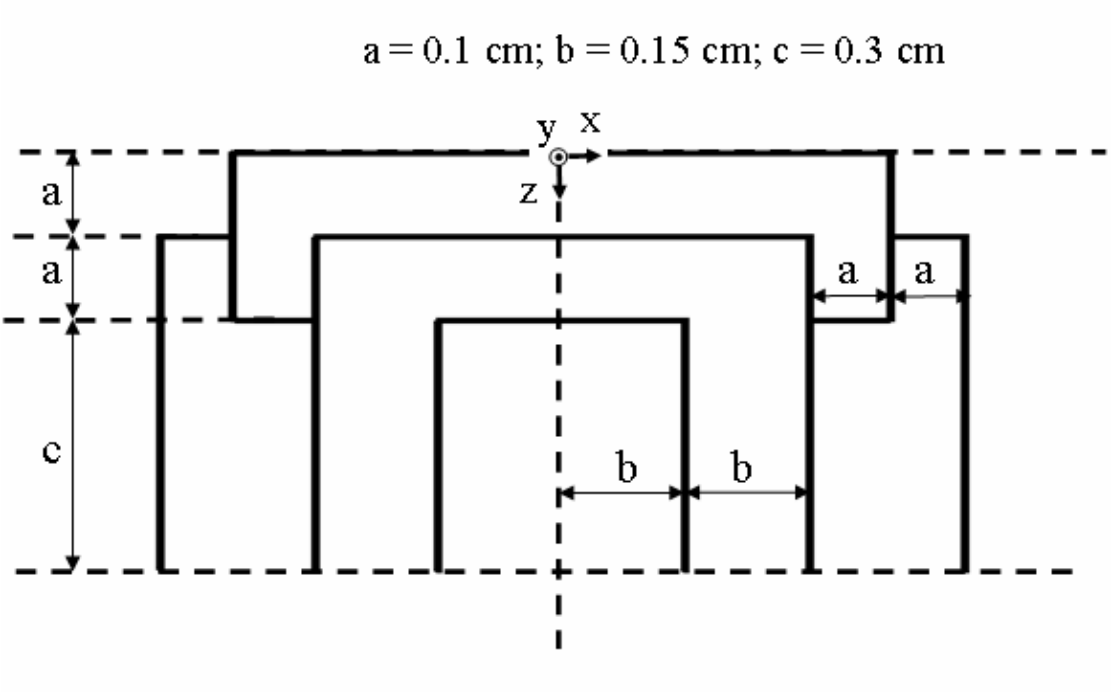

Figure 6.4b Tooth dimension in Monte Carlo model

The optical properties of tooth component have been carefully studied by literature review [109, 110] and are shown below. Gum and pulp optical properties have not been explored yet, some reasonable number is used:

$$\mu_a(\lambda) = \ln 10 \varepsilon(\lambda) 150 / 64500 \quad [6.9]$$

Hemoglobin has a normal concentration of 150g/liter of blood; 64,500 as the gram molecular weight of hemoglobin. The goal of this Monte Carlo model is to provide a toolkit for researchers and clinicians to estimate the PDT dosage. We assume that there are 95% oxy-hemoglobin (μ_a: 488 cm^{-1}/M) and 5% deoxy-hemoglobin (μ_a: 3796 cm^{-1}/M). We assume that the blood content in the pulp is 10%. The absorption coefficient μ_a is from reference [87]. The program also provides the user to input optical properties of tooth by themselves, since tooth optical properties vary for

different samples.

λ=633nm	μ_s [cm^{-1}]	μ_a [cm^{-1}]	g [-]
Enamel	15	0.4	0.7
Dentine	260	3	0.9
Gum	150	0.3	0.9
Pulp	100	0.35	0.97

Table 6.1 Tooth optical properties

6.3.2 Data structure of MCMB

For data structure, the main change of the Monte Carlo tooth model to the original MCML program is new vertical layers. In the layer structure, vertical or horizontal layer and layer position information is added. In the photon structure, the current vertical layer where the photon stays is added. At any time, the vertical layer of the current photon will be recorded because different vertical layer has different optical properties and the boundary handling function will also be changed to adapt vertical layer crossing.

6.3.3 Light source implementation

One of the goals for this tooth Monte Carlo program is to find what is the best position for the incident light and the proper light source type (point spread light, pencil beam or etc.) Therefore, the light source implement need to be very flexible such that all the possibilities could be tested. In MCML, the incident point of the light source is fixed and it will always be a pencil beam. (Other type of light is tested using a program called CONV [99].) This will not meet our requirement. We need to write our own light source code.

The photon data structure includes the position of the photon (x, y, z) and the direction

of the photon (ux, uy, uz) as shown below. These parameters are defined in the function “LaunchPhoton”.

```
Photon_Ptr->x    =    0.0;

Photon_Ptr->y    =    0.0;

Photon_Ptr->z    =    0.0;


Photon_Ptr->ux   =    0;

Photon_Ptr->uy   =    0;

Photon_Ptr->uz   =    1;
```

The above codes represent that the incident light at the central point of the first layer surface and it is a pencil beam with the direction parallel to the z axis as shown in Figure 6.5 light source #1.

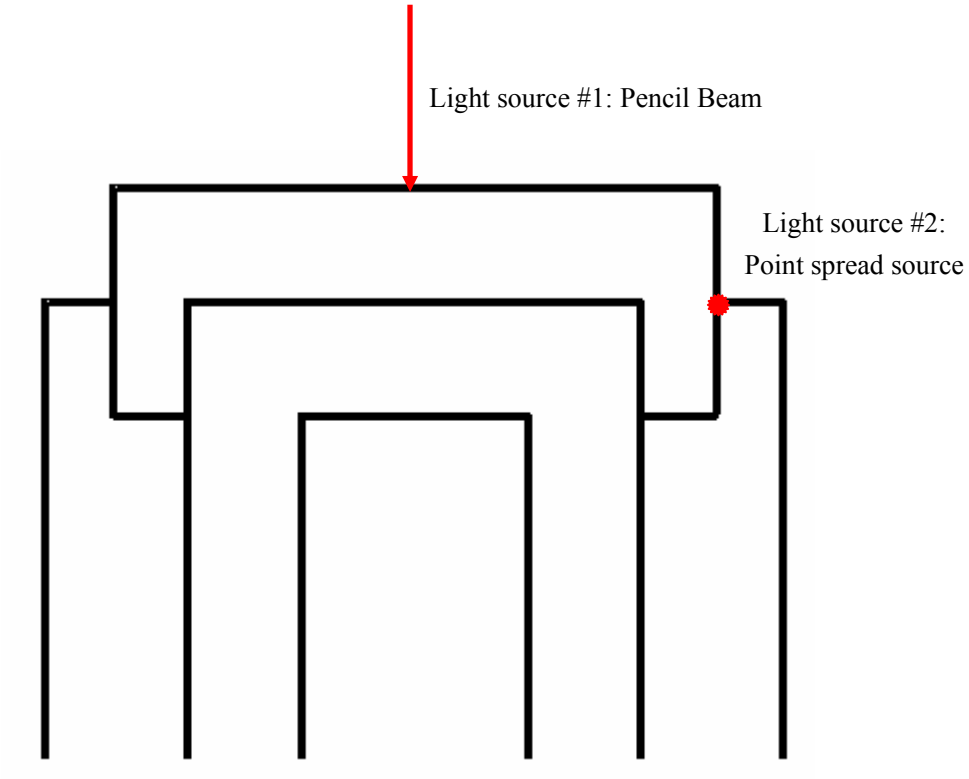

Figure 6.5 Light sources in tooth model

If the light source is a point spread light at the point between enamel and gum, the definition in “LaunchPhoton” is:

```
Photon_Ptr->x    =    0.3;
```

```
Photon_Ptr->y   =   0.0;

Photon_Ptr->z   =   0.25;


ux0             =   1-2*RandomNum();

uy0             =   1-2*RandomNum();

uz0             =   1-2*RandomNum();

uR              =   sqrt(ux0*ux0 + uy0*uy0 + uz0*uz0);

Photon_Ptr->ux =    ux0/uR;

Photon_Ptr->uy =    uy0/uR;

Photon_Ptr->uz =    uz0/uR;
```

The istropic point spread light source is also shown in Figure 6.5 as light source #2. After the photon is launched, the first thing is specular reflectance if there is a mismatched boundary at the tissue/air interface. The refractive indices of the outside medium and tissue are n_1 and n_2. According to Snell's Law, the specular reflectance, R_{sp} is:

$$R_{sp} = \frac{(n_1 - n_2)^2}{(n_1 + n_2)^2} \quad [6.10]$$

6.3.4 Function for photons crossing boundary

The boundary handling strategy is quite different for the tooth model because the geometry structure of Monte Carlo program has changed. There are several vertical boundary implemented in this program. A new “HitBoundary” function is developed for either vertical or the tilt layers crossing.

When a photon is going to hit the boundary, there will be two steps. The first step is to calculate the distance between the original point and the point in the boundary the photon will cross. The photon will be moved to this point in the boundary and if the photon will be reflected or cross the boundary depends on this equation:

$$R(\alpha_i) = \frac{1}{2}\left[\frac{\sin^2(a_i - a_t)}{\sin^2(a_i + a_t)} + \frac{\tan^2(a_i - a_t)}{\tan^2(a_i + a_t)}\right] \quad [6.11]$$

A random number will be generated to determine if the photon reflected or crossed. If it is reflected, the photon will be moved further in the reflected direction and deposit the weight. For the crossed case, the step size will be converted in the new tissue for new optical properties.

The main difference for the 3D program is the vertical layers. I used the above strategy to handle it. When the hitting boundary will happen, I will firstly determine which boundary it will hit by comparing the distance from original point to the boundary points and determine the new optical properties. The conversion of step size is actually converting the step size to a possibility for different layers.

6.3.5 Monte Carlo Output

For the MCML program, a cylindrical coordinate system is used. Each point at the same radius to the central r and depth z will have the same effect for flux and energy deposition. Therefore the data structure for the output is store as r-z coordinate.

The output of MCMB will also be different because the cylindrical symmetry has been broken induced by the light source location and direction change. Light source will not only be in the central point of the first layer surface; it could be any where in the tooth. The result record will be stored from θ-r-z coordinate to x-y-z coordinate. This change means the size of storage space will be significantly larger. Fortunately, the user will only care about the output for certain layers, for example the central layer or the layer where the light source or the PDT treatment target locates. Therefore, only certain layer of the fluence rate and energy deposition will be stored in the MCMB program in a 50x100 array (corresponding to the 50x100 pixels in X-Z in tooth geometry model).

A Matlab program is developed to read the output file from MCMB program and generate the images of the results. The results of the Matlab include energy deposition and fluence rate, as shown in Figure 6.6

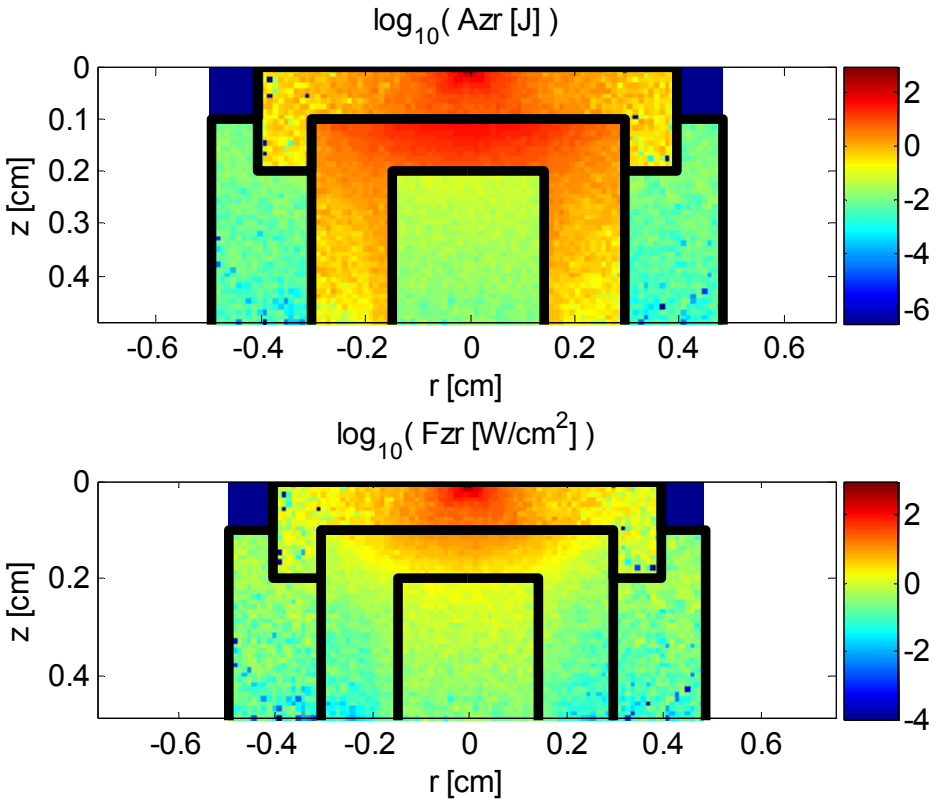

Figure 6.6 An example of MCMB output

The top figure in Figure 6.6 is the energy deposition distribution in the tooth model. It shows the X-Z distribution the central slice in the Y axis. 100,000 photons were launched and the energy deposit in each pixel was recorded. In the bottom figure of Figure 6.6, fluence rate is also documented. Fluence rate is always continuous although there are boundaries in the tooth model.

6.4 Use Cases

Two use cases are presented in this section based on practical PDT application. In a PDT treatment, required dosage delivered to the target region should meet the treatment requirement but surround tissue should not be damaged. The first case is to compare the delivered dosage profile between a broad beam and a narrow beam for

the same amount of input energy at the same incident point. The second case is compare different incident point for the same light source type and input energy.

6.4.1 Light source comparison: broad beam vs. narrow (pencil) beam

Broad collimated beam has the same size (diameter) as the enamel in our tooth model. Pencil beam is collimated and the size of the beam is extremely narrow (1 voxel in this case). In general, pencil beam has more concentrated energy to the target region. However it may also put more energy into the pulp, which is very vulnerable to light irradiation. In this study, the tooth energy deposition profile was compared between broad beam and pencil beam as shown in Figure 5.7a. This comparison will help clinician to decide which light source is better. 500,000 photons were launched for each light source and energy deposition A_{rz} in the tooth is documented and displayed as Figure 6.7 b and c.

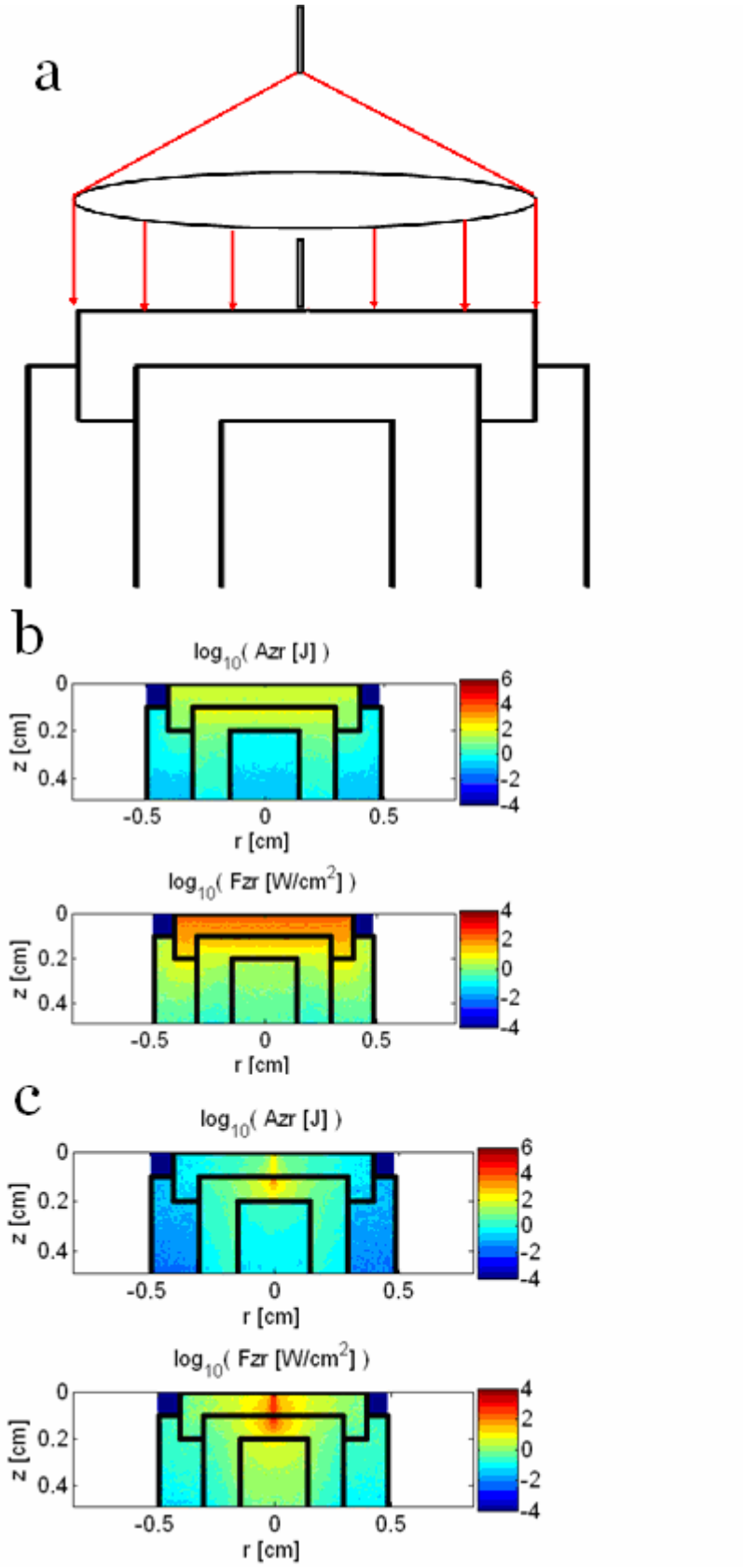

Figure 6.7: Use case #1: Board Beam vs. Narrow Beam (a) Experiment Design (b) Broad beam Result (Top: Energy deposition, Bottom: Fluence rate) (c) Narrow Beam

Result (Top: Energy deposition, Bottom: Fluence rate)

6.4.2 Compare incident light position

In a PDT treatment, the clinician needs to determine which the best point to place the incident light source is. The criteria of best incident point are the more energy deposits to the target region and other region does not have enough light energy to damage the tissue. Monte Carlo tooth program was run for different incident light location and the energy deposition results are compared.

Figure 6.8a shows the setup of MC tooth experiment to determine which the best incident point is. In this experiment, there is one voxel with target cells (bacteria) at position X = 0.25, Y = 0 and Z = 0.15cm. The bacteria voxel size is 0.01x0.01x0.01 in cm. The density of bacteria is roughly 1 gram/cm^3. According to the photodynamic therapy result, the bacteria in this voxel require PDTth1=6.60x10^{13} photons to successfully accomplish the PDT treatment.

Pencil beam was used as light source in this case. Two incident points were tested with Monte Carlo program as shown in Figure 6.8 a. In each test, 500,000 photons were launched in the incident point; the energy deposition at the bacteria position was documented for each test and compared. Figure 6.8 b show the MC tooth result for the two incident points.

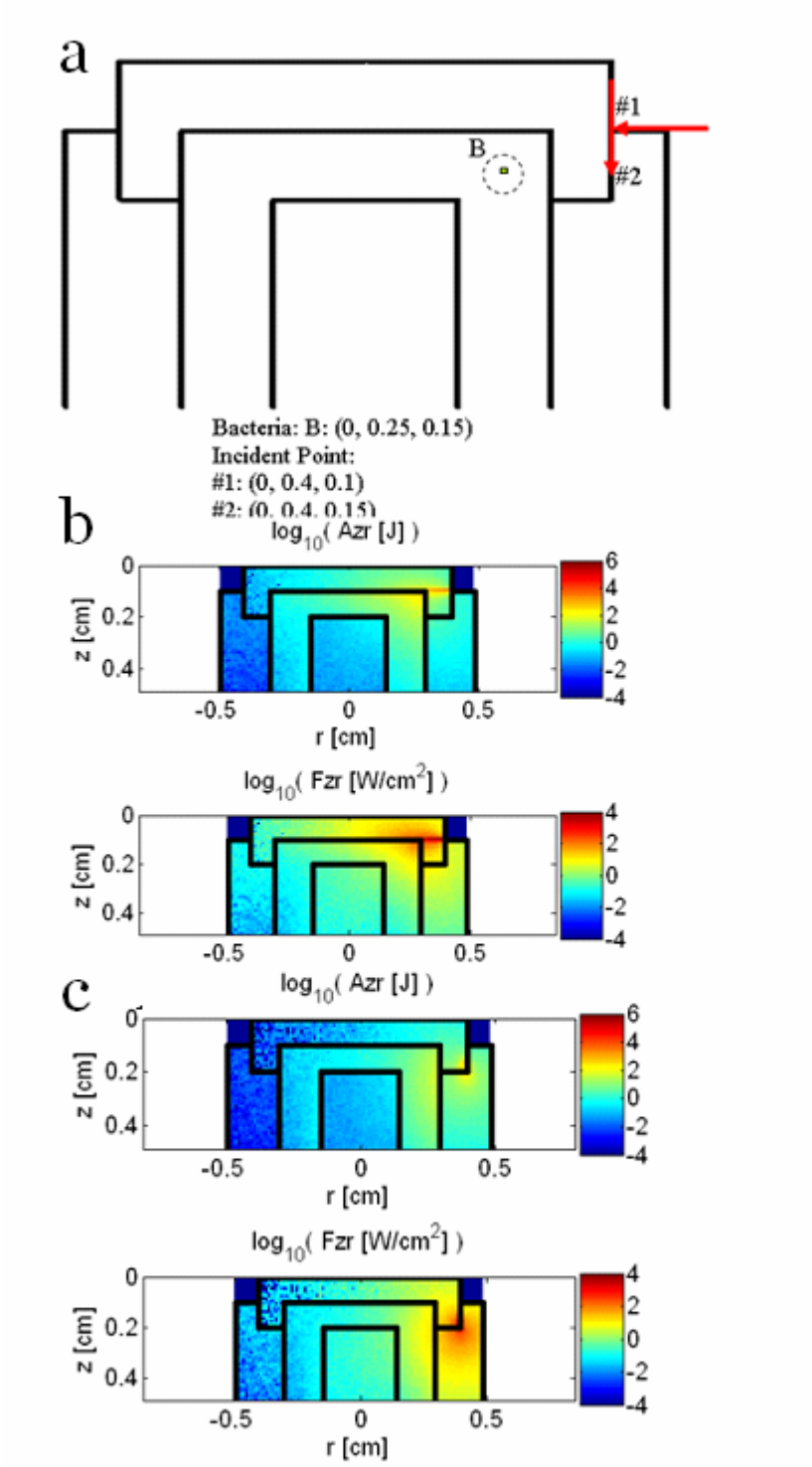

Figure 6.8: Use case #2: Comparison between 2 incident point of doctor's choice (a) Experiment Design (b) Incident Point #1 Result (Top: Energy deposition, Bottom: Fluence rate) (c) Incident Point #2 Result (Top: Energy deposition, Bottom: Fluence rate)

The energy deposition A in photon weight at the incident point is displayed as Table 6.2. We can get transmission T from the energy deposition.

$$T = \frac{A}{N_{ph} V \mu_{a\_dentine}} \quad [6.12]$$

N_{ph} is the initial photon (500,000) and V is the voxel volume (10^{-6} cm^{-1}) and μ_{a_dentin} is the absorption coefficient of dentine. According to the required energy deposition PDTth1 for one voxel is 6.60×10^{13} photons to accomplish PDT. PDTth1 is as the following equation:

$$PDTth1 = Q \mu_{a\_PS} T \frac{\lambda}{hc} \quad [6.13]$$

Q is the required energy delivered in the incident point for PDT requirement. μ_{a_PS} is the absorption coefficient for the photosensitizer in the bacteria cell (1.1×10^{3} cm^{-1}). λ is wavelength (633nm in this case), h is Planck constant and c is the speed of light.

	#1	#2
Energy deposition [photon] @ target point B for dentin per 500,000 photon	81.8	17.9
Energy required at incident point [mJ]	6.3	28.8

Table 6.2: Result for Case #2

In this equation, the only unknown term in Q. The higher Q value means more energy needs to be delivered to the tooth. We want to find the best incident point with least irradiation energy to the tooth. As table 6.2 shows, in this case incident point #1 is the best point since it needs delivery less light for enough PDT dosage.

The above case only considers one voxel of bacteria; in clinical practice, the bacteria region is usually larger than one voxel size. We can still calculate the energy required

for each voxel and in most cases the bacteria absorption is relatively small and won't change the Monte Carlo result significantly. If the bacteria region is quite large, perturbation theory can be used to create some negative light source and balance the absorption effect of bacteria.

6.5 Conclusion and Discussion

The oral biofilm will not always grow in the surface of tooth; sometimes it may also growth in the crack or the cavity of tooth. Some novel designs of PDT light source based on optical fiber has been designed for light power delivery. However, in some cases the fiber still can't access the biofilm. The light needs to irradiate on the surface and penetrate into the tooth.

In this chapter Monte Carlo tooth model is developed as a tool for clinician application. Light propagation into the tooth geometry model is simulated statistically. According to the results in the photodynamic therapy dosage, two use cases are presented to demonstrate the light source type comparison and incident point comparison. The computation time is less than 30 seconds to get a quite good result for tooth model. This will be feasible to design a clinical photodynamic therapy plan in the dentist's office.

Chapter 7:
General Discussion and Conclusion

This dissertation has presented theoretical model and analysis approach for oral antibiotics based photodynamic therapy. Photosensitizer distribution and deposition, light source calibration and light diffusion, photodynamic therapy dosage threshold which are all key factors of photodynamic therapy application have been discussed.

Because of the nature of the target cells: oral bacteria in planktonic state and biofilm state, some traditional approaches to studied photodynamic therapy are not suitable. A novel light propagation model for confocal microscope was validated and applied (Chapter 2B) in this study for photosensitizer distribution analysis in biofilm. Reflectance spectroscopy was yielded to determine the photosensitizer deposition in planktonic bacteria cells (Chapter 2A). PDT light source was calibrated (Chapter 3) and PDT result was analyzed as survival curves (Chapter 4). PDT dosage was determined (Chapter 5). A 3D Monte Carlo simulation model was developed and applied for light propagation in tooth to estimate the light irradiation dosage (Chapter 6).

7.1 Confocal microscopy model for PS distribution in biofilm

The confocal reflectance signal follows exponential decay equation 2.8. Local reflectivity ρ can be expressed as equation 2.11 and attenuation μ can be expressed as equation 2.10 if absorption can be ignored. In the other words, local reflectivity and attenuation has a 2-2 correspondence to the optical properties of the subject (tissue or

phantom). When the subject is measured using confocal microscope, the optical properties can be determined by fitting the confocal signal curve and convert ρ and μ to μ_s' and g.

When absorber is added into the subject, comparing the difference between equation 2.10 and equation 2.13, the adding absorber effect can be calculated and the added absorber concentration can be determined. In Chapter 3, polystyrene sphere and Toluidine Blue O (TBO) solution was made to validate this model. Different polystyrene sphere concentration was yield for scattering dominated case and absorber dominated case. In each case, polystyrene sphere only and polystyrene sphere with different concentration of TBO solution were measured by confocal microscope. TBO concentration was determined and compared to real concentration. The error is less than 15%.

Estimating the PS concentration in the biofilm is to ensure any location in the biofilm has enough PS for PDT. In the biofilm photosensitizer (TBO) concentration measurement experiment, the concentration of TBO is not homogeneous in the biofilm. However the equation 2.13 for light propagation in biofilm can still be applied. Biofilm with no TBO added and with TBO added was measured by confocal microscope. A biofilm holder was designed to ensure the coordinator registration for the two measurements. The only difference between the two measurements are equation 2.14, thus the summation of TBO concentration from top layer to the measurement layer can be calculated. And finally each layer TBO concentration can be determined.

Because of the dimension of biofilm and heterogeneous distribution of photosensitizer, estimation of PS concentration quantity is quite difficult. This method used reflectance mode confocal microscope, the resolution is 0.8 um and it can get the local PS concentration in any position in the biofilm.

7.2 Planktonic state PS uptake

The PS has selectivity for the target cells; in this study, TBO has selectivity to the S. mutans cells. Selectivity is very important property of PS to ensure the PDT happen in the target cells and eliminate the damage of surrounding cells. Therefore, the TBO concentration in the S.mutans cells will be much higher than the initial TBO concentration.

S.mutans with TBO (after waiting for TBO deposition) was collected using centrifuging method. Polystyrene sphere and collected S. mutans cells were put together. Reflectance spectrum was measured. The reflectance spectrum depends on the reduced scattering coefficient (mostly from polystyrene sphere) and absorption coefficient (mostly from the S. mutans with TBO). The concentration of polystyrene sphere was calibrated using standard (polystyrene sphere and pure TBO) therefore, the reduced scattering coefficient is known. The only unknown factor absorption coefficient can be determined with measured spectrum; TBO concentration in the S. mutans cells can be determined. Different initial TBO concentration and different waiting time were used and TBO concentration is each case was determined. A model of TBO diffusion into the S. mutans cells was built.

To measure the absorption in the S. mutans cells with TBO, transmission measurement and reflectance measurement could be the two candidates. Actually both methods have been tested. We found that the transmission measurement won't be accurate because the absorption of S. mutans with TBO is very small and any inaccuracy in the measurement will result dramatic different of the final TBO concentration. For the reflectance method, the measurement is relative robust since the measurement is a combination of TBO absorption and polystyrene sphere scattering.

7.3 Light calibration and PDT dosage analysis

To compare the light dosage for different groups using different light source, our light source need to be calibrated to a certain wavelength. In the S. mutans PDT case, we will calibrate our tungsten filament to 633 nm.

To calibrate the light source, the OceanOptics spectrometer is calibrated from arbitrary unit to real unit (mW) firstly. A HeNe laser (633 nm) was measured for power with a power meter. Then the HeNe laser was measured using the spectrometer. From those two measurements, the convert value from arbitrary unit to real unit is found for 633 nm. In the next step, a tungsten light source with vendor provided irradiation spectrum was measured with OceanOptics spectrometer. Since we know the shape of tungsten light irradiation spectrum and we also measured it using the OceanOptics spectrometer, we are able to calculate the shape of convert value curve (from arbitrary unit to real unit) for the OceanOptics spectrometer. Because we know the convert value at 633 nm, we can get each number in the convert value curve.

With a calibrated spectrometer, we used it to measure our light source (a 500W tungsten filament), all our measurement were in real unit. We also measured the absorption spectrum of TBO. Therefore, we were able to calculate the effective dosage which is defined as how much of the light in 633 nm is equal to the effect of our current light source.

With the calibrated light source, PDT experiments were studied with survival curve using CFU counting. The threshold dose was calculated according to survival curve and compared with other groups. With measured TBO concentration, the PDT dosage threshold as how much of photon is needed to kill 1 gram of target cell was also measured. It has been shown than the dosage threshold of planktonic bacteria is around 10^{21} photon/g.

7.4 Monte Carlo simulation

While the light dosage is estimated by the previous studies, the next question will be how much of the light will be irradiated to the target region. This answer will be obvious if the target region is in superficial layer of tooth, however it will not always be that case. Sometimes the biofilm resides in the crack of the tooth. We need to find the proper irradiation and the proper position to shine the light. The goal is ensure the light deposition is enough for the target cells and not too much to damage the other tissue.

Light propagation is more complicated than other models because it includes both scattering and absorption. Especially in a complicated geometry model, the analytical solution is usually impossible. In biomedical fields, people use a statistical base method Monte Carlo simulation to study those issues. In this dissertation, a 3D Monte Carlo model was developed. Different light source and different boundary conditions was implemented into this model. Both energy deposition and light irradiation in the tooth is calculated.

We also developed several use cases to demonstrate the 3D tooth Monte Carlo model. In the use cases, the different light sources (pencil beam and broad beam) were compared for PDT result. Different light incident points were also compared to help the clinician to find the proper incident point with better light irradiation results. The goal of this study was using Monte Carlo tooth model to meet the PDT light dosage requirements and not to induce too much light to damage the surrounding tissue such as tooth pulp.

7.5 Antibiotics PDT perspective

Photodynamic therapy for antibiotic purposes has a bright perspective however there is still a lot work to be done before the clinical application to benefit the human beings. PDT success needs collaboration of microbiologist, biomedical scientist,

dentists. It was very lucky for me to find professors supporting me from different fields. From the biomedical optics point of view, we can provide approaches to quantitive light propagation analysis, photosensitizer distribution and deposition analysis. Those are very important because we need to make sure the PDT has enough killing effects to prevent the bacteria to grow again, also PDT won't induce damage to the other tissues.

Since it has been demonstrated that PDT has significant killing effect for S. mutans bacteria in both planktonic state and biofilm, some clinical work will be necessary to prove it works well for human being without significant side effects. It will also be nice to find better photosensitizer with properties of selectivity, cheap, and no side effects.

Besides those studies just mentioned above, researchers begins to work on other interesting issues such as pain management in PDT process, bacteria regrowth behavior after PDT and etc. Also biofilm behavior and PDT mechanism for biofilm are not clear yet; it would be quite important to understand those fundamental issues.

BIBLIOGRAPHY

[1] Neu. H., “The crisis in antibiotic resistance” Science, Vol. 257 (5073): pp. 1064-1073. 1992

[2] Grand AL., V. Hogerzeil H, H. FM, “Intervention research in rational use of drugs: a review”, Health Policy and Planning Vol. 14 (2): pp89-102. 1999

[3] Vanderweil S., Pelletier A., Hamedani A., Gonzales R, Metlay J., Camargo C., “Declining antibiotic prescriptions for upper respiratory infections, 1993-2004”, Acad Emerg Med Vol. 14 (4): pp366-369. 2007

[4] Hamblin M. and Hasan T., “Photodynamic therapy: a new antimicrobial approach to infectious disease?” Photochem. Photobiol. Science, Vol. 3: pp. 436-450. 2004

[5] Wainwright M., “Photodynamic antimicrobial chemotherapy (PACT)”, Antimicrob Chemother J., Vol. 42: pp13-28. 1998

[6] Wainwright M., D.A. Phoenix, Laycock S.L., Wareing D.R. and Wring P.A., “photobactericidal activity of phenothiazinium dyes against methicillin-resistant strains of Staphylococcus aureus”, FEMS Microbiol, Lett, Vol. 160: pp. 177-181. 1998

[7] Star W.M., "Light dosimetry in vivo," Phys. Med. Biol. 42, 763-87. 1997

[8] Wilson B.C., Patterson M.S., Lilge L., "Implicit and Explicit Dosimetry in Photodynamic Therapy: A New Paradigm," Lasers Med. Sci. 12(1): pp. 82-99. 1997

[9] Beck JD, Garcia RI, Heiss G, Vokonas PS, Offenbacher S, “Periodontal disease and cardiovascular disease. J Periodontol” Vol. 67: pp.1123-1137. 1996

[10] Rinaldo Cubeddu, Antonio Pifferi, Paola Taroni, Alessandro Torricelli, Gianluca Valentini, Daniela Comelli, Cosimo D’Andrea, Valentina Angelini and Gianfranco Canti, “Fluorescence Imaging During Photodynamic Therapy of Experimental Tumors in Mice Sensitized with Disulfonated Aluminum Phthalocyanine” Photochem Photobiol, Vol. 72(5): pp. 690-695. 2000

[11] Ochsner M., “Photophysical and photobiological processes in the photodynamic therapy of tumours”, Photochem J.. Photobiol., B, Vol. 39: pp. 1-18. 1997

[12] Athar M., Mukhtar H. and Bickers D. R., “Differential role of reactive oxygen intermediates in photofrin-I- and photofrin-IImediated photoenhancement of lipid peroxidation in epidermal microsomal membranes”, J. Invest. Dermatol., Vol. 90: pp 652-657. 1988

[13] Redmond R. W. and Gamlin J. N., “A compilation of singlet oxygen yields from biologically relevant molecules”, Photochem. Photobiol., Vol. 70: pp 391-475. 1999

[14] Hass B. S. and Webb R. B., “Photodynamic effects of dyes on bacteria. IV. Lethal effects of acridine orange and 460- or 500-nm monochromatic light in strains of Escherichia coli that differ in repair capability”, Mutat. Res., Vol. 81: pp 277-285. 1981

[15] Bertoloni G., Lauro F. M., Cortella G. and Merchat M., “Photosensitizing activity of hematoporphyrin on Staphylococcus aureus cells”, Biochim. Biophys. Acta, Vol. 14: pp 169-174. 2000

[16] Y.Nitzan, Gutterman M., Malik Z. and Ehrenberg B., “Inactivation of gram-negative bacteria by photosensitized porphyrins”, Photochem. Photobiol., Vol. 55: pp 89-96. 1992

[17] Hall-Stoodley L., Costerton J.W., Stoodley P., “Bacterial biofilms: from the natural environment to infectious diseases”, Nat. Rev., Microbiol. Vol. 2: pp 95-108. 2004

[18] Henderson BW, Bellnier DA, Greco WR, Sharma A, Pandey RK, Vaughan LA, Weishaupt KR, Dougherty TJ: “An in vivo quantitative structure-activity relationship for a congeneric series of pyropheophorbide derivatives as photosensitizers for photodynamic therapy, Cancer Res. Vol. 57 (18): pp 4000- 4007. 1997

[19] Jori G, Fabris C, Soncin M, Ferro S, Coppellotti O, Dei D, Fantetti L, Chiti G, Roneucci G, “Photodynamic therapy in the treatment of microbial infections: Basic principles and perspective applications”, J Clin Laser Med Surg Vol. 38 (5): pp 468-481. 2006

[20] Nielsen KP, Juzeniene A, Juzenas P, Stamnes K, Stamnes JJ, “Moan J, Choice of optimal wavelength for PDT: The significance of oxygen depletion” Photochem. Photobiol. Vol. 81 (5): pp 1190-1194. 2005

[21] Henderson BW, Busch TM, Snyder JW “Fluence rate as a modulator of PDT mechanisms” Lasers Surg Meds Vol. 38 (5): pp 489-493. 2006

[22] Robinson DJ, de Bruijn HS, van der Veen N, Stringer MR, Brown SB, Star WM “Fluorescence photobleaching of ALA-induced protoporphyrin IX during photodynamic therapy of normal hairless mouse skin: The effect of light dose and irradiance and the resulting biological effect” Photochem. Photobiol. Vol. (1): pp 140-149. 1998

[23] Tomaselli F, Maier A, Sankin O, Anegg U, Stranzl U, Pinter H, Kapp K, Smolle-Juttner FM "Acute effects of combined photodynamic therapy and hyperbaric oxygenation in lung cancer - A clinical pilot study" Lasers Surg Med Vol. 28 (5): pp 399-403. 2001

[24] Anthony W. Smith "Biofilms and antibiotic therapy: Is there a role for combating bacterial resistance by the use of novel drug delivery systems?" Adv. Drug Deliv. Rev., Vol. 57: pp 1539-1550. 2005

[25] Gilbert P., Collier P.J., Brown M.R.W., "Influence of growth rate on susceptibility to antimicrobial agents: biofilms, cell cycle, dormancy, and stringent response", Antimicrob. Agents Chemother. Vol. 34: pp 1865-1868. 1990

[26] Costerton J.W., Stewart P.S., Greenberg E.P., "Bacterial biofilms: a common cause of persistent infections", Science, Vol. 284: pp 1318-1322. 1999

[27] Lewis K., "Riddle of biofilm resistance", Antimicrob. Agents Chemother. Vol. 45: pp 999-1007. 2001

[28] Mah T.-F.C., O'Toole G.A., "Mechanisms of biofilm resistance to antimicrobial agents", Trends Microbiol. Vol. 9: pp 34-39. 2001

[29] Brown M.R.W., Smith A.W., "Antimicrobial agents and biofilms", Medical Implications of Biofilms, Cambridge University Press, Cambridge, pp 36-55. 2003

[30] Gilbert P., Maira-Litra´n T., McBain A.J., Rickard A.H., Whyte F.W., "The physiology and collective recalcitrance of microbial biofilm communities", Adv. Microb. Physiol. Vol. 46: pp 202-256. 2002

[31] Zimmerli W., Trampuz A., Ochsner P.E., "Prosthetic-joint infections", N. Engl. J. Med. Vol. 351: pp 1645-1654. 2004

[32] Peter Meisel, Thomas Kocher, "Photodynamic therapy for periodontal disease: state of the art", Journal of photochemistry and photobiology B: Biology Vol. 79: pp 159-170. 2005

[33] Mea A. Weinberg, D.M.D., M.S.D., R.Ph., "Periodontal Diseases and Systemic Health"
http://www.uspharmacist.com/oldformat.asp?url=newlook/files/Feat/peridontal.cfm&pub_id=8&article_id=434

[34] Wainwright M., Crossley K.B., "Photosensitising agents- circumventing resistance and breaking down biofilms: a review", Int. Biodeterior. Biodegrad. Vol. 53:

pp 119-126. 2004

[35] O'Neill J.F., Hope C.K., Wilson M., "Oral bacteria in multispecies biofilms can be killed by red light in the presence of toluidine blue", Lasers Surg. Med. Vol. 31: pp 86-90. 2002

[36] Simon Wood, Brain Nattress, Jennifer Kirkham, Roger Shore, Steven Brookes, John Griffiths, Colin Robinson, "An in vitro study of the use of photodynamic therapy for the treatment of natural oral plaque biofilms formed in vivo", J. Photochem, Photobiol, B: Vol. 50: pp 1-7. 1999

[37] Marsh P. D., Bradshaw D.J., "Dental plaque as a biofilm", J, Ind. Microbiol, Vol. 15: pp 169-175. 1995

[38] Brub-Buisson C., "New technologies and infection control practices to prevent intravascular catheter-related infections", Am. J. Respir. Crit. Care Med. Vol. 164: pp 1557-1558. 2001

[39] Tony P. Paulino, Prislaine P. Magalhaes, Geraldo Thedei, Jr. Antonio, C. Tedesco and Pietro Ciancaglini, "Use of Visible Light-based Photodynamic Therapy to Bacteria Photoinactivation", Biochem Mol Biol Educ, Vol. 33(1): pp 46-49. 2005

[40] Altmann SW, Davis HR, Zhu LJ, Yao XR, Hoos LM, Tetzloff G, Iyer SPN, Maguire M, Golovko A, Zeng M, Wang LQ, Murgolo N, Graziano MP, "Niemann-Pick C1 like 1 protein is critical for intestinal cholesterol absorption" Science Vol. 303 (5661): pp 1201-1204. 2004

[41] Panyam J, Labhasetwar V, "Biodegradable nanoparticles for drug and gene delivery to cells and tissue" Adv Drug Deliv Rev Vol. 55(3): pp 329-347. 2003

[42] Smith AW, "Biofilms and antibiotic therapy: Is there a role for combating bacterial resistance by the use of novel drug delivery systems?" Adv Drug Deliv Rev Vol. 57(10): pp 1539-1550. 2005

[43] Konan YN, Gurny R, Allemann E, "State of the art in the delivery of photosensitizers for photodynamic therapy" J. Photochem. Photobiol. B, Biol. Vol. 66 (2): pp 89-106. 2002

[44] Berard V, Rousseau JA, Cadorette J, Hubert L, Bentourkia M, van Lier JE, Lecomte R, "Dynamic imaging of transient metabolic processes by small-animal PET for the evaluation of photo sensitizers in photodynamic therapy of cancer" J. Nucl Med Vol. 47 (7): pp 1119-1126. 2006

[45] Chen B, Pogue BW, Luna JM, Hardman RL, Hoopes PJ, Hasan T, "Tumor

vascular permeabilization by vascular-targeting photosensitization: Effects, mechanism, and therapeutic implications," Clin Canc Res Vol. 12 (3): pp 917-923. 2006

[46] Rick K, Sroka R, Stepp H, Kriegmair M, Huber RM, Jacob K, Baumgartner R, "Pharmacokinetics of 5-aminolevulinic acid-induced protoporphyrin IX in skin and blood," J. Photochem. Photobiol. B, Biol. Vol. 40 (3): pp 313-319. 1997

[47] Moan J, Berg K, "The photodegradation of porphyrins in cells can be used to estimate the lifetime of singlet oxygen" Photochem. Photobiol. Vol. 53 (4): pp 549-553. 1991

[48] Nick S. White, Rachel J. Errington, "Fluorescence techniques for drug delivery research: theory and practice" Adv Drug Deliv Rev Vol. 57: pp 17-42. 2005

[49] Owen T. Price, Christopher Lau, and Robert M. Zucker, "Quantitative Fluorescence of 5-FU–Treated Fetal Rat Limbs Using Confocal Laser Scanning Microscopy and LysoTracker Red" Cytometry: Part A Vol. 53A: pp 9-21. 2003

[50] Hamblin MR, O'Donnell DA, Murthy N, Contag CH, Hasan T, "Photodynamic treatment of wound infections in vivo monitored by luminescence imaging", Photochem Photobiol, Vol. 75: pp 51-57. 2002

[51] Komerik N., Nakanishi H., MacRobert A. J., Henderson B., Speight P., and Wilson M., "In Vivo Killing of Porphyromonas gingivalis by Toluidine Blue-Mediated Photosensitization in an Animal Model", Antimicrob Agents Chemother, Vol. 47(3): pp 932-940. 2003

[52] Komerik N., Curnow A., MacRobert A.J., Hopper C., Speight P.M. and Wilson M., "Fluorescence Biodistribution and hotosensitising Activity of Toluidine Blue O on Rat Buccal Mucosa", Lasers Med Sci, Vol.17: pp 86-92. 2002

[53] Nikolaos S. Soukos, Sigmund S. Socransky, Stephen E. Mulholland, Shun Lee, and Apostolos G. Doukas, "Photomechanical Drug Delivery into Bacterial Biofilms", Pharmaceut Res, Vol.17(4): pp 405-409. 2000

[54] Stenuddl C., Nordlund A., Johansson M. R, KdIIestail C., "The Association of Bacterial Adhesion with Dental Caries", J Dent Res Vol. 80(11): pp 2005-2010. 2001

[55] Owen T. Price, Christopher Lau, and Robert M. Zucker, "Quantitative Fluorescence of 5-FU–Treated Fetal Rat Limbs Using Confocal Laser Scanning Microscopy and LysoTracker Red" Cytometry Part A, Vol. 53A: pp 9-21. 2003

[56] Drakaki E., Psycharakis S., Makropoulou M., Serafetinides A.A.: "Optical

Properties and chromophore concentration measurement in tissue like phantoms" Optic Comm, Vol. 254: pp 40-51. 2005

[57] Michael S. Patterson and Brian W. Pogue, "Mathematical model for time-resolved and frequency-domain fluorescence spectroscopy in biological tissues", Appl Optic, Vol. 33(10): pp 1963-1974. 1994

[58] Slots J, Rams TE, Listgarten MA, "Yeasts, enteric rods and pseudomonads in the subgingival flora of severe adult periodontitis." Oral Microbiol Immunol Vol. 3: pp 47-52. 1988

[59] Kevin R. Diamond, Michael S. Patterson, and Thomas J. Farrell, "Quantification of fluorophore concentration in tissue-simulating media by fluorescence measurements with a single optical fiber" Appl Optic, Vol. 42(13): pp 2436-2442. 2003

[60] Robert Weersink, Michael S. Patterson, Kevin Diamond, Shawna Silver, and Neil Padgett, "Noninvasive measurement of fluorophore concentration in turbid media with a simple fluorescence-reflectance ratio technique", Appl Optic, Vol. 40(34): pp 6389-6395. 2001

[61] Hamblin MR, O'Donnell DA, Murthy N, Contag CH, Hasan T, "Photodynamic treatment of wound infections in vivo monitored by luminescence imaging", Photochem Photobiol, Vol. 75: pp 51-57. 2002

[62] Roesler CS, Perry MJ, "In-situ Phytoplankton Absorption, Fluorescence Emission, and Particulate Backscattering Spectra Determined from Reflectance" J Geophys Res C Oceans Vol. 100(C7): pp 13279-13294. 1995

[63] Dragana Stasic, Thomas J Farrell and Michael S Patterson, "The use of spatially resolved fluorescence and reflectance to determine interface depth in layered fluorophore distributions," Phys Med Biol Vol. 48: pp 3459-3474. 2003

[64] Gardner CM, Jacques SL, Welch AJ, "Fluorescence spectroscopy of tissue: Recovery of intrinsic fluorescence from measured fluorescence" Appl Optic Vol. 35 (10): pp 1780-1792. 1996

[65] Johansson A, Johansson T, Thompson MS, Bendsoe N, Svanberg K, Svanberg S, Andersson-Engels S, "In vivo measurement of parameters of dosimetric importance during interstitial photodynamic therapy of thick skin tumors" J Biomed Optic Vol. 11(3): pp 034029. 2006

[66] Murat Canpolat and Judith R. Mourant," Monitoring photosensitizer concentration by use of a fiber-optic probe with a small source–detector separation,"

Appl Optic Vol. 39(34): pp 6508-6514. 2000

[67] Jacques SL, R. Samatham, N. Choudhury, Y. Fu, D. Levitz, “Measuring tissue optical properties in vivo using reflectance-mode confocal microscopy and OCT”, Proc SPIE6864;10, 2008

[68] Moan J, Peng Q, evensen If, Berg K, Western A, Rimington C: “Photosensitizing efficiencies, tumor-uptake and cellular-uptake of different photosensitizing drugs relevant for photodynamic therapy of cancer” Photochem Photobiol vol. 46 (5): pp 713- 721. 1987

[69] Soukos NS, Ximenez-Fyvie LA, Hamblin MR, “Targeted antimicrobial photochemotherapy”Antimicrob Agents Chemothe Vol. 42 (10): pp 2595-2601. 1998

[70] Bhatti M, MacRobert A, Meghji S, Henderson B, Wilson M “A study of the uptake of toluidine blue O by Porphyromonas gingivalis and the mechanism of lethal photosensitization” Photochem Photobiol Vol. 68 (3): pp 370-376. 1998

[71] Patterson MS, Wilson BC, Graff R, “Invivo tests of the concept of photodynamic threshold dose in normal rat-liver photosensitized by aluminum chlorosulfonated phthalocyanine” Photochem Photobiol Vol. 51 (3): pp 343-349. 1990

[72] Ferreira J, Moriyama LT, Kurachi C, Sibata C, Silva OCE, Zucoloto S, Bagnato VS “Experimental determination of threshold dose in photodynamic therapy in normal rat liver” Laser Phys Lett Vol. 4 (6): pp 469-475. 2007

[73] Henderson BW, DoughertY TJ “How does photodynamic therapy work” Photochem Photobiol Vol. 55 (1): pp 145-157. 1992

[74] Hatz S, Lambert JDC, Ogilby PR “Measuring the lifetime of singlet oxygen in a single cell: addressing the issue of cell viability” Photochem Photobiol Vol. 6 (10): pp 1106-1116. 2007

[75] Jori G “Tumour photosensitizers: Approaches to enhance the selectivity and efficiency of photodynamic therapy” J of Photochem Photobiol B Vol. 36 (2): pp 87-93. 1996

[76] Demidova TN, Hamblin MR “Photodynamic therapy targeted to pathogens” Int J Immunopathol Pharmacol Vol. 17 (3): pp. 245-254. 2004

[77] Zanin ICJ, Goncalves RB, Brugnera A, et al. “Susceptibility of Streptococcus mutans biofilms to photodynamic therapy: an in vitro study” J Antimicrob Chemother Vol. 56 (2): pp 324-330. 2005

[78] Maisch T, Baier J, Franz B, Maier M, Landthaler M, Szeimies RM, Baumler W "The role of singlet oxygen and oxygen concentration in photodynamic inactivation of bacteria" Proc. Natl. Acad. Sci. U.S.A Vol. 104 (17): pp 7223-7228. 2007

[79] Johansson A, Svensson J, Bendsoe N, Svanberg K, Alexandratou E, Kyriazi M, Yova D, Grafe S, Trebst T, Andersson-Engels S "Fluorescence and absorption assessment of a lipid mTHPC formulation following topical application in a non-melanotic skin tumor model" J Biomed Opt Vol. 12 (3) 034026. 2007

[80] Gareau DS, In vivo confocal microscopy in turbid media, PhD Dissertation, Oregon Health & Science University, Portland, OR, 2006

[81] Jacques SL, Samatham R., Choudhury N., Gareau D. S., Specifying tissue optical properties using axial dependence of confocal reflectance images: confocal scanning laser microscopy and optical coherence tomography, Proc. SPIE 6446-22. 2007

[82] L. Henyey and J. Greenstein, "Diffuse radiation in the galaxy," Astrophys. Journal, vol. 93, pp. 70-83. 1941.

[83] Bohren, Craig F., Donald R. Huffman, Scattering of Light by Small Particles, Wiley, New York. 1983

[84] Boyle RW, Dolphin.D. "Structure and biodistribution relationships of photodynamic sensitizers" Photochem. Photobiol. Vol. 64 (3): pp 469-485. 1996

[85] O'Riordan K, Akilov OE, Chang SK, Foley JW, Hasan T "Real-time fluorescence monitoring of phenothiazinium photosensitizers and their anti-mycobacterial photodynamic activity against Mycobacterium bovis BCG in in vitro and in vivo models of localized infection" Photochemical and Photobiological Science Vol. 6 (10): pp 1117-1123. 2007

[86] Farrell T. J., Patterson M. S., and Wilson B. C., "A diffusion theory model of spatially resolved, steady-state diffuse reflectance for the non-invasive determination of tissue optical properties in vivo," Med. Phys. Vol. 19: pp 879-888. 1992

[87] Takatani S. and Graham M. D., "Theoretical analysis of diffuse reflectance from a two-layer tissue model," IEEE Trans. Biomed. Eng., BME-26: pp 656-664. 1987

[88] American Dental Association "Oral Health Topics A-Z: Tooth whitening treatments, Online FAQ", available:
http://www.ada.org/public/topics/whitening_faq.asp

[89] Wilson M "Lethal photosensitisation of oral bacteria and its potential application in the photodynamic therapy of oral infections" Photochem Photobiol Vol. 3 (5): pp

412-418. 2004

[90] Kidd, E.A.M. and Smith, B.G.N.. Pickard's Manual of Operative Dentistry, Sixth Edition. Chapter 1 - Why restore teeth? Oxford Medical Publications 1990

[91] Barajas O, Ballangrud AM, Miller GG, Moore RB, Tulip J "Monte Carlo modelling of angular radiance in tissue phantoms and human prostate: PDT light dosimetry" Phys Med Biol Vol. 42 (9): pp 1675-1687. 1997

[92] Wang LH, Jacques SL, Zheng LQ "MCML - Monte-carlo modeling of light transport in multilayered tissues" Comput Methods Programs Biomed Vol. 47 (2): pp 131-146. 1995

[93] Monte Carlo Modeling of Light Transport in Multi-layered Tissues in Standard C (MCML Manual) Lihong Wang, Steven L. Jacques,

[94] Monte Carlo Simulation in Finance, available:
global-derivatives.com

[95] Lux, I., and L. Koblinger, "Monte Carlo Particle Transport Methods: Neutron and Photon Calculations", CRC Press 1991.

[96] Mcguire AF, Hapke BW "An experimental-study of light-scattering by large, irregular particles" ICARUS Vol.113 (1): pp 134-155. 1995

[97] Press W. H., Teukolsky S. A., Vetterling W. T., Flannery B.P: "Numerical Recipes in C++ Second Edition." Cambridge University Press, UK. 2002

[98] Henyey L. C. and. Greenstein J. L, ''Diffuse radiation in the galaxy,'' Astrophys. J. Vol. 93: pp 70–83. 1941

[99] Wang LH, Jacques SL, Zheng LQ "CONV - convolution for responses to a finite diameter photon beam incident on multi-layered tissues" Comput Methods Programs Biomed Vol. 54 (3): pp 141-150. 1997

[100] Ryan KJ; Ray CG. "Sherris Medical Microbiology, 4th ed.", McGraw Hill. 2004

[101] Vaarkampt J, Boscht JJ, Verdonschott EH "Light propagation through teeth containing simulated caries lesions" Phys. Med. Bid. Vol. 40: pp 1375-1387. 1995

[102] Farrell TJ, Wilson BC, Patterson MS, Olivo MC "Comparison of the in vivo photodynamic threshold dose for photofrin, mono- and tetrasulfonated aluminum phthalocyanine using a rat liver model" Photochem Photobiol Vol. 68 (3): pp 394-399. 1998

[103] Iriana C, Junqueira Z, Reginaldo B, Gon C, Aldo BJ, Christopher KH, Jonathan P, “Susceptibility of Streptococcus mutans biofilms to photodynamic therapy: an in vitro study” J. Antimicrob. Chemother. Vol. 56: pp 324-330. 2005

[104] Williams JA, Pearson GJ, Colles MJ, Wilson M, “The photo-activated antibacterial action of toluidine blue O in a collagen matrix and in carious dentine” Caries Res. Vol. 38(6): pp 530-536. 2004

[105] Loesche WJ. “Microbiology of Dental Decay and Periodontal Disease.” In: Baron's Medical Microbiology (Baron S et al, eds.), 4th ed., Univ of Texas Medical Branch. 1996

[106] Madigan M; Martinko J, “Brock Biology of Microorganisms, 11th ed.”, Prentice Hall. 2005.

[107] Klein, J.P.; Scholler, M.. "Recent Advances in the Development of a Streptococcus mutans Vaccine". Eur. J. Epidemiol. Vol. 4 (4): pp 419-425. 1998

[108] Hajishengallis G and Russell MW. "Molecular Approaches to Vaccination against Oral Infections", in Molecular Oral Microbiology. Caister Academic Press. 2008

[109] Sekal W., Fried D., Featherstone JDB., and Borzillary SF.: “Light Deposition in Dental Hard Tissue and Simulated Thermal Response”, J Dent Res Vol. 74(4): pp 1086-1092. 1995

BIBLIOGRAPHICAL NOTES

Yongji Fu was born in Beijing, China. He entered Tsinghua University in Beijing China in 1995. He received the B.S degree in Biomedical Engineering in 1999 and M.S degree in 2002 also in Biomedical Engineering. From 2002 to 2003, he worked as a medical imaging engineer in Siemens Medical Solution. In September 2003, he matriculated in Biomedical Engineering department at Oregon Health and Science University. Currently, he is a researcher in ShaUniversity. Currently, he is a researcher in Sharp Laboratories of America.